

AD-A044 208

SPERRY RESEARCH CENTER SUDBURY MASS
OPTOSWITCH CROSSTALK STUDY. (U)

F/6 17/2

AUG 77 R A SOREF
SCRC-CR-77-22

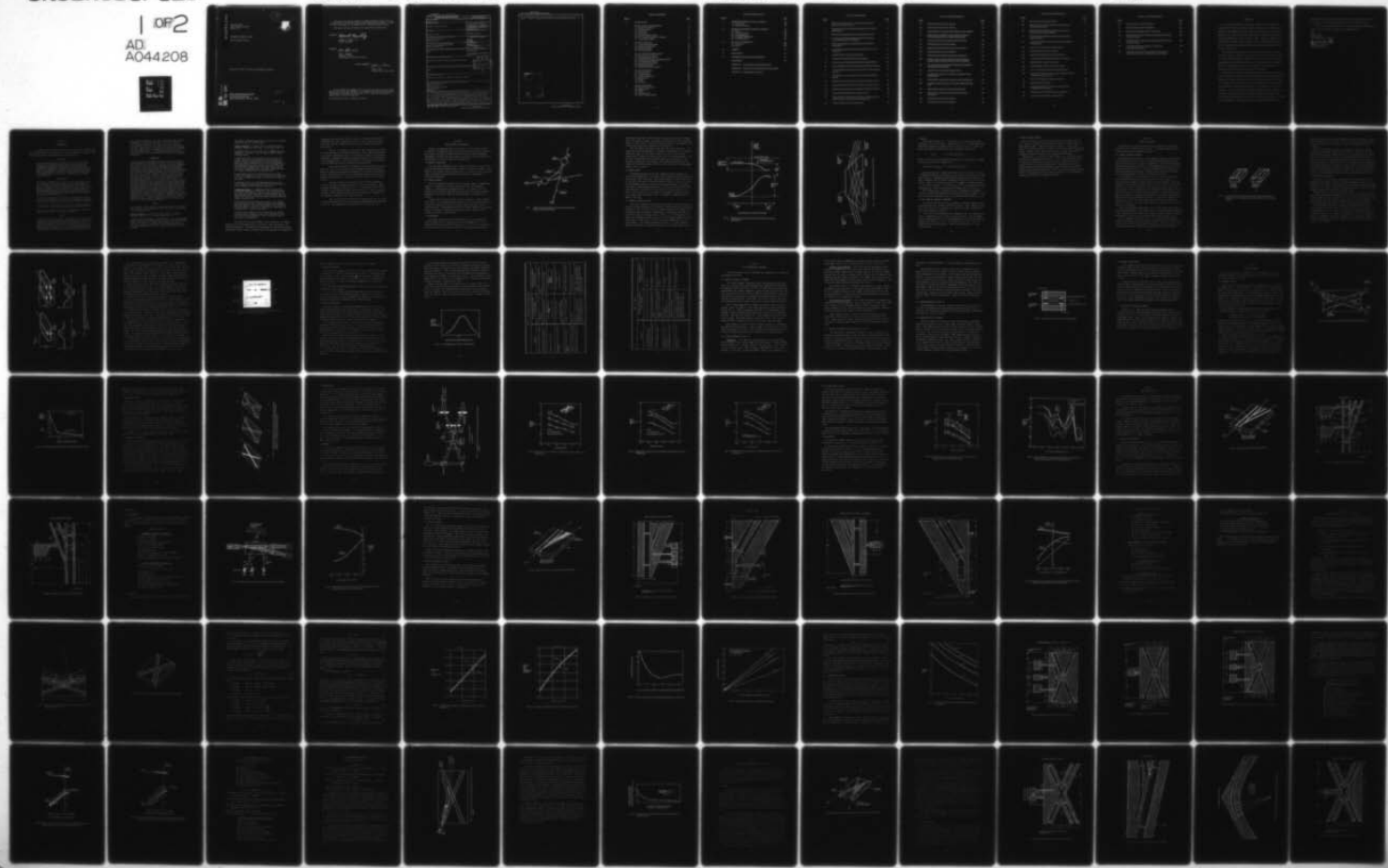
F30602-76-C-0129

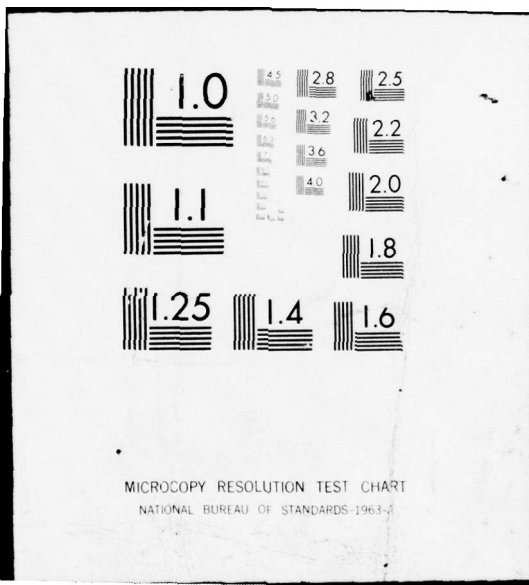
NL

UNCLASSIFIED

1 OF 2
AD
A044208

RADC-TR-77-260





MICROCOPY RESOLUTION TEST CHART
NATIONAL BUREAU OF STANDARDS-1963-A

AD A044208

RADC-TR-77-260
Final Technical Report
August 1977

12



OPTOSWITCH CROSSTALK STUDY

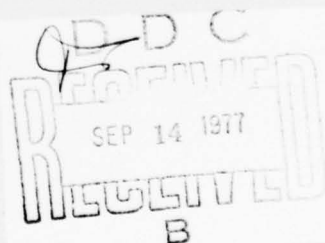
Sperry Research Center

OPTOSWITCH CROSSTALK STUDY

Approved for public release; distribution unlimited.

AD NO. _____
DDC FILE COPY

ROME AIR DEVELOPMENT CENTER
Air Force Systems Command
Griffiss Air Force Base, New York 13441



This report has been reviewed by the RADC Information Office (OI) and is releasable to the National Technical Information Service (NTIS). At NTIS it will be releasable to the general public including foreign nations.

This report has been reviewed and is approved for publication.

APPROVED:

Richard C. Benoit, Jr.

RICHARD C. BENOIT, JR
Project Engineer

APPROVED:

Fred I. Diamond

FRED I. DIAMOND
Technical Director
Communications & Control Division

FOR THE COMMANDER:

John P. Huss

JOHN P. HUSS
Acting Chief, Plans Office

If your address has changed or if you wish to be removed from the RADC mailing list, or if the addressee is no longer employed by your organization, please notify RADC (DAP), Griffiss AFB NY 13441. This will assist us in maintaining a current mailing list.

Do not return this copy. Retain or destroy.

UNCLASSIFIED

SECURITY CLASSIFICATION OF THIS PAGE (When Data Entered)

REPORT DOCUMENTATION PAGE		READ INSTRUCTIONS BEFORE COMPLETING FORM
1. REPORT NUMBER RADC-TR-77-260	2. GOVT ACCESSION NO.	3. RECIPIENT'S CATALOG NUMBER
4. TITLE (and Subtitle) OPTOSWITCH CROSSTALK STUDY		5. TYPE OF REPORT & PERIOD COVERED Final Technical Report February 1976 - March 1977
7. AUTHOR(s) Richard A. Soref		6. PERFORMING ORG. REPORT NUMBER SCRC-CR-77-22
9. PERFORMING ORGANIZATION NAME AND ADDRESS Sperry Research Center Sudbury MA 01776		8. CONTRACT OR GRANT NUMBER(s) F30602-76-C-0129
11. CONTROLLING OFFICE NAME AND ADDRESS Rome Air Development Center (DCLT) Griffiss AFB NY 13441		10. PROGRAM ELEMENT, PROJECT, TASK AREA & WORK UNIT NUMBERS 62702P 45191908
14. MONITORING AGENCY NAME & ADDRESS (if different from Controlling Office) Same		12. REPORT DATE August 1977
		13. NUMBER OF PAGES 127
		15. SECURITY CLASS. (of this report) UNCLASSIFIED
		15a. DECLASSIFICATION/DOWNGRADING SCHEDULE N/A
16. DISTRIBUTION STATEMENT (of this Report) Approved for public release; distribution unlimited.		
17. DISTRIBUTION STATEMENT (of the abstract entered in Block 20, if different from Report) Same		
18. SUPPLEMENTARY NOTES RADC Project Engineer: Richard C. Benoit, Jr. (DCLT)		
19. KEY WORDS (Continue on reverse side if necessary and identify by block number) Optical Communications Wave Propagation Communications Techniques Microelectronics Thin Film		
20. ABSTRACT (Continue on reverse side if necessary and identify by block number) A multimode electro-optical switch that has low crosstalk between channels has been demonstrated experimentally in a 70- μm -thick plate of Z-cut LiTaO ₃ . The fiber-compatible four-port switch is intended for integration into an optical matrix. The crosspoint consists of an in-plane crossover, two simple optical switches, and a curved connecting waveguide. Taken alone, the crossovers had 40 dB optical isolation. Compound crosspoints were tested using convergent TM-polarized input light with an 0.07 numerical aperture. About 10% of the initially channeled light was transferred into the crosschannel, and the (Cont)		

DD FORM 1 JAN 73 1473 EDITION OF 1 NOV 65 IS OBSOLETE

UNCLASSIFIED

SECURITY CLASSIFICATION OF THIS PAGE (When Data Entered)

D D C

REF ID: A651473 SEP 14 1977

B

MICROFOTOGRAFIA 408-198

UNCLASSIFIED

SECURITY CLASSIFICATION OF THIS PAGE(When Data Entered)

optical switching ratio of the crosschannel was 26 dB using 450 volts dc for control. Optical transmission loss of the 6-cm-long switch was 1.6 dB.

A

ACCESSION for	
NTIS	White Section <input checked="" type="checkbox"/>
DDC	Buff Section <input type="checkbox"/>
UNA UNCLASSED	<input type="checkbox"/>
JUSTIFICATION	<input type="checkbox"/>
DISTRIBUTION AND SECURITY CODES	
S-0-0-A	
A	

UNCLASSIFIED

SECURITY CLASSIFICATION OF THIS PAGE(When Data Entered)

TABLE OF CONTENTS

Section		Page
1	INTRODUCTION	1
2	OPTICAL MATRIX REQUIREMENTS	5
	2.1 Compound Crosspoints	5
	2.2 Tapoff Switching	5
	2.3 Terminology	5
	2.4 Matrix Layout	7
	2.5 Improved Crosspoint Model	7
	2.6 The "Compound Compound" Crosspoint	10
	2.7 Large Crossover Angles	11
3	CHOICE OF APPROACH	12
	3.1 Thermal Diffusion Approach	12
	3.2 Electro-Optic Approach	14
	3.3 Preferred Approach	18
	3.4 Passive Waveguiding	18
4	DEVICE FABRICATION PROCEDURE	22
	4.1 Initial Clean-up of Crystal	22
	4.2 Photolithography of Side "A"	22
	4.3 Turning the Crystal over for Access to Side "B"	23
	4.4 Photolithography of Side "B"	24
	4.5 Completion of the Sandwich	24
	4.6 Cutting and Polishing	26
	4.7 Mounting and Electrical Contact	26
5	PASSIVE CROSSOVERS	27
	5.1 Crossover Theory	27
	5.2 Crosstalk Sources	30
	5.3 Crossover Construction	30
	5.4 Measurements	32
	5.5 Results	32
	5.6 Discussion	37
6	SIMPLE CROSSPOINTS	40
	6.1 Design and Construction	40
	6.2 Measurements	44
	6.3 Results	44
	6.4 Spoiler Structure	47
	6.5 Spoiler Crosspoint Results	47

TABLE OF CONTENTS (Cont.)

<u>Section</u>		<u>Page</u>
7	COMPOUND CROSSPOINT (INITIAL VERSION)	56
	7.1 Initial Design	56
	7.2 Experimental Results	65
8	COMPOUND CROSSPOINT (IMPROVED VERSION)	78
	8.1 Design	78
	8.2 Device Construction	80
	8.3 Initial Measurements	85
	8.4 Throughput Measurements	91
	8.5 Final Measurements	93
9	DEFLECTION CROSSPOINT	98
	9.1 Construction	100
	9.2 Results	105
10	SUMMARY	111
11	CONCLUSIONS	114
12	RECOMMENDATIONS FOR FURTHER WORK	117
	REFERENCES	119
	APPENDIX A – Crosstalk Reduction in Optical Switching	
	APPENDIX B – Properties of the Terminated Optical Crossbar Matrix	
	APPENDIX C – Crosstalk Model for Crossover	

LIST OF ILLUSTRATIONS

<u>Figure</u>		<u>Page</u>
1	Model of compound crosspoint including cross-scattering and radiation from connecting guide.	6
2	Representation of four-port device showing definitions of optical switching terms.	8
3	Matrix of compound crosspoints (3 X 3) interfaced with fibers.	9
4	Two types of multimode waveguide crossovers constructed by thermal diffusion of Cu ⁺⁺ into LiNbO ₃ .	13
5	Dipolar and quadripolar electrooptic channels with associated index profiles.	15
6	Experimental examples of electrooptic channeling in 70-μm-thick LitaO ₃ plate.	17
7	Estimated behavior of passive channeling effect.	19
8	Cross-section of laminar electrooptic device package.	25
9	Plan view of planar intersecting channels showing angle definitions.	28
10	Typical dependence of interchannel coupling versus intersection angle.	29
11	Three electrode geometries that were used to make in-plane waveguide crossovers.	31
12	Experimental set-up for measuring optical isolation of intersecting channels.	33
13	Measured S/C ratio as a function of collection cone angle for a Fig. 11.	34
14	Measured S/C ratio as a function of collection cone angle for a Fig. 11.	35
15	Measured S/C ratio as a function of collection cone angle for a Fig. 11.	36
16	Measured S/C versus collection cone angle for Fig. 11.	38
17	Spatial distribution of crossover crosstalk light on focal plane for two values of applied voltage and for two observation cones.	39
18	Layout of three-port simple crosspoint device.	41

LIST OF ILLUSTRATIONS (Cont.)

<u>Figure</u>		<u>Page</u>
19	Photoresist mask for actual Fig. 18 device.	42
20	Photoresist mask for actual Fig. 18 device.	43
21	Experimental set-up for electro-optical testing of simple crosspoint.	45
22	Measured output of straight-through and branch channels as a function of gate potential for a simple crosspoint device.	46
23	Layout of three-port simple crosspoint device with spoiler.	48
24	Photoresist mask for actual Fig. 23 device.	49
25	Detail of side A photoresist mask for actual Fig. 23 device.	50
26	Photoresist mask for actual Fig. 23 device.	51
27	Detail of side B photoresist mask for actual Fig. 23 device.	52
28	Measured output of straight-through and branch channels as a function of gate-and-spoiler potential for two Fig. 23 devices.	53
29	Plan view of compound crosspoint electrodes showing dimensions and angles used in switch design.	57
30	Layout of four-port compound crosspoint device.	58
31	Induced index perturbation in LiNbO_3 and LiTaO_3 as a function of applied field.	61
32	Critical angle in LiNbO_3 and LiTaO_3 as a function of applied field.	62
33	Geometric coupling loss versus light-divergence-angle/branch-angle ratio.	63
34	Optical isolation of barrier as a function of barrier width.	64
35	Minimum bend radius of multimode channel versus channel critical angle.	66
36	Photoresist mask for actual Fig. 30 device.	67
37	Photoresist mask for actual Fig. 30 device.	68

LIST OF ILLUSTRATIONS (Cont.)

<u>Figure</u>		<u>Page</u>
38	Photoresist mask for actual Fig. 30 device.	69
39	Measured output of straight-through and crosschannels as a function of gate potential.	71
40	Measured output of straight-through and crosschannels as a function of gate-and-spoiler potential.	72
41	Top view of initial compound crosspoint showing location of undesired radiation.	75
42	Z-component of electric field along a line midway between two "capacitor plates."	77
43	Layout of four-port compound crosspoint device.	79
44	Photocresist mask for actual Fig. 43 device.	81
45	Detail of side A photoresist mask for Fig. 43 device.	82
46	Further detail of side A photoresist mask for Fig. 43 device.	83
47	Photoresist mask for actual Fig. 43 device.	84
48	Photomicrograph of polished end of CC-3-4 device.	86
49	Top view of actual CC-3-4 compound crosspoint device.	87
50	Experimental arrangement for electro-optical signal and crosstalk measurements on CC-3-4 devices.	88
51	Test of CC-3-4 device with convergent input light.	89
52	Output light of CC-3-4 device.	90
53	Intensity distributions from straight-through channel and crosschannel of CC-3-4 device.	92
54	Observed output of straight-through and crosschannels.	94
55	Layout of four-port deflection crosspoint device.	99

LIST OF ILLUSTRATIONS (Cont.)

<u>Figure</u>		<u>Page</u>
56	Photoresist mask for actual Fig. 55 device.	101
57	Photoresist mask for actual Fig. 55 device.	102
58	Detail of side A photoresist mask for Fig. 55 device.	103
59	Observed output of straight-through and crosschannels as a function of deflector voltage.	104
60	Observed output of straight-through and crosschannels as a function of deflector voltage.	106
61	Light output of deflection crosspoint in reflective and transparent-deflector states.	108
62	Optical switching ratio and optical tapoff ratio as a function of observation cone angle for two deflection-crosspoint devices.	110

EVALUATION

This work has established the probable feasibility of constructing a high-level, military, nationwide, packet switching, optical communication network of multi-megabit per second capacity. The fiber optic transmission capability has, within the past year, been publicly shown to be possible by installed experimental links of multimode fibers. When that capability is combined with the modest sized, multimode, optical-switching matrices which can very reasonably be extrapolated from this work, such a network's feasibility is quite clear.

The switching ratios achieved in this work are sufficient for digital switching. They are, however, not sufficient for either an analogue network or a mixed red-black network. However, the fact that all optical crossover implementations tried during the course of the work had similar crosstalk leads us to surmise that much of the crosstalk was from input-surface to output-surface double scattering and could be eliminated.

The principle of guiding light within undisturbed electro-optic crystal slabs by reducing the refractive index electro-optically at the boundaries of the guide is a major advance which has been reduced to practice in this work. It will permit the use of dopants outside the light paths in order to reduce the crosstalk by absorbing scattered light, as is pointed out in the conclusions. It is also clear that similarly doped areas could be temporarily included within the shunt path of a compound crosspoint in order to make a very high switching ratio in the shunt path, thereby relieving the stringent cutoff requirement of the present crosspoint designs and introducing the

possibility of using reflection switching with its lower losses while overcoming the poorer crosstalk characteristics of the reflection switch.

Thus, the original design goals of a red-black-network compatible matrix might still be met with relatively little additional work.

Mark W. Levi

MARK W. LEVI
Initiating Project Engineer

Richard C. Benoit, Jr.

RICHARD C. BENOIT, JR
Project Engineer

Section 1

INTRODUCTION

The goals of this contract are stated very well in the original RADC Work Statement which is reprinted here. The Work Statement also defines many of the terms that are used throughout this Final Report.

OBJECTIVE

This twelve month effort is intended to prove the feasibility of an optical crosspoint which will have an acceptably low transmission attenuation combined with a sufficiently high crosstalk attenuation to be compatible with the crosstalk level which can be achieved in an optical fiber transmission medium. Such a demonstration is needed to satisfy possible requirements for handling both "red" and "black" information in a common switching matrix.

DEFINITIONS

An "optical crosspoint" is a device, single or compound, which can be located at the intersection of two optical waveguides and is capable of causing the interchange of the signals in the guides in response to an externally applied signal (which may or may not be optical). This is known as a four port switch in electromagnetic terminology, but that terminology would be confusing in a communications environment where the word "switch" has a specialized connotation.

A "matrix" is an array of crosspoints (not necessarily square) which are interconnected so as to have a multiplicity of inputs and a number of outputs, based upon a given blocking probability.

"Red and black information" are respectively information which is classified or unclassified either in content or destination.

A "passive crossover" is a planar or pseudo-planar crossover of optical channels which has no active elements.

SCOPE

The scope of the effort shall be to demonstrate a single optical crosspoint in a form suitable to integration into a matrix of modest size, and whose crosstalk and attenuation are such as to satisfy the objectives above. The products shall be an experimental model, tests of the model, and a report documenting the work and results of the tests. Since previous work has shown a high theoretical probability that the objectives cannot be met

with a simple crosspoint, the scope of this work shall include a compound crosspoint but shall not extend to a matrix of such compound crosspoints. The control of such a matrix is also outside the scope of this effort other than insuring that excessive control powers or voltages or currents are not needed, and that stray fields from controlling one crosspoint shall not adversely affect others. A simple crosspoint is needed by itself to provide data on what should be expected of a compound crosspoint.

BACKGROUND

A preceding study titled "Optical Switch Study" whose results are documented in AD a007009 of the same title has established many characteristics which must be met by an optical crosspoint if it is to be used in a matrix carrying both red and black information. Thus study was based on the premise of information transmission via optical fibers. Some of the characteristics are needed so that attenuation through the matrix will not be excessive (e.g., 10 dB). Others are needed so that crosstalk will be minimized (e.g., -80 dB). In the past, much has been said about the possibility of putting red and black traffic through common equipment. As a practical matter, however, it was found impossible to do so as a result of the large crosstalk which was caused by common grounding and coupling problems both in the electrical transmission media and in the junctures with switching equipment. The advent of optical transmission media has shown a possible way around those difficulties so that such common hardware can be considered in a more plausible light. It was found that the physical mechanisms which might be used to implement a crosspoint are such that the crosstalk from a single stage would be excessive; consequently a topology was devised in which two simple crosspoints and a passive crossover could be combined to give a complex crosspoint having the requisite properties in a planar integrable fashion.

TASKS

The contractor shall provide all engineering services, materials and facilities for the design, fabrication and test of the structures specified below.

Passive Crossover. A passive crossover shall be designed, fabricated and tested. The design goals shall be:

Scattering from one channel of the crossover to the second channel should be at least 80 dB down from the level in the first channel. Output coupling losses from the second channel are not to be considered as part of the 80 dB. The crossover should satisfy this goal independently of which channel is chosen as the "first channel".

The passive crossover design shall be such as to be readily integrable into the switch designs.

Simple Crosspoint. A simple optical crosspoint shall be designed, constructed and tested. Design goals shall be:

A switching ratio at least 40 dB over a 1/10000 fractional bandwidth. This ratio is not to include input or output coupling losses.

A transmission loss in the unswitched state better than 0.5 dB. This low an attenuation is needed in order to prevent excessive attenuation in a matrix configuration. Input and output coupling losses are not to be included in the transmission loss since neither loss will appear more than once when crosspoints are later made into a matrix, nor will the coupling methods necessarily remain the same in a larger configuration to be pursued later.

A transmission loss in the switched state better than 5.0 dB. This parameter is not so critical as the unswitched loss since a signal traversing a matrix could see only one such loss.

A switching time of less than 100 nanoseconds to attain the off channel attenuation within 3 dB (reference level to be the steady-state off channel attenuation).

Compound Crosspoint. A compound optical crosspoint shall be designed, constructed and tested. The design goals are the same as those for the simple crosspoint except for the switching ratio which should be at least 80 dB and shall be within 5 dB of twice the switching ratio achieved during the simple crosspoint task.

All measurements and designs may be taken at any suitable wavelength provided that suitable allowances and extrapolations are made to a free space wavelength of one micrometer. This wavelength is chosen as a representative wavelength for transmission over optical fiber media.

The tasks may be combined to the extent that the separate structures may be combined on one or two substrates rather than on individual substrates. This is permitted since a prime goal is integrability.

This report presents experimental results obtained at the Sperry Research Center on multimode passive crossovers, simple crosspoints, and compound crosspoints. Construction and performance are described in detail. The multimode tapoff switches developed under this contract are intended for

integration into an optical crossbar, that is, a network control switch for a multimode fiber-optic communication system. These active devices also have other fiber-optic applications such as access coupling and optical multiplexing.

Early in the contract, an all-electro-optic approach was selected as the optimum means of meeting the RADC goals. Then, the fiber-compatible electro-optic technology was applied step-by-step to devices of increasing complexity, starting with channel crossings and going on to sub-components of the compound switch. In the final quarter of the contract, two versions of a high-isolation four-port crosspoint were demonstrated.

This report begins with a background discussion of matrix requirements (Sec. 2) to set the stage for the switching research that follows. Section 3 compares two competing technologies for crosspoint switching and presents the criteria used to select the optimum approach (electro-optic). Complete specifications for fabricating electro-optical devices are given in Sec. 4.

The next four Sections present results on device performance. Section 5 describes crosstalk measurements on passive crossovers. Simple crosspoint performance is detailed in Sec. 6. Experimental results on two versions of the compound crosspoint are given in Secs. 7 and 8. Section 9 describes a novel crosspoint whose switched transmission is comparable to the compound crosspoint, but in a shorter length.

Our research and development work is summarized in Sec. 10. Conclusions drawn from the results and implications for matrixing are discussed in Sec. 11. Recommendations for further work are given in Sec. 12.

Section 2

OPTICAL MATRIX REQUIREMENTS

Because the long-range goal of the contract is matrixing, we wish to review matrix requirements and properties before going into device specifics. This section describes the nature of matrix switches, defines switching terminology, describes the matrix layout, and presents recent refinements in calculations of the matrix signal-to-crosstalk ratio.

2.1 COMPOUND CROSSPOINTS

In a 1975 paper (Appendix A of this report), we pointed out the signal-to-crosstalk enhancement produced by a "tandem" or compound crosspoint. The layout of this optical switch is shown in Fig. 1, where the circles represent simple crosspoints and the solid lines denote optical signal paths (3-dimensional waveguides).

2.2 TAPOFF SWITCHING

All the crosspoints developed under the present contract, compound and simple, are intended for a specific kind of matrix — the terminated crossbar — rather than the permutation matrix. The reason is that the crosspoints are optical tapoff switches rather than "all-or-none" switches. Appendix B of this report shows how tapoff switches are sufficient for a crossbar.

Tapoff devices have a "leaky bar" state in addition to their "perfect cross" state. In the leaky bar state, about 10 to 50% of the input signal is transferred (tapped off) into the crossguide rather than 100% as in an idealized switch. The permutation matrices that other authors have discussed require "perfection" in both the bar and cross states, which is a more stringent requirement than faced here.

2.3 TERMINOLOGY

The latter sections of this report make use of the switching terms "optical tapoff ratio", "switching ratio" and "throughput loss". Let us specify now exactly what we mean by these terms. To do this, we examine the two output ports of a crosspoint (called the "first and second channels")

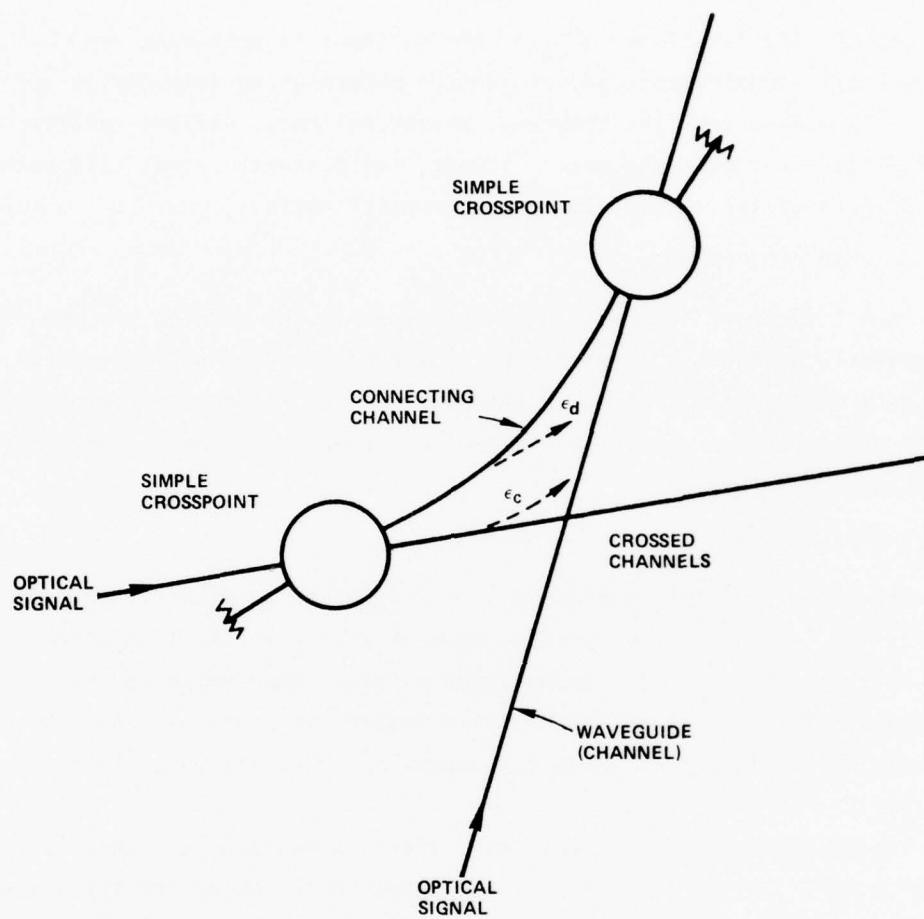


FIG. 1 Model of compound crosspoint including cross-scattering and radiation from connecting guide.

and we observe how the transmitted optical intensity varies with the magnitude of the control voltage. A schematic representation of both crosspoint outputs is shown in Fig. 2, where the switching voltages corresponding to the cross and bar states have been labeled on the abscissa.

The first-channel emission is lower than the optical input level. We define the optical throughput loss (switched or unswitched) as the difference between the input and this channel output in the cross or bar states, respectively, as shown. The tapoff ratio is the cross channel output in the bar state, divided by the first channel output in the cross state. The optical switching ratio, also known as the signal-to-crosstalk ratio, is simply the crosschannel output in the bar state, divided by the crosschannel output in the cross state.

2.4 MATRIX LAYOUT

We examined the properties of the terminated optical crossbar in a recent paper (Appendix B). The length, width, signal-to-crosstalk ratio, and insertion loss were calculated. The crossbar layout was given symbolically in Fig. 2A of that paper. From that figure and from Fig. 1 above, we arrive at a preliminary design for a matrix of compound crosspoints. The layout (top view) is shown schematically in Fig. 3, including the input and output fiber coupling. Termination of the matrix ends is discussed in Sec. 11 below. If we define L_{cc} as the length of the compound crosspoint, and W_{cc} as its width, then the length of the $N \times N$ crossbar is $(2N-1)L_{cc}$ and its width is $(2N-1)W_{cc}$.

2.5 IMPROVED CROSSPOINT MODEL

Our previous compound crosspoint model (Appendix B) did not include the effect of optical scattering at the channel crossing (which exists inside the crosspoint), nor the effect of optical leakage from the curved channel connecting the simple crosspoints. Accordingly, we now refine this model to include these effects as shown in Fig. 1, where ϵ_c is the fractional crosstalk of the waveguide crossover, and ϵ_d is the fractional leakage out of the curved guide. (Recall that ϵ_a is the cross state leakage and ϵ_b the bar state leakage.) The channel-to-channel scattering, ϵ_c and the guided-to-unguided scattering ϵ_d are present in both the cross and bar states of the

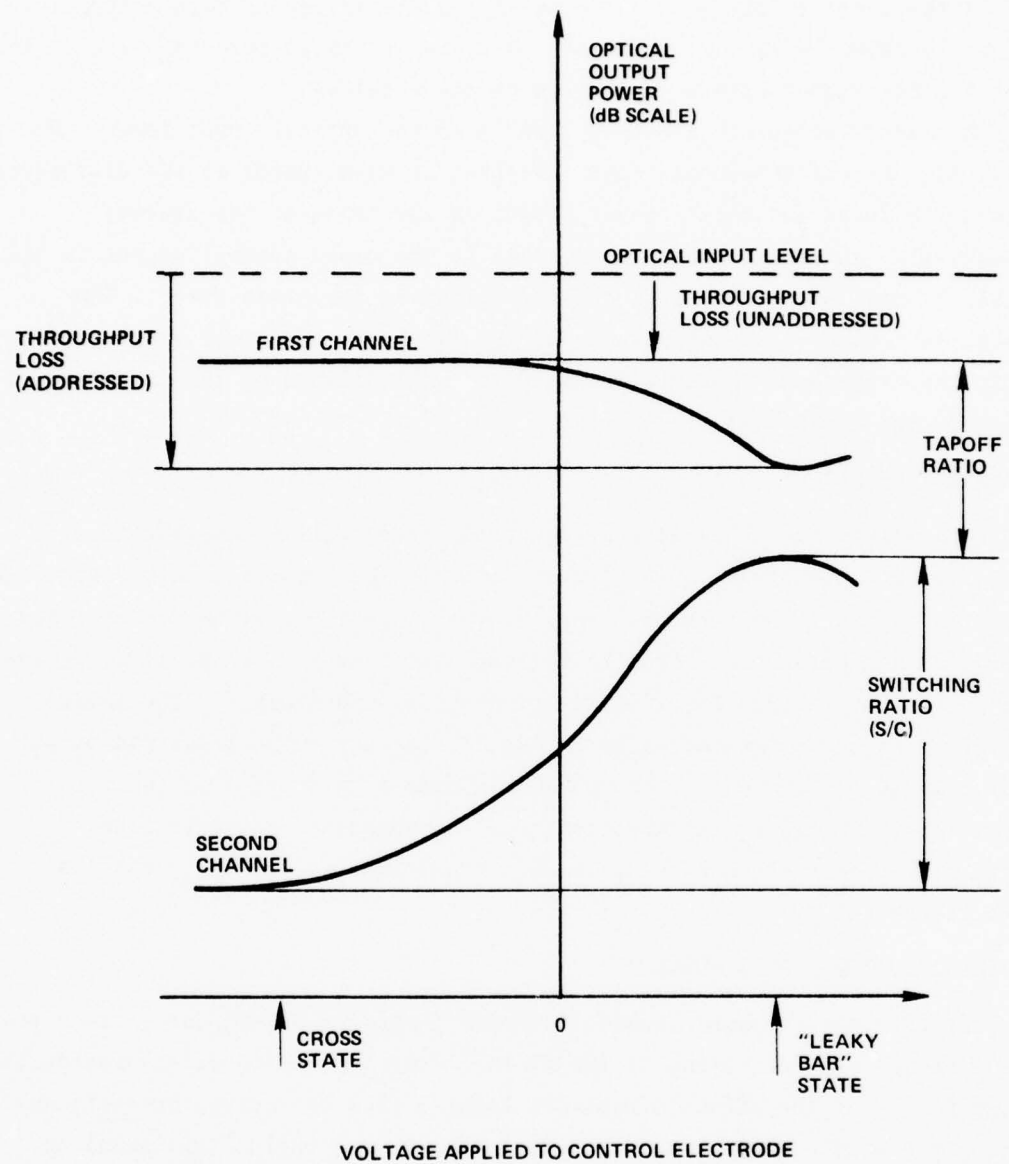


FIG. 2 Representation of four-port device showing definitions of optical switching terms.

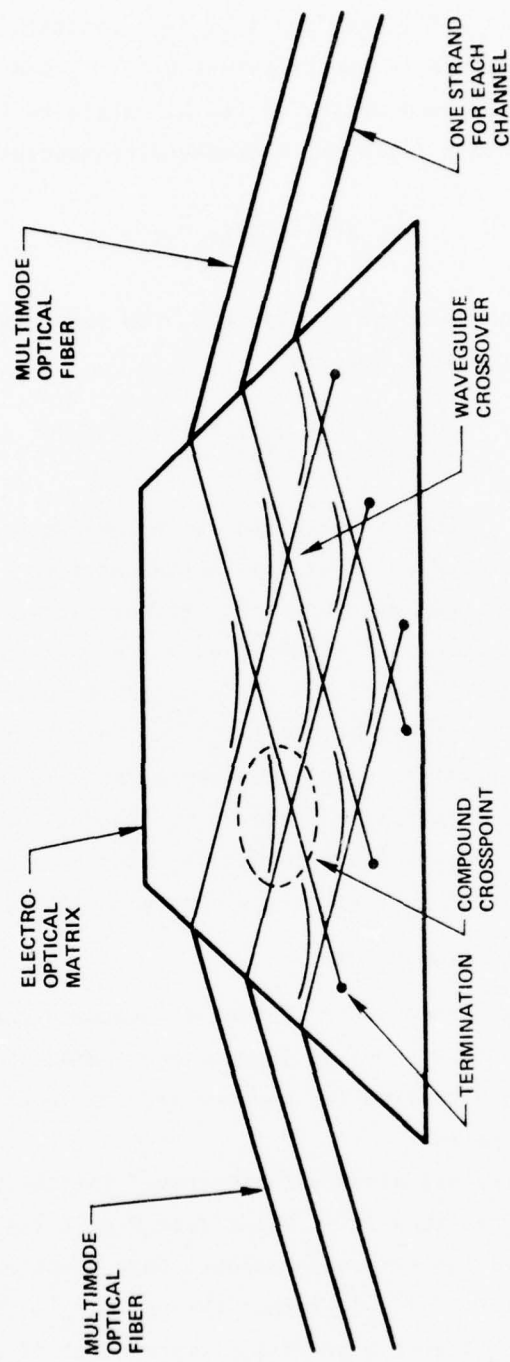


FIG. 3 Matrix of compound crosspoints (3×3) interfaced with fibers.

crosspoint.

In the approximation $\epsilon_a \ll 1$, we find that the crosstalk of the compound device in its cross state is approximately $\epsilon_a^2 + \epsilon_c^2$ and that the signal transmission through the compound device in its bar state is $(1-\epsilon_b)^2(1-\epsilon_d)$. Hence, the signal-to-crosstalk ratio for a compound crosspoint is:

$$S/C|_{cc} = (1-\epsilon_b)^2(1-\epsilon_d)/(\epsilon_a^2 + \epsilon_c^2) .$$

For an $N \times N$ matrix of such compound crosspoints, the lowest value of signal-to-crosstalk at any matrix output port is:

$$\text{worst-case } S/C|_{\text{matrix}} = (1-\epsilon_b)^2(1-\epsilon_d)/(N-1)(\epsilon_a^2 + \epsilon_c^2) .$$

Light goes only once through a bar state in the matrix because N out of N^2 compound crosspoints are addressed at any instant of time (one per row and one per column). Depending upon which path an optical signal traverses, it passes through a different number of unaddressed switches (zero to $N-1$ cross states). Thus, the insertion loss of the $N \times N$ matrix is bracketed between $1 - \{(1-\epsilon_b)^2(1-\epsilon_d)\}$ and $1 - \{(1-\epsilon_b)^2(1-\epsilon_d)(1-\epsilon_z)^{N-1}\}$, not including the in/out coupling losses. These insertion losses are nearly the same since $\epsilon_a \ll 1$.

The foregoing results on matrix S/C and on throughput loss emphasize the need for minimizing crosstalk from the passive crossover (making $\epsilon_c \ll \epsilon_a^2$) and for minimizing propagation loss in the connecting guide (making $\epsilon_d \rightarrow 0$).

2.6 THE "COMPOUND COMPOUND" CROSSPOINT

The question has been raised as to whether a "compound compound" cross-point would offer any crosstalk benefits in practice. What would this four-fold device look like? To visualize it, replace the simple crosspoints in Fig. 1 with compound crosspoints.

If the cross-scattering was already "bothersome" for the compound cross-point (ϵ_c comparable to ϵ_a^2), then it is clear from Fig. 1 that crosstalk will be equally annoying in the compound-compound case because the crosstalk component will now be $\epsilon_c + (\epsilon_a^2 + \epsilon_c^2)^2$ rather than $\epsilon_c + \epsilon_a^2$. Thus, the tandem-tandem switch will not give a practical improvement if ϵ_c is the limiting factor.

2.7 LARGE CROSSOVER ANGLES

There is incentive to make the angle between crossed guides large in Fig. 3 because the optical isolation between channels is greatest when the angle approaches 90^0 . Then the matrix has a square, or nearly square, layout; so the 90^0 case offers a savings in "real estate" because the matrix now has a length of NL_{cc} compared with $(2N-1)L_{cc}$, nearly a 50% reduction, although the matrix is now wider, NL_{cc} compared with $(2N-1)W_{cc}$.

Unfortunately, to realize the length savings, it is necessary to put a 90^0 bend in the connecting guide (Fig. 1). Due to space limitations, this is usually not permissible in practice because the bend radius must be greater than 10 cm to avoid radiation loss. Conceptually, one could use straight connecting guides and miniature specular reflectors to redirect optical signals through large angles. But it is not clear how such mirrors would be "sculptured" into the crystalline substrate, so the 90^0 layout is probably not feasible for compound crosspoints.

Section 3

CHOICE OF APPROACH

Two approaches to optical waveguiding and switching were investigated during the first two months of the contract. The approach judged superior was then pursued in the remaining ten months.

3.1 THERMAL DIFFUSION APPROACH

Some preliminary experiments on ionic doping of LiNbO_3 in late 1975 and early 1976 led us to believe that the thermal diffusion approach was promising for meeting the present contract requirements. We succeeded in diffusing deep multimode optical channels. Three-dimensional guides like this had not been reported previously. In February and March 1976, we applied our diffusion technology to waveguide crossovers and constructed both in-plane and out-of-plane channel crossings as illustrated in Fig. 4.

In both instances, we started with a $3/4'' \times 5/8'' \times 11\text{-mil-thick}$ Z-cut plate of LiNbO_3 that had been optically polished on all six faces. To delineate optical channels, copper strips, 2 mils wide and 920 \AA thick, were evaporated in vacuum on the crystal surface. For the device in Fig. 4A, the strips crossed on the top surface at 5.3° , whereas, in the Fig. 4B device, there was one strip on the top and one on the bottom surface, again at a 5.3° angle with respect to each other, but out-of-plane. The crystals were then placed in a furnace in a flowing oxygen ambient. The furnace was heated to 900° and held at that temperature for 20 min. Conversion of metallic Cu to CuO occurred, and Cu^{++} ions were driven into the lattice more than $50 \mu\text{m}$ beneath the surface. The copper-doped regions had a higher refractive index than their surroundings.

Using a Mach-Zehnder interferometer, the crossover plates were examined along (and perpendicular to) the channel axes. From the interference patterns it was concluded that the higher-index regions were half-cylindrical in shape, approximately 3 mils deep, with a maximum index shift of about 1×10^{-3} .

With the apparatus discussed in Sec. 5.4, we found that the optical signal-to-crosstalk ratio of the in-plane diffused crossover was about 48 dB with the input light polarized normal to the Z axis (TE modes), and the out-of-plane crossover had a signal-to-crosstalk ratio of about 56 dB under

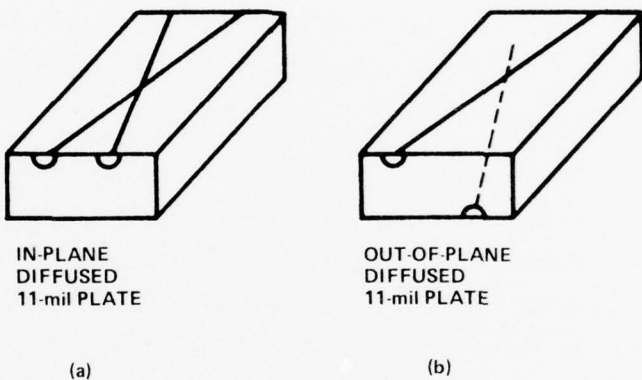


FIG. 4 Two types of multimode waveguide crossovers constructed by thermal diffusion of Cu^{++} into LiNbO_3 : (a) planar intersection; (b) out-of-plane crossing.

similar conditions. The measurement apparatus picked up light from a 3-millimeter-diameter region of the crystal end. Since the crystal was 370% thicker than the collection pupil, the signal-to-crosstalk ratio may have been overestimated.

Prospective switching techniques were devised for thermally diffused channels, including both in-plane and out-of-plane crosspoints. The idea was to arrange two doped channels parallel to one another, about 25 μm apart over a 1.0 cm length, and to alter the interchannel index profile with applied electric fields from parallel-stripe electrodes (usually situated on one crystal-surface). With the field off, the diffused index distribution of the channels would overlap slightly, but there would be a lower-index valley or barrier between them, isolating the channels. For switching, the applied electric field distribution raises and flattens this valley (eliminating it) thereby permitting multimode coupling (energy transfer) between channels.

3.2 ELECTRO-OPTIC APPROACH

Experiments on electro-optic channeling were also performed before the beginning of the contract, and were extended to waveguide crossovers during February and March 1976. This technique required thinner crystal plates than diffusion. The crystals were pure (undoped) and perfectly uniform (including a complete poling) in the absence of applied fields.

Although side-by-side electrodes on one surface are possible for channeling as first demonstrated by Channin (Ref. 1), we preferred instead a top-to-bottom geometry for the electrodes. Here the electric field strength is more uniform within the crystal and the channels are more nearly circular in cross-section, which facilitates efficient coupling to multimode fibers.

We investigated two kinds of electro-optic waveguides shown in Fig. 5. The first kind, or dipolar channel, uses one pair of electrode stripes. It is illustrated at the left. There, the input light is channeled directly between the stripes. As is shown in the crystal's refractive index profile (lower left diagram), the voltage is applied with a polarity that opposes the crystal's spontaneous polarization, which serves to increase the crystal index locally (Δn_z) as shown.

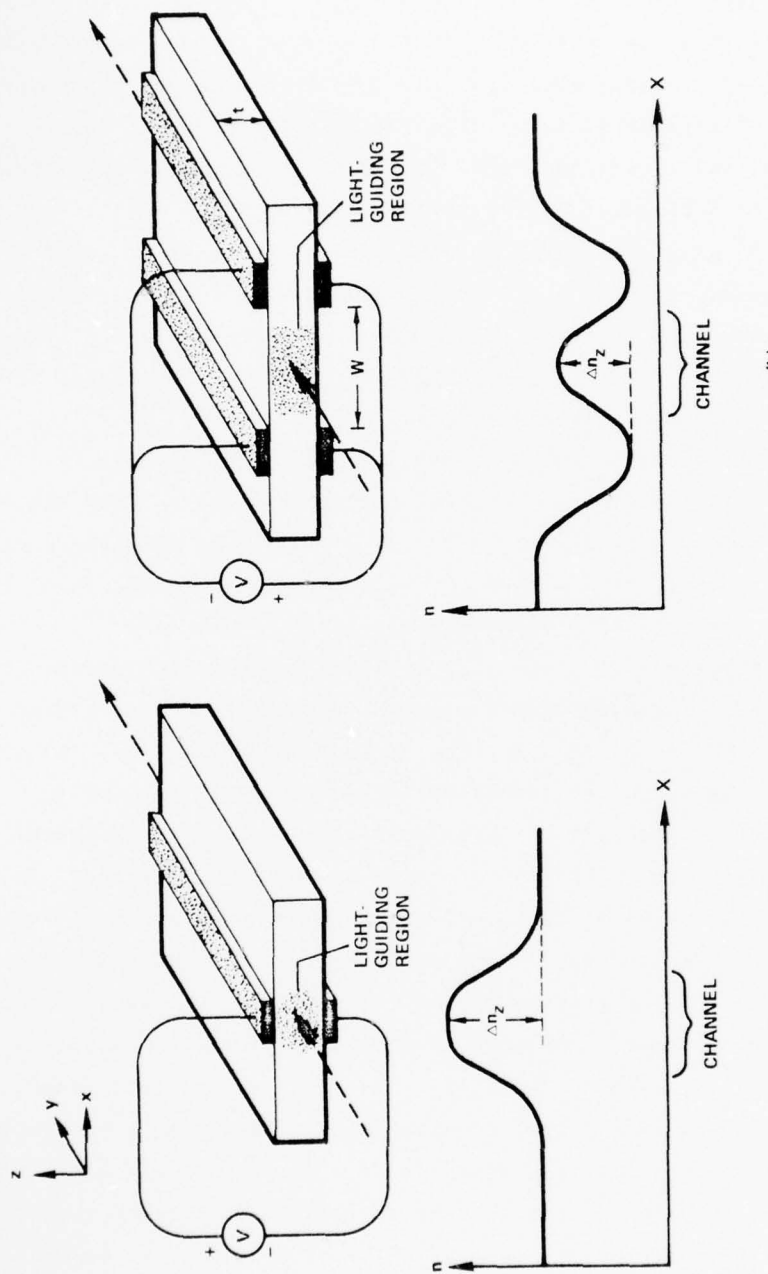


FIG. 5 Dipolar and quadripolar electrooptic channels with associated index profiles: (a) guiding under stripe electrodes; (b) guiding between stripe-pairs.

The second type of electro-optic channel, which we call "quadripolar", is illustrated at the right (Fig. 5B). Two pairs of stripe electrodes are employed. The voltage polarity is the reverse of that in Fig. 5A. Two lower-index "tubes" are formed, corresponding to the troughs in the index profile (lower right diagram). These tubes tend to expel light. Light is guided between the pairs of stripes as shown at the higher-index "hump" labeled Δn_z . Generally speaking, the lower-index tube is a wall or barrier that reflects multimode light over a range of angles at grazing incidence.

Light in Fig. 5B does not travel directly under the metallic areas as in the two-stripe channel of Fig. 5A. This is advantageous for two reasons: 1) the optical attenuation is lower in non-metal-clad regions and 2) the quadripole midregion is, for the most part, free from electric fields which help minimize optical damage effects that may arise.

In practice, it was not necessary to interpose a thin lower-index dielectric cladding layer between the metal and the crystal because the metal cladding loss was comparatively small. Dr. A. R. Nelson of our laboratory had previously found that aluminum and chromium had higher losses than silver and gold, but that the optical attenuation was small in any case.

An opposed-stripe modulator like that in Fig. 5A was first reported by Nelson et al (Ref. 2). Drawing upon that work, we built low-loss end-coupled channels of both kinds as per Fig. 5. The crystal plate thickness was chosen to match the core diameter of available multimode fibers (2 to 3 mils).

The operation of a four-stripe electro-optic channel is shown in the photographs of Fig. 6, near-field views of the waveguide output end. In the upper two photographs, parallel light "flooded" the channel and adjacent areas at the input. Focused input light was used in the lower two photographs, the focal spot being contained completely within the quadripole midregion. The second and fourth photographs show how light becomes trapped as the applied voltage is raised to 450 V dc. The light was well-confined.

Crosspoint switching in the electro-optic case relies upon a controllable lower-index barrier in the crystal, about 25 μm wide, between locally parallel electro-optic channels. Since this barrier is induced by voltage applied to top-and-bottom stripes, its height can easily be altered (or it can be eliminated) by altering the applied voltage magnitude and/or polarity.

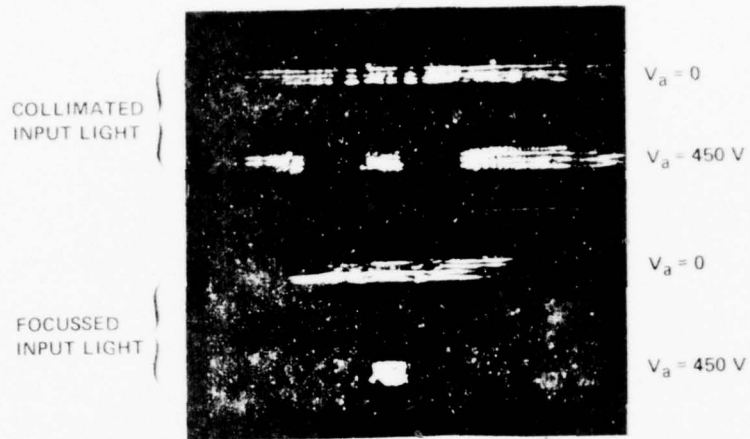


FIG. 6 Experimental examples of electrooptic channeling in 70- μ m-thick LiTaO₃ plate (end views of four-stripe guide).

Then the channels will fuse locally and will share optical power.

3.3 PREFERRED APPROACH

We compared the thermal-diffusion and electro-optic approaches on a number of points, and did further experiments where necessary, to decide which was best. Perhaps the most crucial finding was that the optical attenuation of multimode copper-doped channels was approximately 2 dB/cm at a doping level that gave $\Delta n(\text{max}) = 1 \times 10^{-3}$, a far larger propagation loss than in the electro-optic case.

The results of investigating the relative merits of the two techniques are summarized in Table 1 below.

For all of the reasons cited in the above table, we conclude that the electro-optic method is the preferred approach. We therefore pursued the electro-optic approach for the remainder of the contract, even though greater emphasis had been placed originally on the diffusion method.

3.4 PASSIVE WAVEGUIDING

As a final comment on electro-optic channeling, we wish to describe a passive effect that was found in such devices. In our devices, metal electrodes are evaporated directly on the clean crystal surface without intervening dielectric layers. A. R. Nelson discovered that these metal overlays on undoped LiTaO₃ and LiNbO₃ crystals can produce strong refractive index shifts. This passive effect was explored briefly by Nelson and the author.

Under a polarizing microscope, it was seen that the index perturbation extended 10 to 50 μm into the crystal. The shift was localized under the metal stripe but also extended laterally, reminiscent of diffusion, about one-half depth on either side of the stripe in a semi-cylindrical region. This effect was found in Y-cut and Z-cut plates.

When two metal overlays faced each other on opposite sides of a 3-mil plate, the net effect was to have an index-shifted 3-mil-high "vane" or wall extending through the crystal. Significantly, the crystal's refractive index always decreased under the metal overlay, making the vane reflective to grazing rays. Two such walls make a passive channel waveguide.

The origin of this effect is not understood at present. Speculations about its cause include ionic migration in the crystal, and oxydation-reduction reactions.

The correlation between the magnitude of the effect and the physical preparation of the sample is also not well understood although, in preparing dozens of samples, we found that the final heating of the sample during processing was important. There is fragmentary empirical evidence to indicate that the passive effect is described by a bell-shaped curve extending from room temperature to 200° C, as illustrated in Fig. 7. The temperature in this graph refers to the crystal's last heating for 1 to 3 minutes, performed when the glass sandwich is completed (Sec. 4.5).

Another important aspect of the passive effect is that it fades with time, which is an important consequence for device performance and reproducibility. Initially, the waveguiding may be equivalent to several hundred volts (dc) applied. After two days, the effect will be down several dB and, after two weeks, the effect has usually faded to zero or to a small residual value.

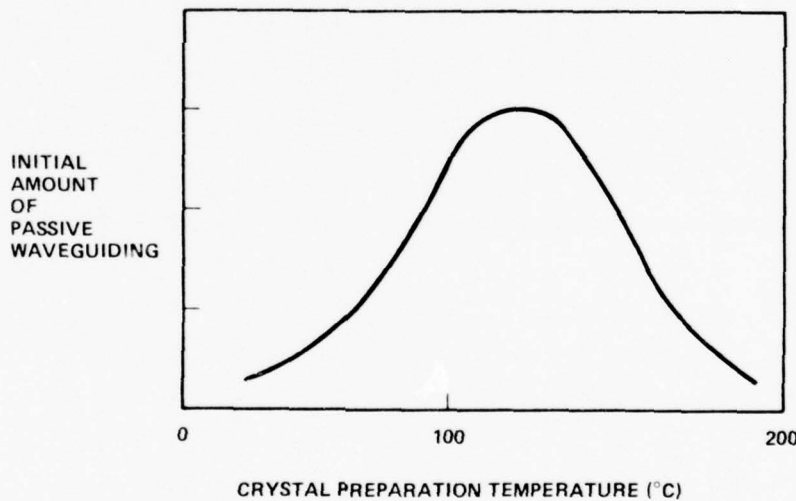


FIG. 7 Estimated behavior of passive channeling effect.

Table 1. Comparison of two approaches

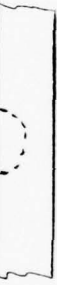
Property	THERMAL DIFFUSION APPROACH (Ionic doping)	ELECTRO-OPTIC APPROACH (Four-stripes)
Optical attenuation in channels	$\sim 2 \text{ dB/cm}$ loss at $\Delta n = 10^{-3}$ and $\lambda = 0.63 \mu\text{m}$	Less than 1 dB/cm propagation loss
Optical damage in channels	Occurs at high light levels	None observed in LiTaO ₃
Channel cross-section		
Input/output optical coupling to device		Edge chipping is a problem.
Available refractive index change	$\Delta n(\text{max}) \approx 10^{-3}$ (non-uniform)	$\Delta n(\text{max}) \approx 10^{-3}$ (fairly uniform)
Isolation of in-plane crossover	About 48 dB	34 to 45 dB (Sec. 5)
Crosspoint switch technology	Difficult: must obtain overlapping index profile of parallel channels; must match E-field distribution to it.	Simple: one electrode pattern provides all index profiling needed. Most aspects of switch have been tested.

Table 1 (Cont.)

Property	THERMAL DIFFUSION APPROACH (Ionic doping)	ELECTRO-OPTIC APPROACH (Four-stripes)
Crystal surfaces used in crosspoint fabrication	One side only (in-plane device)	Both sides
Crystal surface preparation	Critical for reproducible diffusion	Not critical
Crystal breakage problem	Crystal is "naked" in diffusion furnace, and 3-mil plates are fragile	Crystal is always cemented to substrate
Complexity of crosspoint construction	More complex More processing steps	Less complex
Reproducibility of devices	We have had problems reproducing channel size and shape	Good reproducibility
Control required in device processing	More parameters to control and more accurate control needed; copper thickness, surface cleanliness, furnace temp profile, ambient gas, purity, etc.	Less control required

Section 4

DEVICE FABRICATION PROCEDURE

After some initial trials, we developed the following steps to make the electro-optic switches.

4.1 INITIAL CLEAN-UP OF CRYSTAL

The 2.5-mil ultrapure LiTaO₃ plate, optically polished on both large faces, was received from Crystal Technology Inc., Mountain View, California. In shipment, the plate was glued to a 3" x 1" x 1/16" glass microscope slide with paraffin wax. Before attempting to clean or work the crystal, the crystal and glass slide must be heated to 120°C and any air bubbles in the paraffin under the crystal must be squeezed out by gently pressing on the crystal with the wooden end of a cotton swab. Care must be taken at all times during fabrication not to subject the crystal to sudden temperature changes.

After a slow cool-down of the sample, the exposed crystal surface is cleaned. Place the sample in a Petri dish filled with acetone and allow to soak for 30 sec. Slight agitation by hand will aid in washing away excess paraffin. Using an acetone-soaked cotton swab, gently wash away remaining paraffin. This will take several swabs. There should be no visible streaks on the crystal. Some undercutting of crystal may result. If so, reheat sample to 120°C to re-flow wax out to crystal edges; then cool slowly.

Place sample in a beaker of Micro detergent solution (one tablespoon, plus 400 ml DI filtered water). Agitate sample by hand for 30 sec to remove ionic contaminants on crystal. Rinse thoroughly with running filtered water (Barnstead ultrapure) and blow dry with filtered air (4 micron filter).

4.2 PHOTOLITHOGRAPHY OF SIDE "A"

Photoresist. This operation should be done in a clean hood under yellow lighting. Place cleaned sample on Headway spinner. Shipley AZ1350B positive photoresist is filtered through a 4 micron filter. Cover the entire crystal area with resist. Spin the sample at 5000 RPM for 20 sec, which produces a resist layer not more than 2000 Å thick. Edge build-up of resist

on the crystal edges is minimized by covering the entire surface initially. Allow sample to dry in air at room temperature for more than 15 min.

Exposure and development. First clean the mask thoroughly (acetone, trichlor, de-ionized water; ultrasonic bath; blow dry with filtered air). Place the mask and sample onto the alignment fixture. Put mask over sample and make sure that there is intimate contact between them. (If unable to observe interference fringes in central area of sample, it may be necessary to expose off edge buildup of resist on crystal prior to pattern exposure. That is done with opaque shim-stock covering central area).

When intimate contact is obtained, expose photoresist using a collimated 200W Hg arc lamp for 25 sec. Then remove sample and develop for about 10 sec. in Shipley Developer. Rinse sample with distilled water and blow dry with filtered air. Inspect pattern with 70x microscope for sharp edges and complete resist removal where desired.

Metalization and liftoff. Place sample into evaporator equipped with chromium rod source and gold boat source. Pull vacuum in chamber to 1×10^{-6} Torr. Evaporate 50 \AA of chromium and 400 to 500 \AA of gold onto sample. (These thicknesses are less than the photoresist layer thickness, which facilitates liftoff and gives ample metal for conductivity).

Remove sample and place it into a Petri dish filled with acetone. Hand-agitate for 20 to 25 sec, or until the metal has lifted off resist areas. Inspect under microscope. Some metal flecks may still be attached and should be removed by gently wiping area with an acetone-soaked cotton swab.

4.3 TURNING THE CRYSTAL OVER FOR ACCESS TO SIDE "B"

This 180° flip is accomplished as follows. Using a circular glass-cutting saw, make necessary cuts into the side of a glass microscope slide, so that when the side A surface of the crystal is slid over these cut-outs, electrical connection pads will be exposed. The glass slide is cleaned with acetone and placed on a hot plate. The sample is put on the same hot plate and heated to 120°C . When that temperature is reached, the entire A surface of the crystal is covered with glycol pthallate. Glycol pthallate (GP),

also known as Crystalbond #509, is a clear, insulating, thermal-melting cement.

The loosened crystal is slid to the edge of its original slide with a wooden stick. Put GP on the central area of the cutout slide and allow hot plate temperature to rise to 150⁰C. At 150⁰, pick up the crystal slide with tweezers. Turn it over and place it onto the cutout slide so that the crystal is near the edge of the latter. Allow to stand for a minute or two and gently attempt to slide the top glass slide off completely. This will be a slow process. Monitor the hot plate temperature and do not allow it to rise above 190⁰C. When the top glass has been removed, center the crystal on its "new" slide so that no part of the crystal is over the cutouts at this stage of processing. Squeeze out any air bubbles under crystal. Remove from heat and cool slowly. Side B is now exposed. Repeat the initial clean-up process.

4.4 PHOTOLITHOGRAPHY OF SIDE "B"

Photolithography on side B is done in the same way as for side A, except that a microscope (preferably monocular) will be needed to line up (register) the side-B pattern directly over the side-A pattern. Metalization and liftoff are the same as above.

4.5 COMPLETION OF THE SANDWICH

Cutouts are made in a second glass slide (#2) to permit (eventually) electrical contacting to side B. Place sample and cleaned slide #2 on hot plate. Bring temperature of hot plate to 120⁰C, and put GP on cutout regions of glass substrate #1. Slide crystal over cutouts on #1, centering them over side A pads. Put GP onto central area of cutout slide #2. Pick glass up with tweezers, turn it over, and place it onto exposed top surface (B) of crystal to form sandwich. Allow temperature to go up to 185⁰C. Gently press on sandwich to squeeze out excess GP. Allow sandwich to remain at 185⁰ for 2 min. Remove from hot plate and allow to cool slowly to room temperature. A cross-section view of the resulting laminar structure is shown in Fig. 8. A small amount of Torr-Seal epoxy is placed on the sandwich edges so that the sandwich components will not move during subsequent heating.

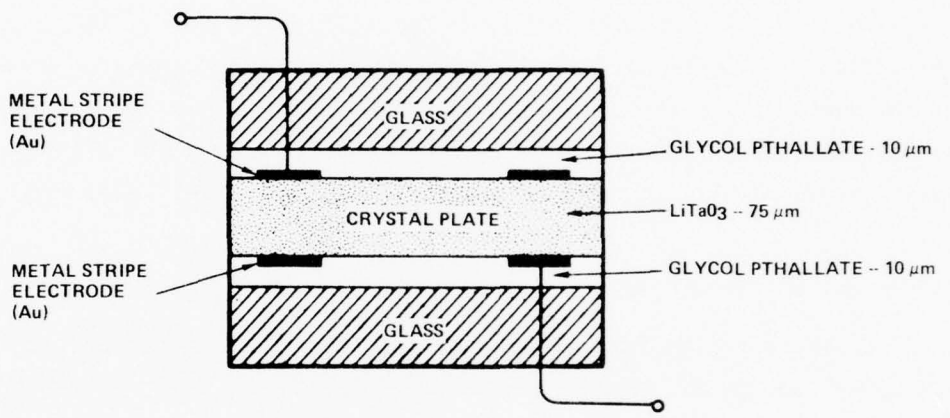


FIG. 8 Cross-section of laminar electrooptic device package.

4.6 CUTTING AND POLISHING

Place sandwich on ceramic block and put both on hot plate. Heat both, and flood sandwich with GP, covering sandwich and attaching it to block. Using a thin diamond-wheel saw, cut the sandwich along both ends of the electrode pattern. Cutting should be done slowly (about 25 min per cut) so as not to crack the crystal. Then remove sandwich from block and clean with acetone.

Sanding and optical polishing is done in four steps: 600-grit paper, 12-micron paper, 4-micron paper, and .03-micron alumina solution on a polishing pad. All operations are done by hand on a 10" diam motor driven wheel. For each step, the sandwich end is polished until it reaches the degree of perfection associated with the particular grit size being used. Both ends of the device are polished flat for direct, end-fire coupling to fibers or to a laser. To get reproducible, flat ends, the sandwich is held against a square brass block that holds it perpendicular to the polishing wheel.

4.7 MOUNTING AND ELECTRICAL CONTACT

Contacts to the sample are made using Acme Conductive Adhesive (E-solder) no. 3025. Using acetone and cotton swabs, clean GP out of electrical pad area. Place a small amount of conductive epoxy on pad using a small wooden stick. Form a trail of conductor away from pad. Strip 1" of insulation from #18 stranded wire and place wire carefully on adhesive trail. Allow adhesive to cure. Then place sandwich onto a glass mounting base that is narrower than the device (but wider), and attach with Torr-Seal. The various wires are attached to the base with epoxy dots for strain relief.

Section 5

PASSIVE CROSSOVERS

This section presents experimental results on in-plane electro-optic waveguide crossovers. The section begins with a discussion of crossover theory and optical noise sources.

5.1 CROSSOVER THEORY

Figure 9 shows a top view of two identical guides that cross in-plane at an oblique angle ϕ . In this diagram, θ_i is the maximum cone angle of input light, θ is the bounce angle of a ray in the guide, θ_c is the critical angle or maximum bounce angle, and θ_o is the maximum output angle collected by the photodetector. All angles are referred to the guide medium and are 2.2 times larger in air. Angles are measured with respect to the axis shown. The four dashed lines in the figure denote continuations of the electro-optic channel walls that may be present at the discretion of the device designer. Their effect is discussed in Sec. 5.3.

We now examine the relationship between the intersection angle and the cross-guide coupling. Theoretically, there are two regimes:

- 1) coupling regime: $\phi \leq 2\theta_c$, power division
- 2) non-coupling regime: $\phi > 2\theta_c$, isolation

Generally, light spreads into the crossguide at the intersection. Rays are incident on the crossguide walls over the angular range from $\phi - \theta_c$ to $\phi + \theta_c$. Ideally, the reflection coefficient at the channel walls is zero for incidence angles exceeding θ_c . Thus, when ϕ is raised to $2\theta_c$, the crosschannel incidence angles range from θ_c to $3\theta_c$, so those rays radiate out and are "lost". Hence, in theory, cross-coupled power goes to zero at $\phi = 2\theta_c$.

Figure 10 illustrates schematically the dependence of cross-coupled power upon intersection angle. At $\phi = 0$, half the power is transferred. Generally, the coupling is the convolution of the modal distribution ($0 < \theta < \theta_c$) with itself, that is, a triangular shape (Fig. 10) for a square distribution. In practice, the wall reflectance does not vanish at θ_c -incidence because the index shift is not discontinuous at the boundary; so there is small cross-coupling at $\phi = 2\theta_c$, but this power diminishes rapidly (becoming orders of

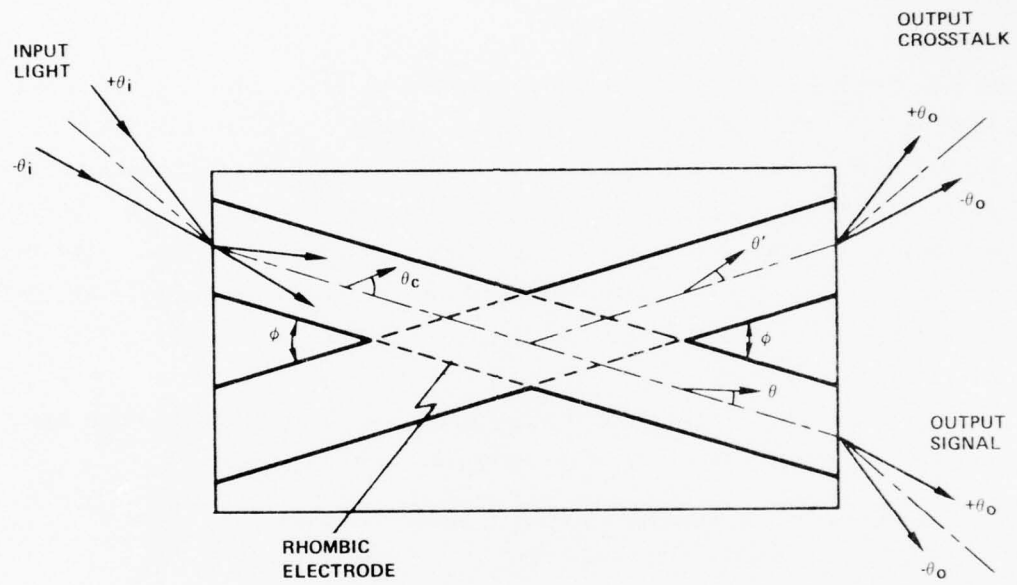


FIG. 9 Plan view of planar intersecting channels showing angle definitions.

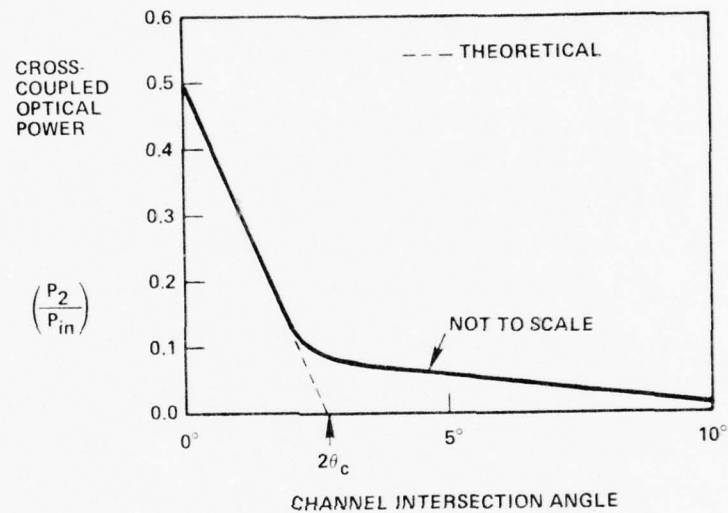


FIG. 10 Typical dependence of interchannel coupling versus intersection angle.

magnitude below the input) as φ is increased beyond 2°_c (Fig. 10). The residual cross-coupled light comes from single and multiple scattering processes. All of our experiments are performed in the isolation regime.

5.2 CROSSTALK SOURCES

Optical crosstalk is the aggregate of several kinds of optical scattering — arising in the bulk of the crystal or at its surfaces. Volume scattering at the channel intersection sends crossguided light to the output. Such first-order scattering comes from crystal imperfections such as microscopic defects, striae, incomplete poling, etc. This light is localized at the terminus of the crosschannel.

The second type of scattering, usually involving surfaces, is a double scattering process. Here the light is often not guided. For example, scattering occurs immediately at the input end. Then those unguided rays travel directly to the output end where they are re-scattered. This type of radiation has a fairly isotropic distribution at the device output.

In Appendix C, we present a simple crosstalk model in which the crosstalk intensity is the sum of single and double scattering terms.

5.3 CROSSOVER CONSTRUCTION

We built planar electro-optic channel crossings in the 4.9 to 6.3° intersection angle range in 3-mil LiNbO_3 and LiTaO_3 . Construction details are given in Sec. 4. We tested three designs: the dipolar channel approach shown in Fig. 11A and the quadripolar approaches shown in Figs. 11B and 11C. The device of Fig. 11C has an open intersection, while the Fig. 11B device has a parallelogram electrode at the crossing (on the top and bottom plate surfaces) as per the dashed lines in Fig. 9. This rhombic electrode was first proposed by D. H. McMahon of our laboratory. The idea of the electrodes is to impede crosschannel flow but not to disturb straight-through flow. This reduces crosstalk if the main noise source is intersection scattering.

Devices B and C had 1-mil-wide stripe electrodes, spaced 6 mils apart. Device A had 3-mil-wide stripe electrodes. Devices were 1.8 cm long.

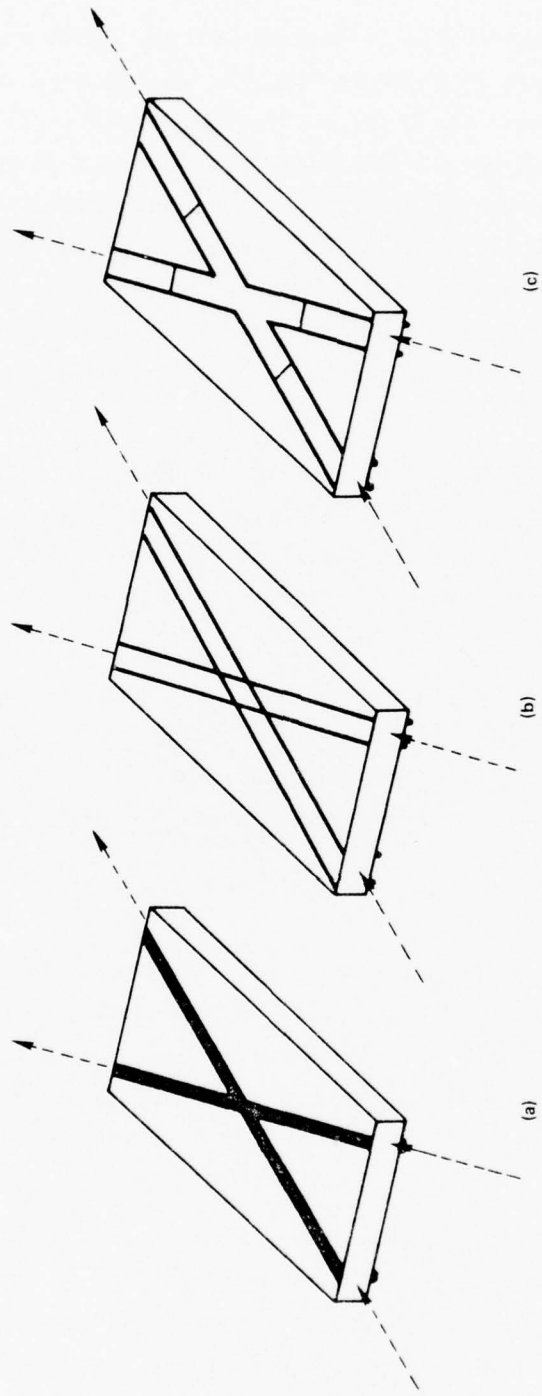


FIG. 11 Three electrode geometries that were used to make in-plane waveguide crossovers: (a) dipolar; (b) quadripolar with rhombic electrode at intersection; (c) quadripolar with open intersection.

5.4 MEASUREMENTS

The experimental arrangement for measuring optical signal and crosstalk strength from the crossovers is shown in Fig. 12. Two focused input beams at an angle of 2.2° are aligned along the axes of the electro-optic channels, and the on-axis outputs are located precisely with the near-field imaging lens and photomultiplier detector (EMI 9558A). With one input beam blocked, the output signal strength at the desired channel is recorded (with an 18 dB attenuator inserted in the output path). The second input beam is admitted (the first beam being blocked) in order to determine crosstalk from the same channel exit. (The 18 dB attenuator is removed during crosstalk determination.)

The output of the photodetector is sent to a logarithmic amplifier. A digital milliammeter connected to the log-amp displayed the output light level directly in dB. The ratio of the two powers measured above tells how well the intersecting channels are isolated from one another.

An adjustable iris on lens L_2 (4 \times objective) determines the output collection cone designated $\pm\theta_o$ in Fig. 9. A rectangular aperture is placed on the detector face, so that it "sees" the channel cross-section and nothing more. The numerical aperture of the input light, proportional to θ_i in Fig. 9 ($NA = \sin[2.2\theta_i]$), is governed by the choice of input lens L_1 (4 \times , 10 \times , or 20 \times objective).

5.5 RESULTS

The observed signal-to-crosstalk ratios for three devices as a function of θ_o are presented in Figs. 13 through 15. The input cone angle, ranging from ± 0.43 to $\pm 1.80^\circ$, was taken as a parameter in the graphs. The observation cone ranged from ± 0.4 to $\pm 1.6^\circ$. The signal-to-crosstalk ratio increased with decreasing θ_i , and the ratio decreased with increasing θ_o , approximately as θ_o^{-2} .

The signal-to-crosstalk ratio ranged from 31 to 41 dB in the first device, and from 34 to 45 dB in the latter two devices, depending on the "angle choice". The lower range in the "simple X" device is attributed to the smaller intersection angle and to passive waveguiding that subtracted from

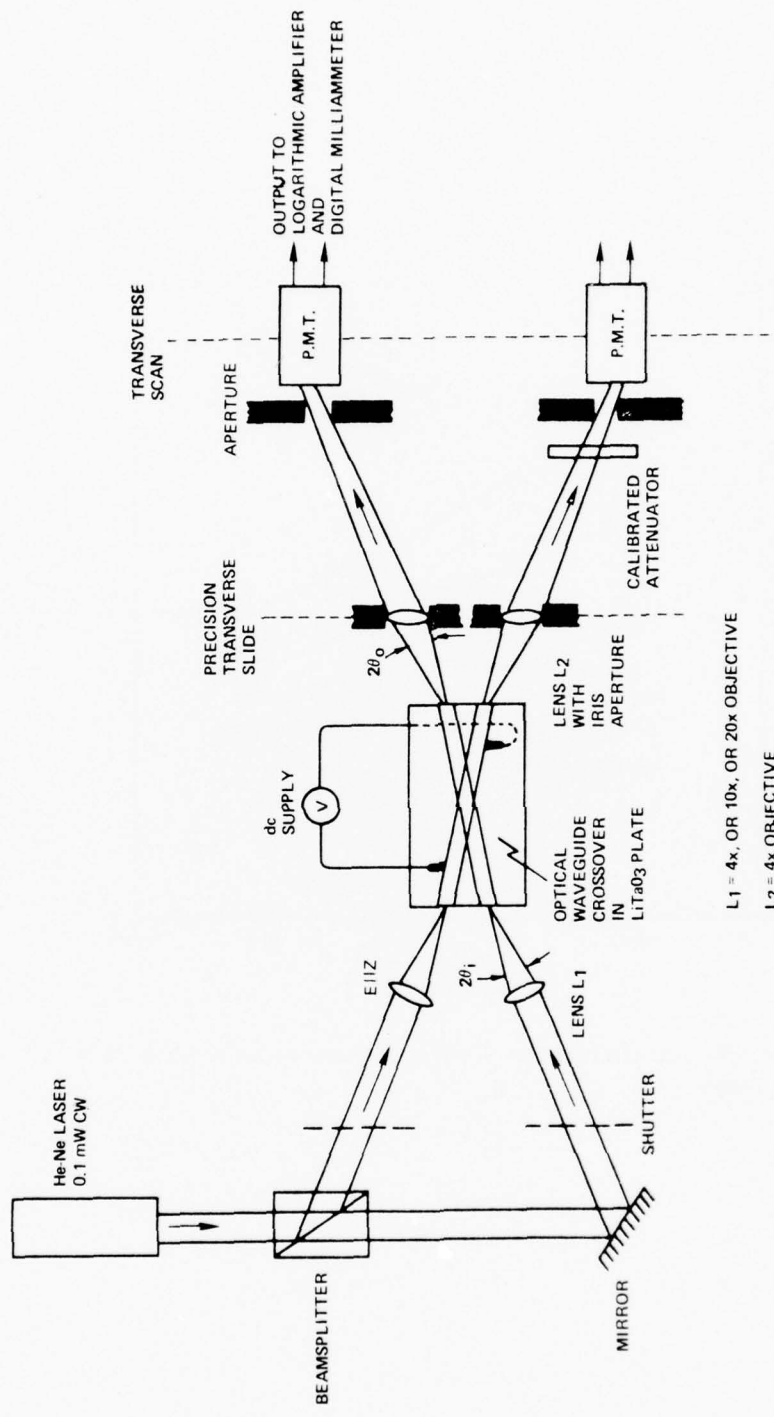


FIG. 12 Experimental set-up for measuring optical isolation of intersecting channels.

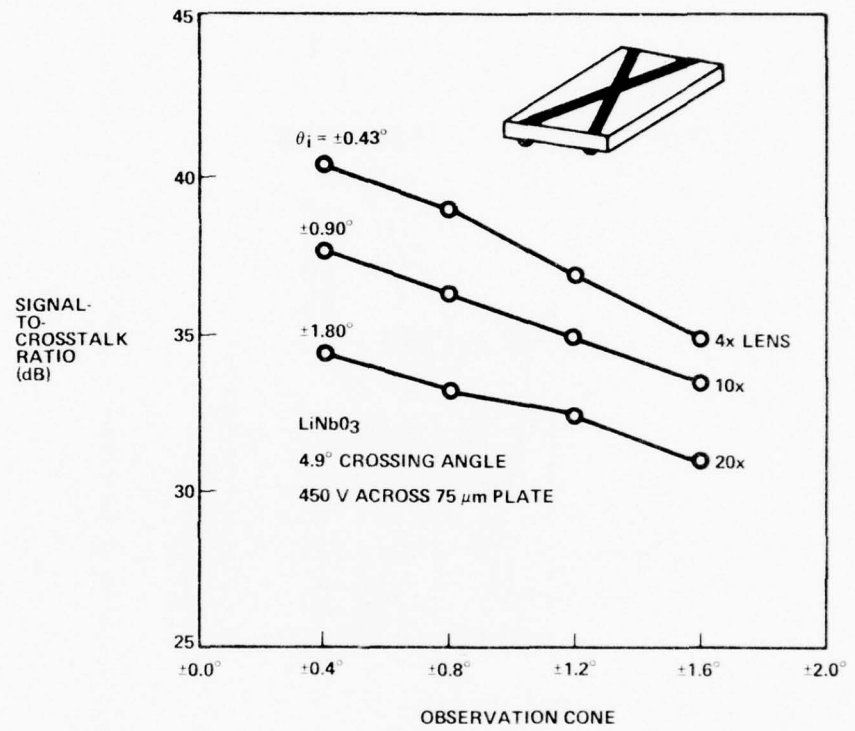


FIG. 13 Measured S/C ratio as a function of collection cone angle for a Fig. 11(a) LiNbO₃ device.

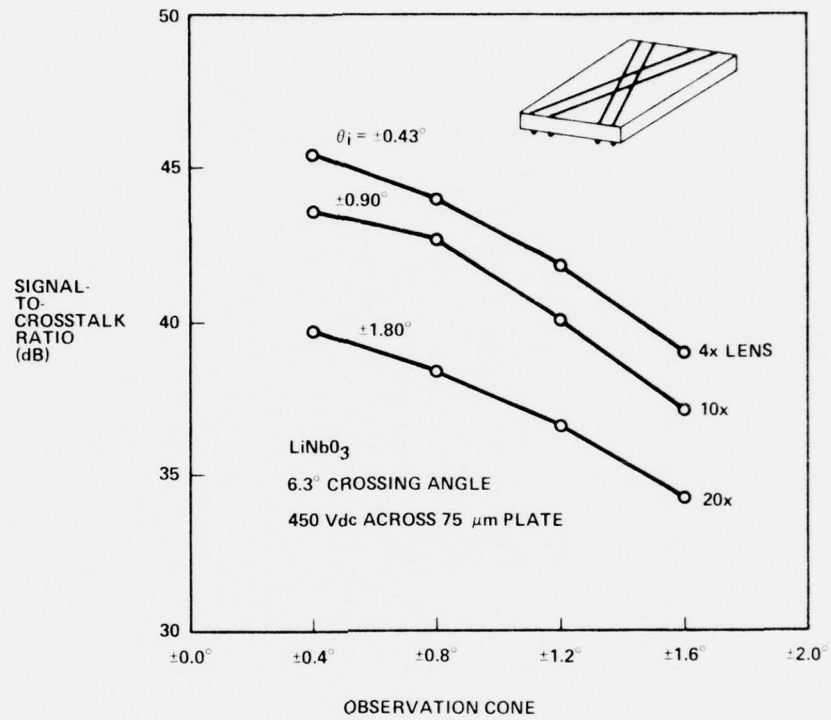


FIG. 14 Measured S/C ratio as a function of collection cone angle for a Fig. 11(b) LiNbO₃ device.

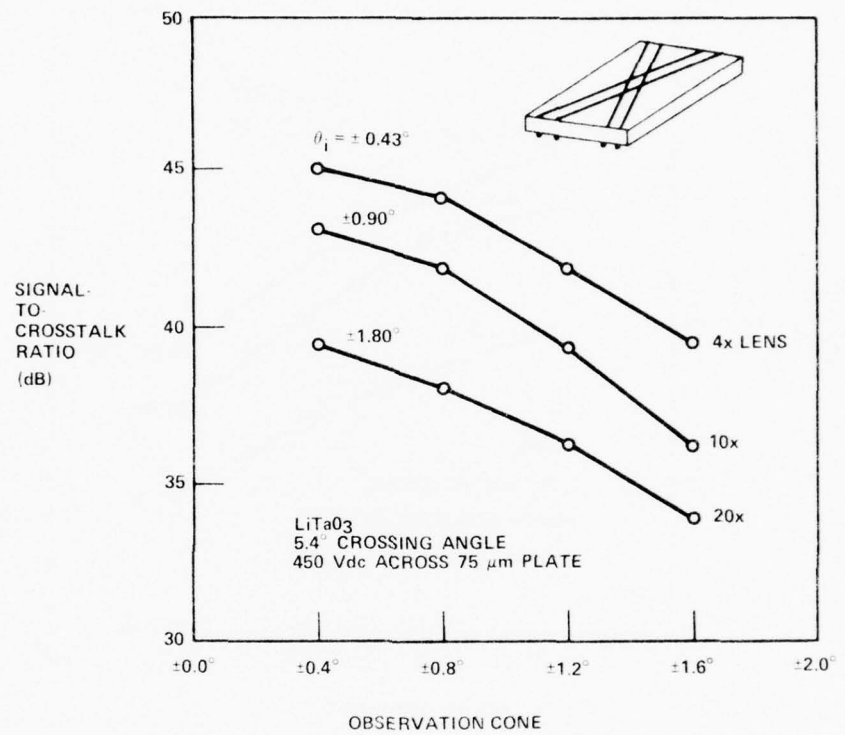


FIG. 15 Measured S/C ratio as a function of collection cone angle for a Fig. 11(b) LiTaO₃ device.

the voltage-induced effect.

A test was performed to find out whether the rhombic electrode gave improved isolation over the open intersection design. Two channel crossovers, one like that in Fig. 11B and one like that in Fig. 11C, were constructed side-by-side in the same 68 μm LiTaO₃ plate. They had the same crossover angle (6°), channel width (170 μm), electrode width (50 μm), length (1.8 cm), and applied voltage (400 V dc). The experimental results are presented in Fig. 16. The observed S/C ratios were the same to within 1 dB, so the expected increase was not found.

We examined the crosstalk distribution on the output end of the device as shown in Fig. 17. With lens L₂ fixed exactly on the crosschannel axis, the detector was moved from side to side on the focal plane to record the light's spatial distribution. Figure 17 presents curves for the voltage-on and voltage-off conditions. Results are given for two different collection cones.

The crosschannel width is 0.6 cm on the image plane. Some localization of optical scattering on the channel exit is seen in Fig. 17. The right-hand peak in the Fig. 17 is high-angle scattering emanating from the other channel.

5.6 DISCUSSION

One expects the channel isolation to get better as the input light becomes more collimated ($\theta_i \rightarrow 0$). This was verified in Figs. 13 — 16.

A simple physical model like the one in Appendix C will aid us in further interpreting the results of Figs. 13 — 16. Single-scattering should dominate in the limit of small θ_o (less than θ_i) and here the S/C ratio should be approximately independent of θ_o . On the other hand, for larger θ_o (greater than θ_c), double-scattering will be prominent and the S/C ratio should fall off as θ_o^{-2} , which is the behavior seen in Figs. 13 — 16. Hence, from an examination of the figures, we conclude that double-scattering was stronger than the "intrinsic" scattering of the device. This explains why the rhombic electrode did not give enhancement: its beneficial effects were masked.

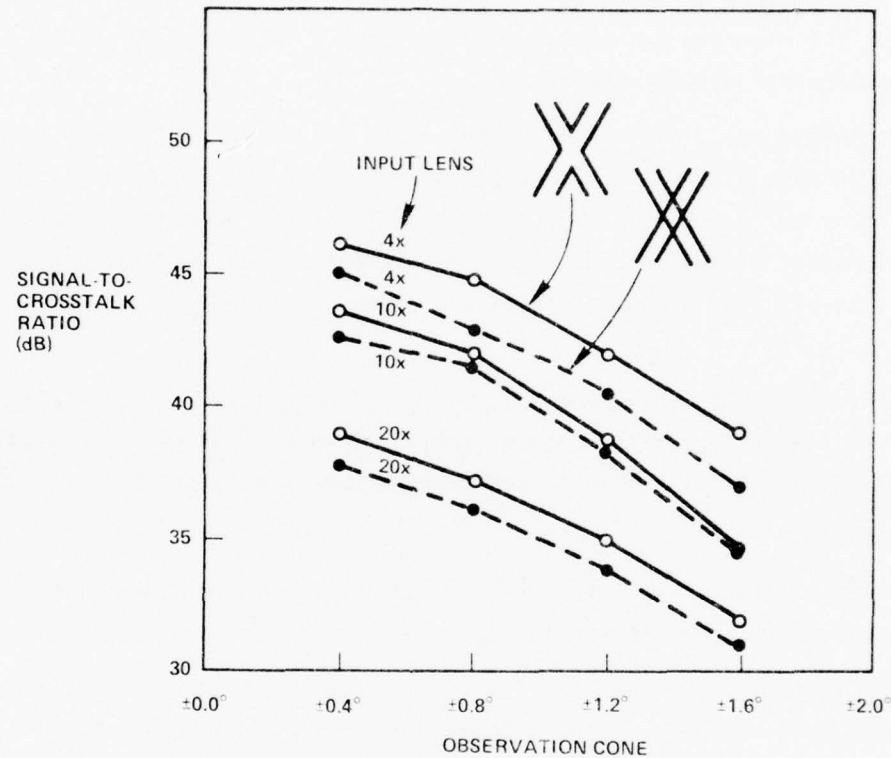


FIG. 16 Measured S/C versus collection cone angle for Fig. 11(b) and 11(c) crossovers, both in the same LiTaO_3 crystal.

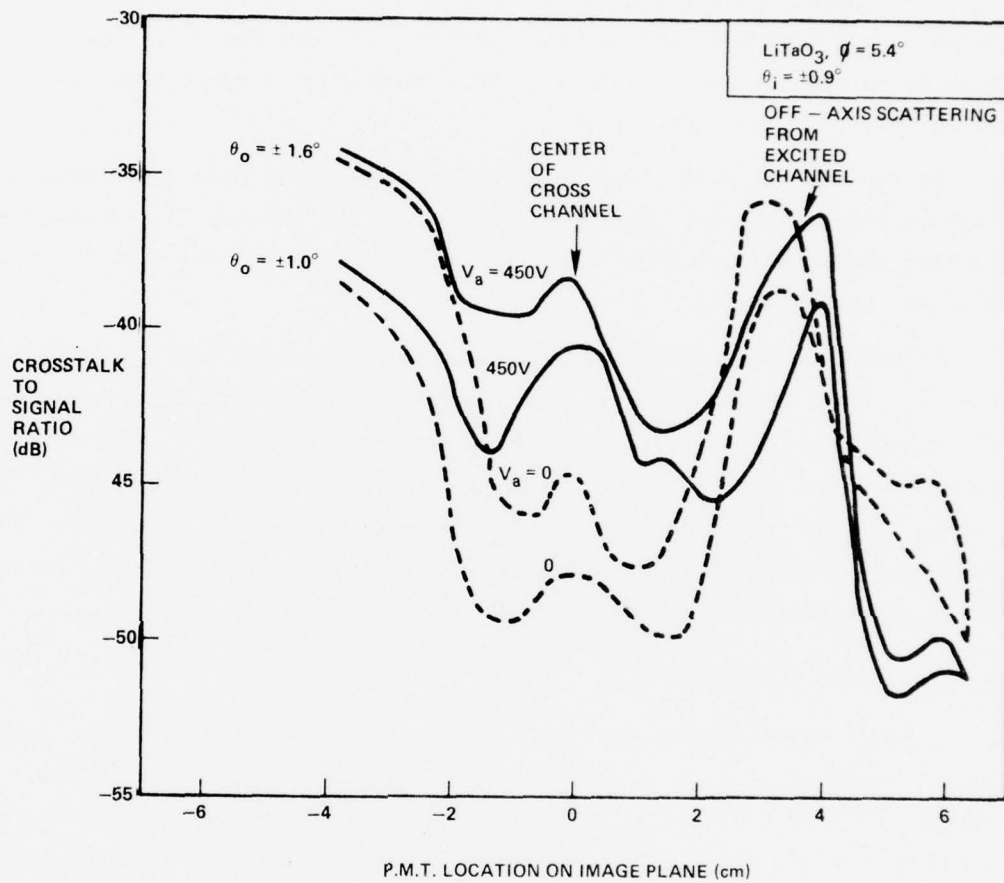


FIG. 17 Spatial distribution of crossover crosstalk light on focal plane for two values of applied voltage and for two observation cones.

Section 6

SIMPLE CROSSPOINTS

The compound crosspoint can be constructed from a simple power-divider crosspoint and a simple power-combiner crosspoint (See Fig. 1). The simplest method is to use three-port switches, so a three-port structure has been adopted for our simple crosspoints.

We reported in June, 1976 (Ref. 3) on a multimode three-port optical switch in which light was guided directly under the channel electrodes. The switching action stemmed from fringing-field coupling or merger of the main and branch channels.

An analogous switching structure can be constructed with quadripolar channels. Here, switching is obtained by interrupting part of the channel wall where the main and branch channels come together in a "Y". These contiguous channels share a single stripe electrode that we call a "gate". By altering the gate potential, the interchannel light-flow is regulated. This multimode electro-optic switch geometry is shown in Fig. 18. It is the one we have employed for the simple crosspoint.

6.1 DESIGN AND CONSTRUCTION

A modal distribution that ranges over $\pm \theta_c$ propagates down the input channel. About 3 dB, at most, of this power will spread into the branch. In choosing the branch angle, θ_b , we note that small values of θ_b allow a large pickoff but create problems in isolating the two channels in that the gate region is not totally opaque when "closed". On the other hand, the tapoff decreases with increasing θ_b , going to zero at $\theta_b = 2\theta_c$. The choice, $\theta_b \approx 0.5 \theta_c$, is a good compromise, and should allow one to approach 3 dB coupling.

An experimental device like that in Fig. 18, designated Sample #1, was constructed by means of the procedures spelled out in Sec. 4. Figures 19 and 20 show the pair of photoresist masks employed for this simple crosspoint device. All dimensions of the metallic electrodes are given in the drawings. The two electrode patterns were registered atop one another on opposite faces

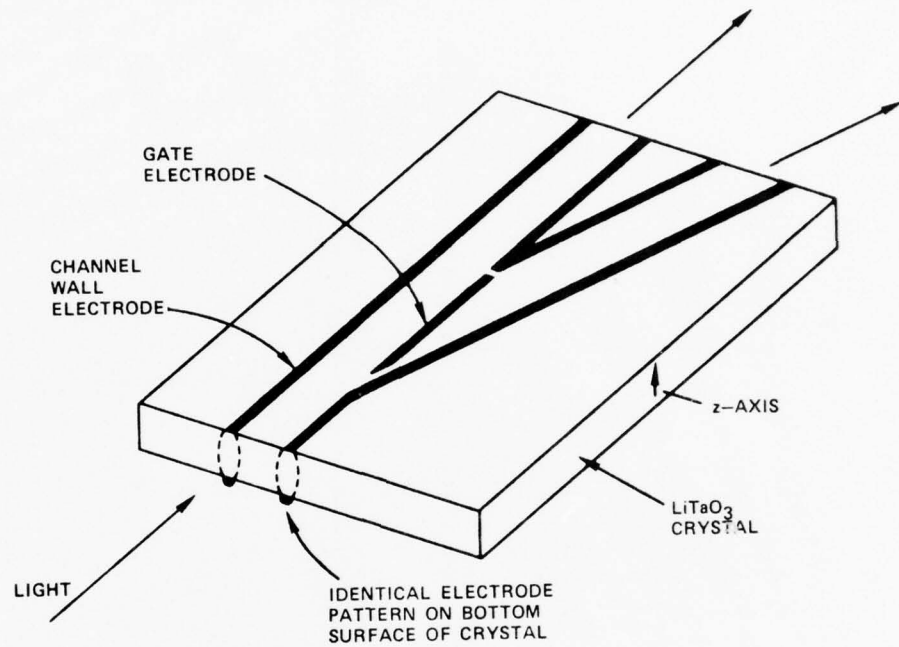
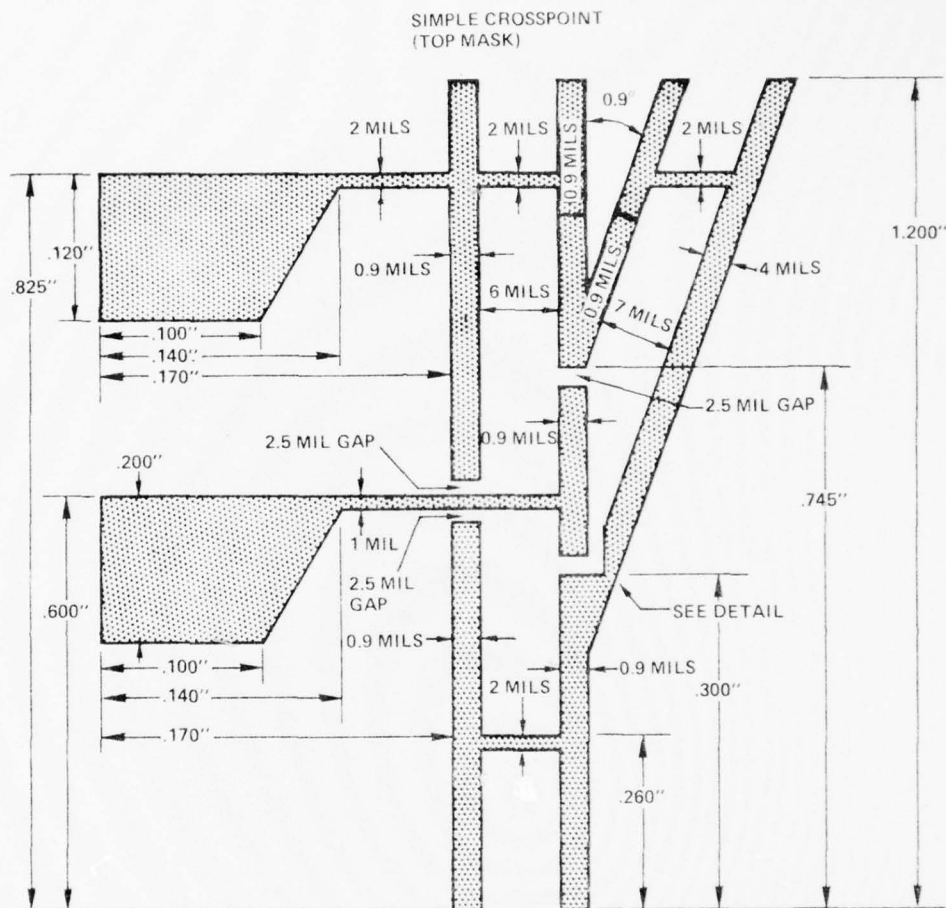


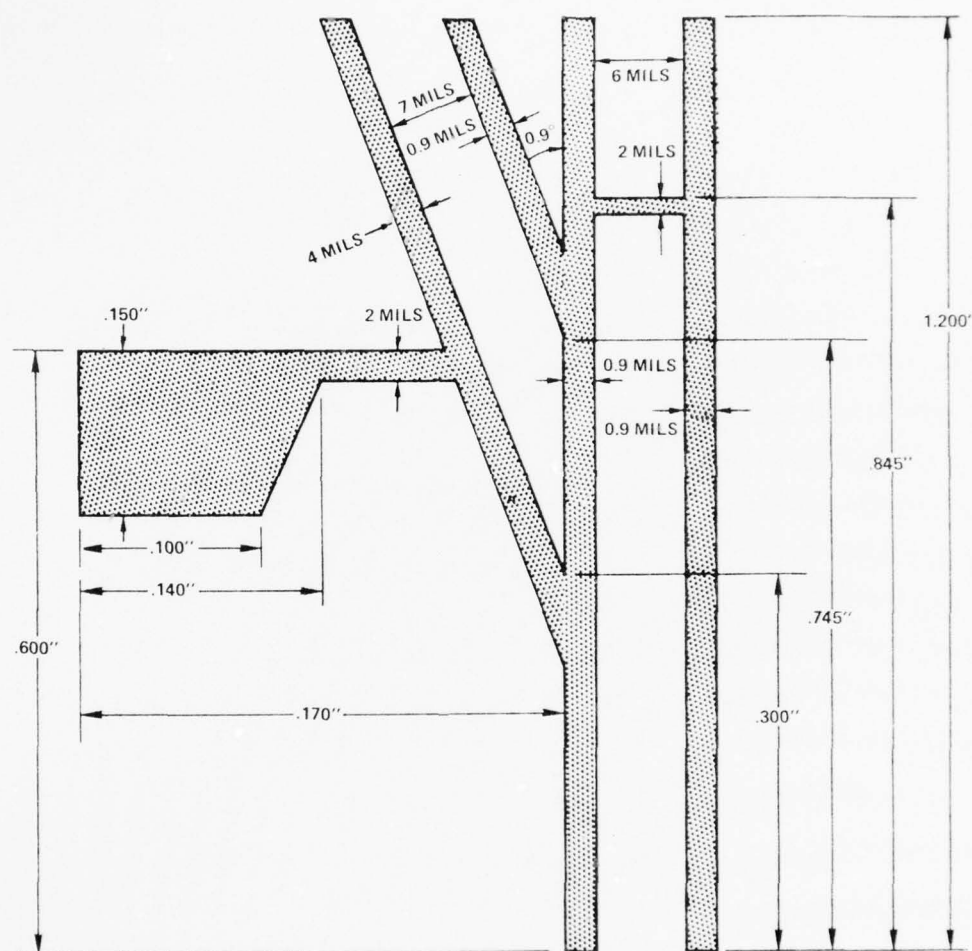
FIG. 18 Layout of three-port simple crosspoint device.



NOT TO SCALE

FIG. 19 Photoresist mask for actual Fig. 18 device (side A).

SIMPLE CROSSPOINT (BOTTOM MASK)



NOT TO SCALE

FIG. 20 Photoresist mask for actual Fig. 18 device (side B).

of the device.

6.2 MEASUREMENTS

The experimental arrangement for measuring switch performance, illustrated in Fig. 21, was virtually the same as for the passive crossovers (Fig. 12). The experimental test conditions and device parameters were as follows.

Simple Crosspoint

STRUCTURE, DEVICE #1 (Fig. 22)

- LiTaO₃, Z-cut plate
- 75 μm plate thickness
- 150 μm channel width (electrode gap)
- 23 μm gate electrode width
- 1.1 cm gate electrode length
- 0.9° branch angle
- 175 μm branch channel width (electrode gap)
- 1.7 cm overall length of device
- passive channeling equivalent to -50 Vdc applied

TEST CONDITIONS (Fig. 22)

- Focussed laser beam input
($\Delta = 0.63 \mu\text{m}$, 1.1 mm beam diam)
- TM polarized, $E \parallel Z$
- 10x input lens
- $\pm 0.9^\circ$ input cone in crystal, on the channel axis
- $\pm 2.0^\circ$ input cone in air (0.04 NA)
- $\pm 5.5^\circ$ output collection cone in air
- 2 mm x 8 mm detector aperture on 38x image plane
- ~ 360 Vdc channel wall bias

6.3 RESULTS

The optical output power from both ports of this switch was measured

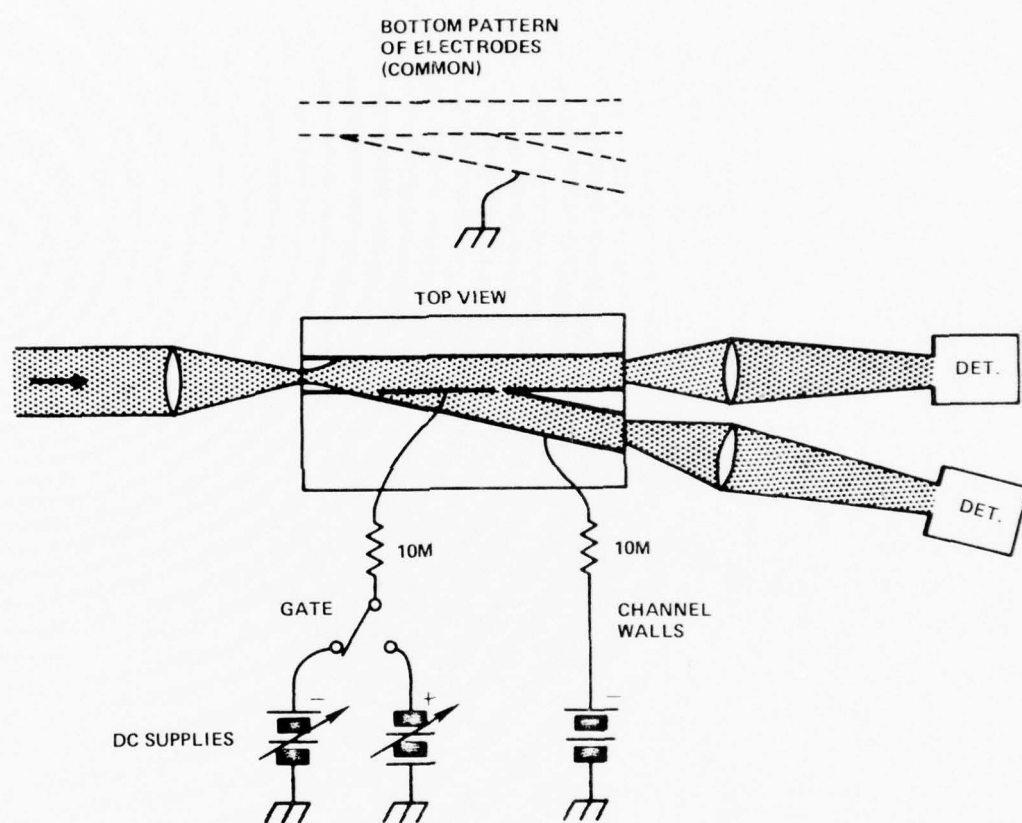


FIG. 21 Experimental set-up for electro-optical testing of simple crosspoint.

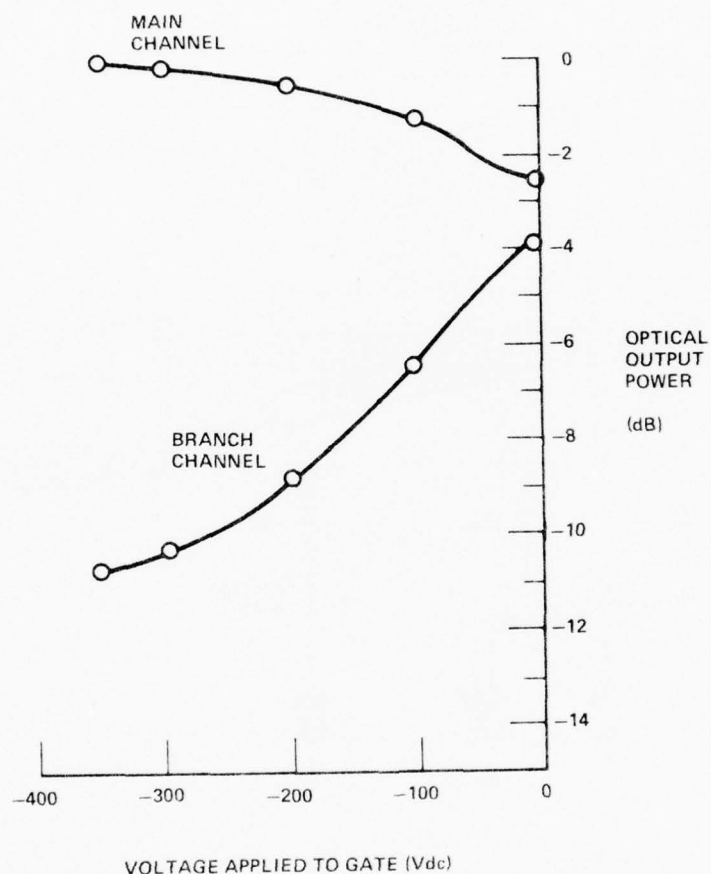


FIG. 22 Measured output of straight-through and branch channels as a function of gate potential for a simple crosspoint device.

as a function of gate voltage with the result presented in Fig. 22. The optical tapoff ratio to the branch at $V_g = 0$ was -3.9 dB relative to the main channel at $V_g = -350$ V dc, but the optical isolation of the branch (with gate closed) was only 10.6 dB below the input level. A way of increasing the isolation was sought.

6.4 SPOILER STRUCTURE

Dr. A. R. Nelson of our laboratory proposed that a pair of electrodes be added to the branch channel to divert unwanted light out of it. These electrodes, termed "spoilers", are simple stripes (or tapered stripes) that go down the midline of the branch. They decrease optical crosstalk in the following way. Negative applied voltage lowers the crystal index under the spoiler, and stray light is reflected out of the channel on either side of this "vane". The spoiler vanishes (becomes transparent) like the gate at zero potential. Usually, gate and spoiler receive the same voltage. Drawing upon these ideas, we designed a new switch.

Figure 23 presents a perspective drawing of the simple crosspoint with the spoiler electrodes. The specific electrode geometry and dimensions that we selected for those devices are shown in the photoresist masks of Figs. 24 — 27 that were used for construction.

6.5 SPOILER CROSSPOINT RESULTS

Two crosspoints with spoilers were built, one of which cracked after a few data points were taken. The amount of passive waveguiding in both devices was large. Strong channeling was found with little or no voltage applied to the channel walls. Useful switching was attained in the zero-bias condition.

Figure 28 shows the output signals of main and branch channels as a function of gate-and-spoiler potential (the gate and spoiler were connected together internally). The results are summarized below, together with a tabulation of device parameters and test conditions.

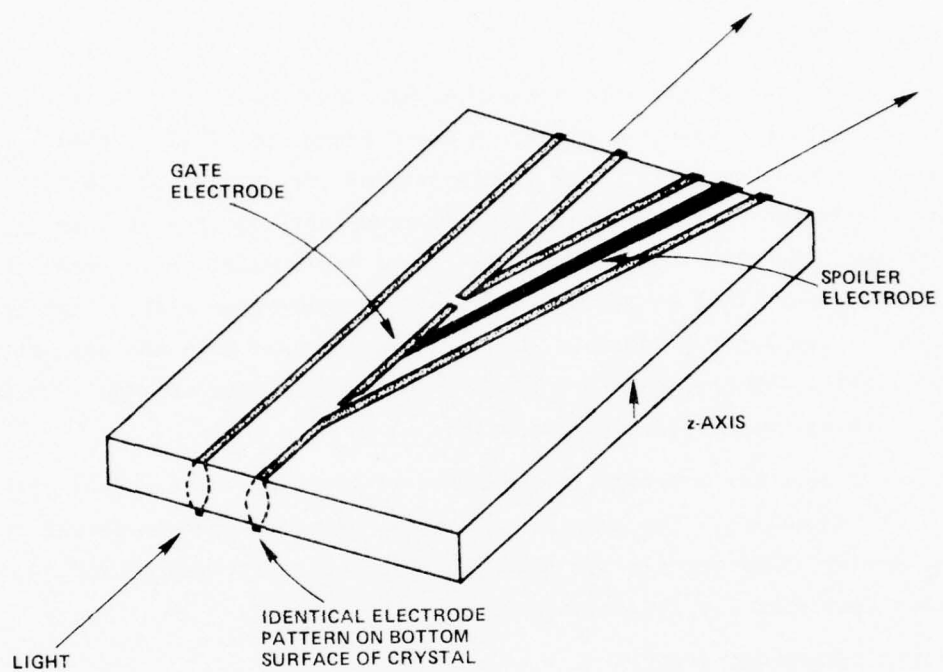
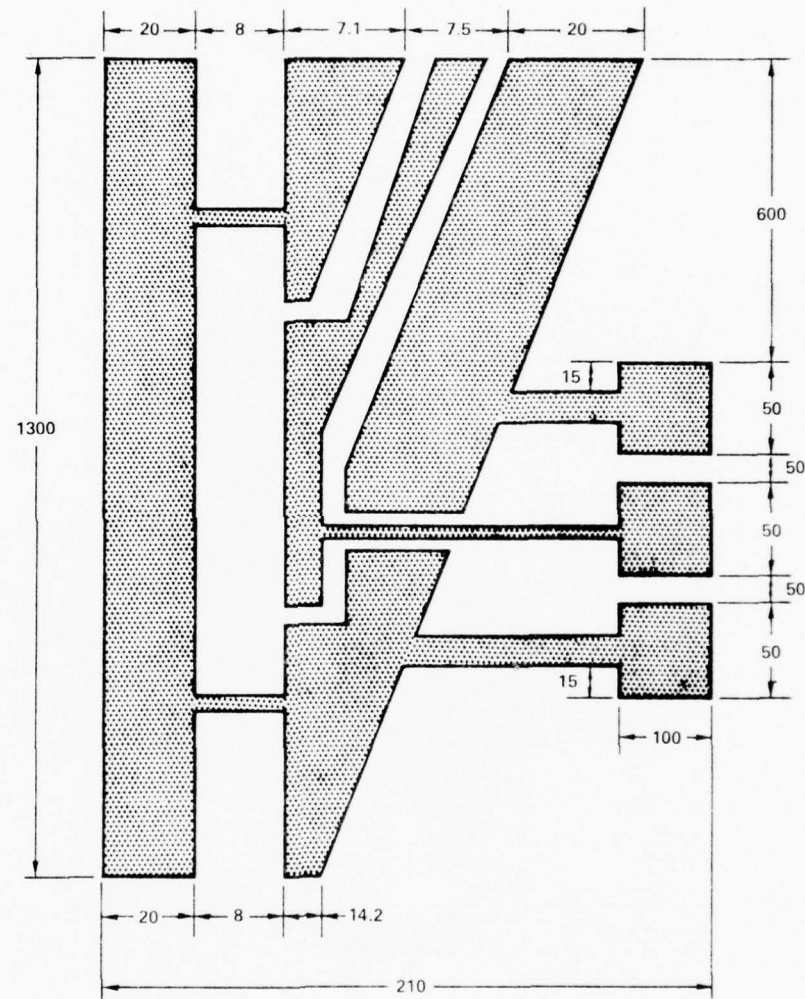


FIG. 23 Layout of three-port simple crosspoint device with spoiler.

SIMPLE CROSSPOINT WITH SPOILER (TOP MASK)



NOT TO SCALE

SHADED AREAS ARE TRANSPARENT ON FINAL MASK
(DIMENSIONS IN MILS)

FIG. 24 Photoresist mask for actual Fig. 23 device (side A).

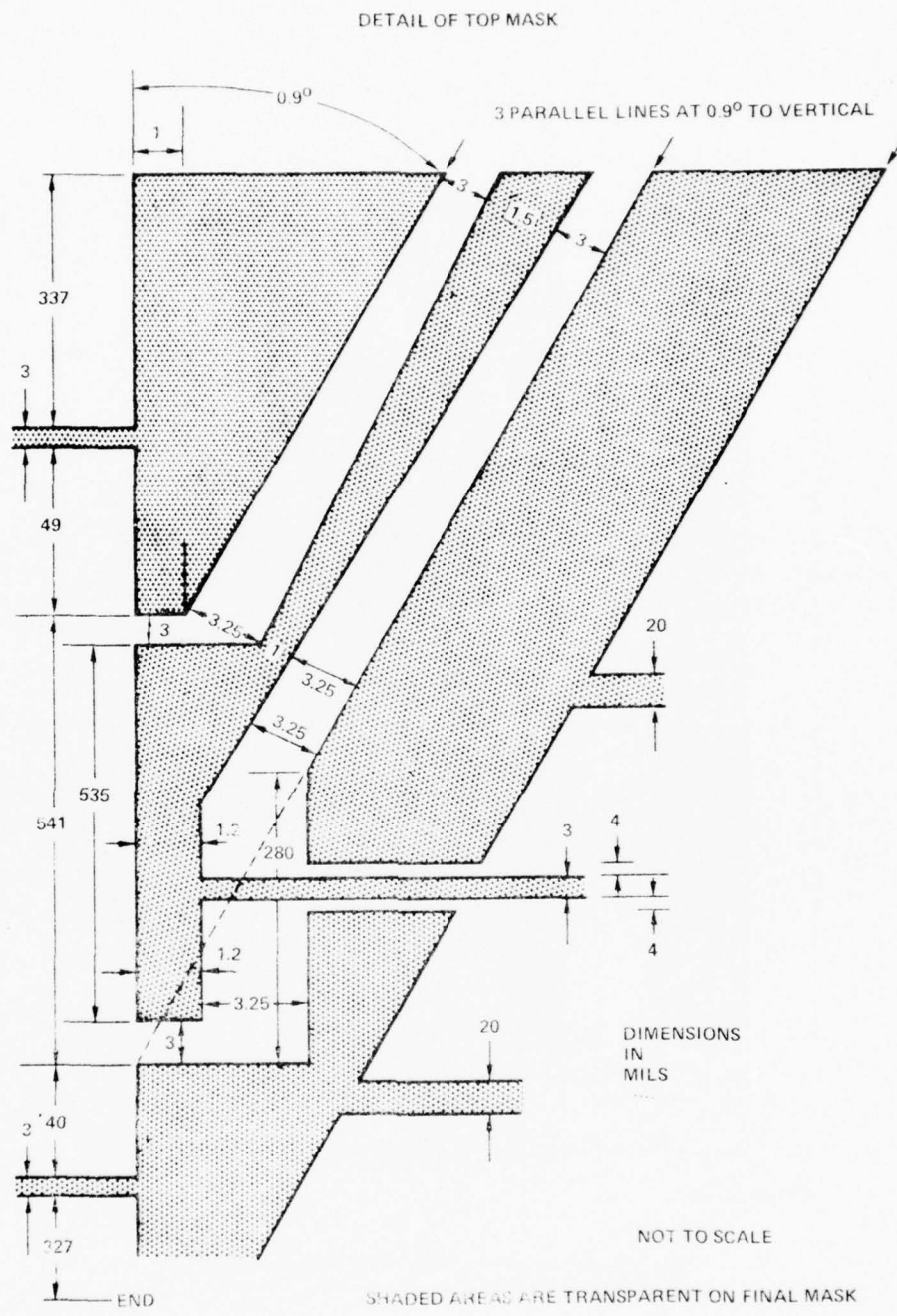
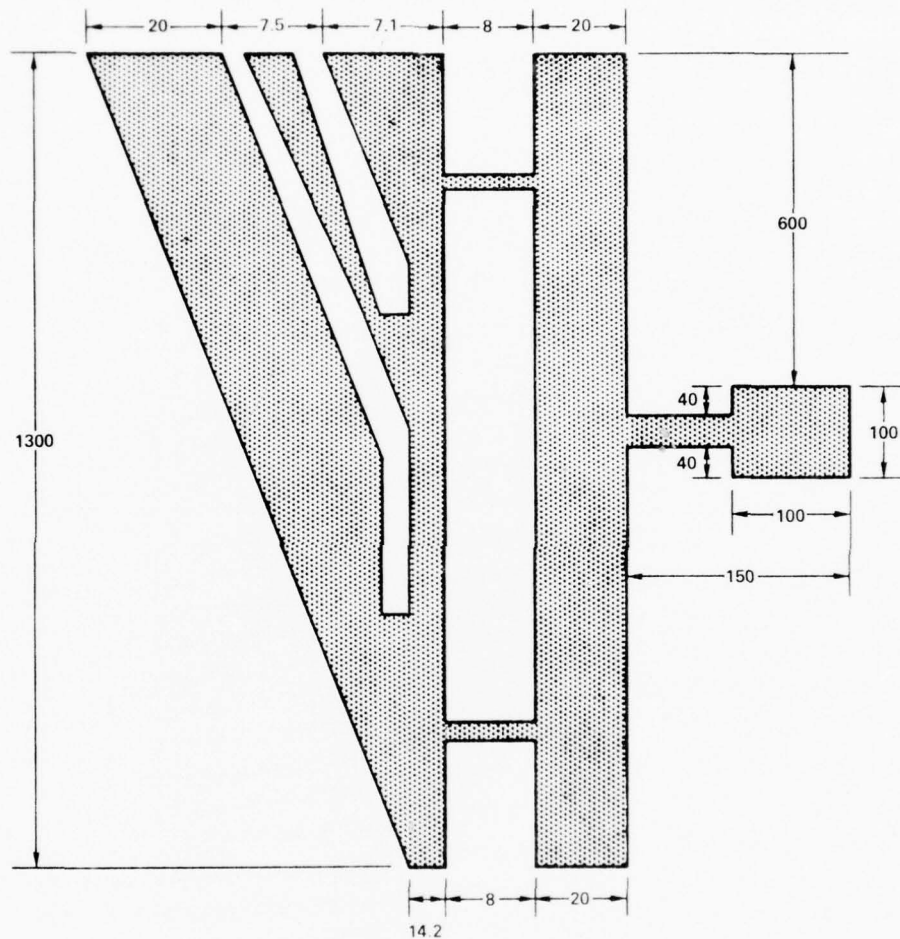


FIG. 25 Detail of side A photoresist mask for actual Fig. 23 device.

SIMPLE CROSSPOINT WITH SPOILER (BOTTOM MASK)



PATTERN REGISTERS EXACTLY TO TOP PATTERN

SHADED AREAS ARE TRANSPARENT ON FINAL MASK
(DIMENSIONS IN MILS)

NOT TO SCALE

FIG. 26 Photoresist mask for actual Fig. 23 device (side B).

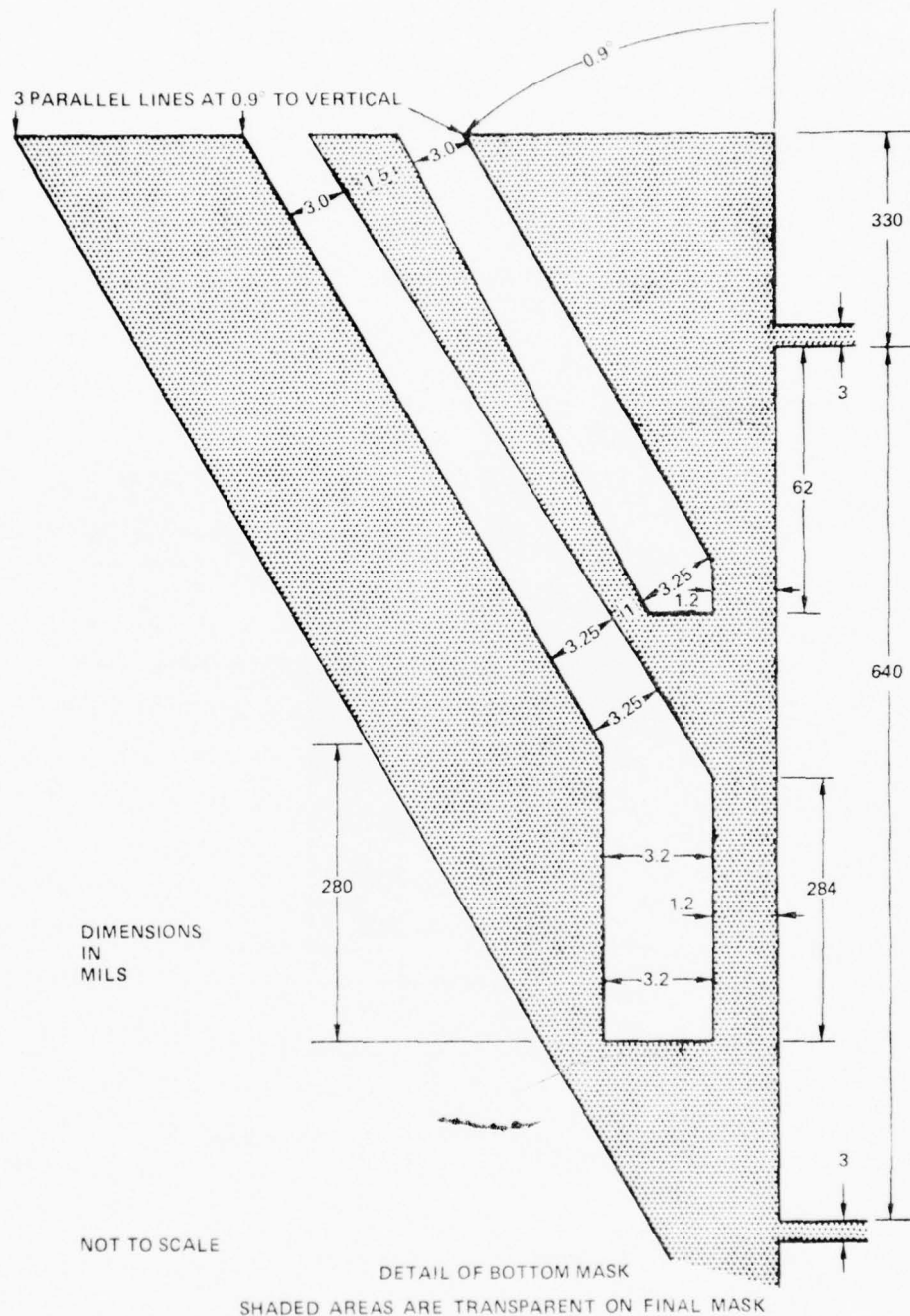


FIG. 27 Detail of side B photoresist mask for actual Fig. 23 device.

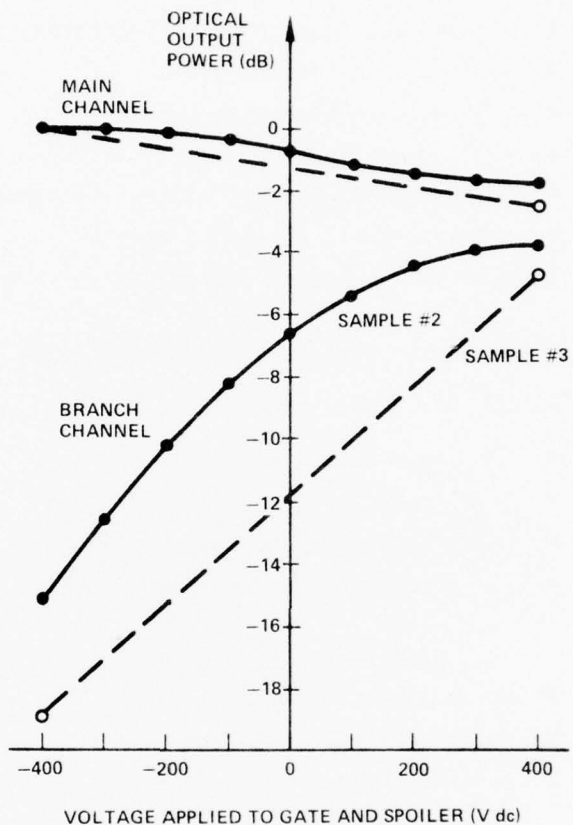


FIG. 28 Measured output of straight-through and branch channels as a function of gate-and-spoiler potential for two Fig. 23 devices.

Simple Crosspoint with Spoiler

STRUCTURE, DEVICE #2

- LiTaO₃, Z-cut plate
- 74 μm plate thickness
- 200 μm main channel width (electrode gap)
- 30 μm gate electrode width
- 1.36 cm gate electrode length
- 0.9° branch angle
- 190 μm branch channel width (electrode gap)
- 1.8 cm overall length of device
- passive channeling equivalent to -170 V dc

TEST CONDITIONS, DEVICES #2 and #3 (Fig. 28)

Same as for Device #1, except

- 20X input lens
- ±4.0° input cone in air
- ±4.0° output collection cone in air
- no voltage applied to channel walls

STRUCTURE, DEVICE #3

- 60 μm plate thickness
- 3.0 cm overall length of device
- passive channeling equivalent to -400 V dc

RESULTS, DEVICE #2

- -4.0 dB optical tapoff ratio into branch at $V_{gs} = +400$ V dc relative to main channel at $V_{gs} = -400$ V dc.
- 11.2 dB optical switching ratio (signal-to-crossstalk of branch at $V_{gs} = +400$ V dc vs $V_{gs} = -400$ V dc).
- 2 dB estimated throughput loss of unswitched channel including both reflection losses.

- 13 pF gate-and-spoiler capacitance
- 101 pF capacitance of bias electrodes (channel walls)

RESULTS, DEVICE #3

- -4.9 dB optical tapoff ratio, device #2 conditions
- 13.9 dB optical switching ratio, device #2 conditions
- 2.5 dB estimated throughput loss, device #2 conditions
- 16.6 pF gate-and-spoiler capacitance
- 192 pF capacitance of bias electrodes (channel walls)

We conclude from the foregoing data that the spoilers operated as predicted. Devices #2 and #3 gave a 4 to 7 dB improvement in the signal-to-crosstalk ratio of the branch compared to Device #1, most of which we attribute to the spoiler electrodes.

Section 7

COMPOUND CROSSPOINT (INITIAL VERSION)

Having demonstrated the feasibility of simple crosspoints and high-isolation crossovers, we began construction of compound crosspoints that unite these devices in one substrate. Our goal was to build the compound switch subject to the following constraints:

- a limit is set on the overall length (L_{cc})
- the plate thickness (t) is comparable to multimode fiber core diameters: 50 to 75 μm
- the switching and bias voltage (V_g and V_w) are limited to 450 V
- the crossover angle (ϕ) is relatively large for low crosstalk
- the branch off angles (θ_b) are relatively small for high tapoff ratios.

Tradeoffs must be made among these requirements since they conflict in certain areas. The length limit is imposed so that several compound crosspoints can be joined into a matrix of reasonable size. For the initial version, we took $L_{cc} = 3$ cm.

7.1 INITIAL DESIGN

Starting with the "optical circuit diagram" of Fig. 1, we substituted the simple-crosspoint layout of Fig. 18 for both switches and used 4-stripe electro-optic channels for all required signal paths. A design for the monolithic compound crosspoint was arrived at in this way. A top view of the electrode pattern for the resulting compound crosspoint is shown in Fig. 29 (which includes labeling for the relevant dimensions and angles), and a perspective view of the device (sans control leads) is shown in Fig. 30. Note that the crosspoint is bidirectional. It functions identically for either direction of light propagation.

Returning to Fig. 29, the specific parameters are determined as follows.

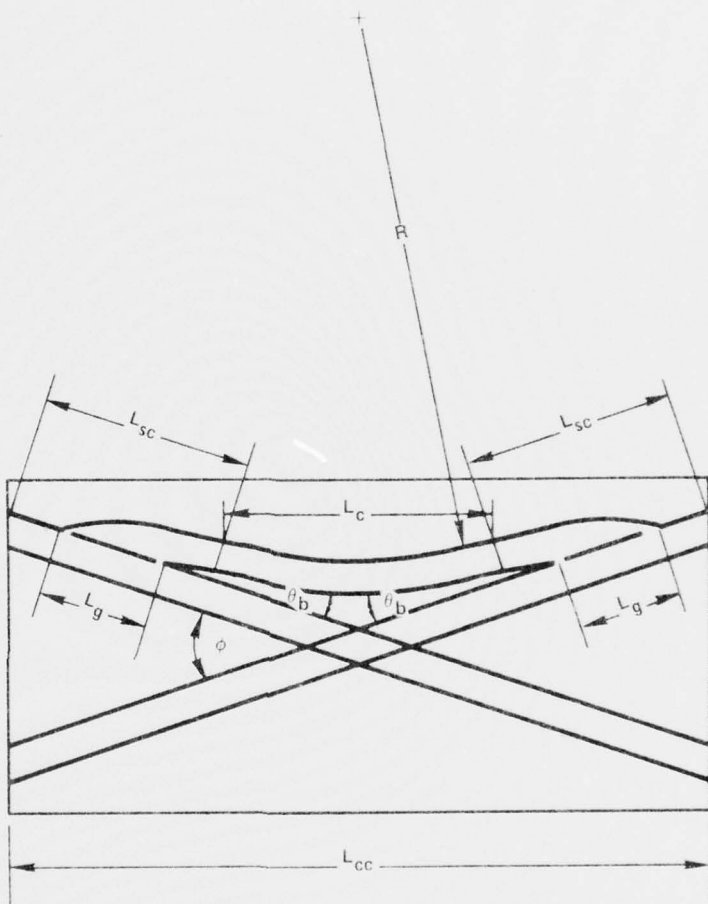


FIG. 29 Plan view of compound crosspoint electrodes showing dimensions and angles used in switch design.

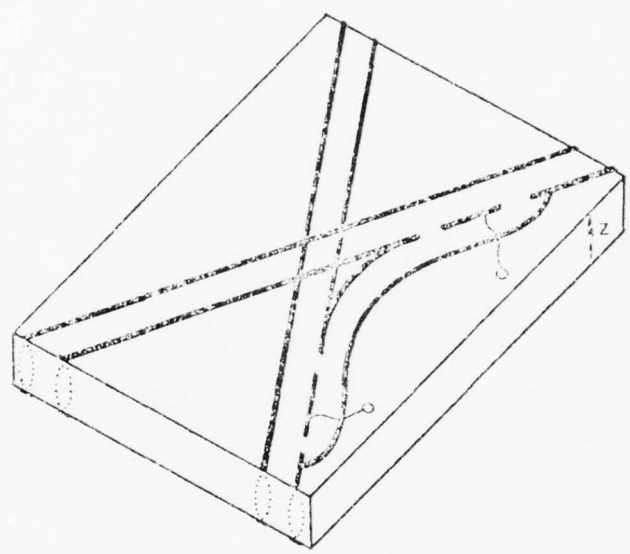


FIG. 30 Layout of four-port compound crosspoint device (first version).

First, the plate thickness is to 50 to 75 μm as above, but we ruled out $t \leq 60 \mu\text{m}$ because of our prior experience with crystal breakage (2.5 mils $\leq t \leq 3.0$ mils).

Next, we need to know the light-confinement properties of the channels. The critical angle θ_c for electro-optic channeling is computed from the allowed switching voltage; then the branch angle is determined from θ_c . The critical angle is related to the induced index shift Δn_z as follows:

$$\theta_c (\text{TM}) = \pm \sqrt{\frac{2\Delta n_z}{n_z}} . \quad (7-1)$$

The TM modes are those polarized with their optical field parallel to the crystal Z axis, and the angle θ_c is measured within the crystal. The refractive index shift along Z is related to the applied electric field (Z component) by the r_{33} electro-optic coefficient of lithium tantalate or lithium niobate as follows:

$$\Delta n_z = \frac{1}{2} n_z^3 r_{33} E_z . \quad (7-2)$$

Previously measured coefficient values from the Chemical Rubber Laser Handbook are:

$$r_{33} (\text{LiTaO}_3, \lambda = 0.63 \mu\text{m}) = 30.3(\text{S}) \times 10^{-6} \text{ micron/V}$$

$$r_{33} (\text{LiNbO}_3, \lambda = 0.63 \mu\text{m}) = 30.8(\text{S}) \times 10^{-6} \text{ micron/V}$$

$$n_z (\text{LiTaO}_3, \lambda = 0.63 \mu\text{m}) = 2.19$$

$$n_z (\text{LiNbO}_3, \lambda = 0.63 \mu\text{m}) = 2.20 .$$

Substitution of these data into Eq. (7-2) gives these numerical results:

$$\begin{aligned} \Delta n_z (\text{LiTaO}_3, \lambda = 0.63 \mu\text{m}) &= 1.59 \times 10^{-4} E_z \\ \Delta n_z (\text{LiNbO}_3, \lambda = 0.63 \mu\text{m}) &= 1.65 \times 10^{-4} E_z \\ \theta_c (\text{LiTaO}_3, \lambda = 0.63 \mu\text{m}) &= 1.21 \times 10^{-2} \sqrt{E_z} \\ \theta_c (\text{LiNbO}_3, \lambda = 0.63 \mu\text{m}) &= 1.22 \times 10^{-2} \sqrt{E_z} . \end{aligned} \quad (7-3)$$

in which the units of E_z are volts per micron and θ_c is in radians. For our electrode geometry, the relation between the applied voltage V_g and the field E_z

$$V_g = E_z/t \quad (7-4)$$

is fairly accurately obeyed in the crystal region directly under a stripe. The relations (7-3) are plotted in Figures 31 and 32 over the 2 to 8 V/ μm field range, which covers practical values. Taking $t = 63 \mu\text{m}$ and $V_g = 450 \text{ Vdc}$, we find from Eqs. (7-4), (7-3), and (7-1) that $E_z \approx 7.1 \text{ V}/\mu\text{m}$ and $\theta_c = 1.83^\circ$ for lithium tantalate. The branchoff angle for each simple crosspoint is taken to be

$$\theta_b \approx \frac{1}{2} \theta_c$$

in order to get a high tapoff ratio. (An approximate ray-optic theory of the optical power division between merged Y-coupled channels has been worked out by D. H. McMahon. Representative results for the coupling ratios versus θ_b/θ_c are given in Fig. 33). Thus for the initial compound crosspoint we chose $\theta_b = 1^\circ$.

The gate length L_g is given by

$$L_g = (W + W_g)/\sin \theta_b \quad (7-5)$$

in which W is the branch channel width (synonymous with the connecting channel width) and W_g is the gate electrode width. According to a barrier-isolation calculation worked out by D. H. McMahon, stripe-like gates are capable of high optical isolation, more than 80 dB when $W_g \geq 25 \mu\text{m}$ (Fig. 34). Accordingly, we took $W_g = 25 \mu\text{m}$ and we also chose $W = 5.5 \text{ mils}$ ($140 \mu\text{m}$) similar to that of the simple crosspoint in Chapter 6, Device #1. Hence, $L_g = 0.94 \text{ cm}$ for this switch. Including the lead-in waveguides (L_i), the simple crosspoint length is $L_{sc} = L_i + L_g$, and taking $L_i = 0.2 \text{ cm}$, we have $L_{sc} = 1.14 \text{ cm}$ for the initial compound crosspoint. Since the overall length is approximately

$$L_{cc} = 2 L_{sc} + L_c \quad (7-6)$$

where L_c is the arc-length of the curved connecting guide, we find that this arc is 0.72 cm long here.

The radius of curvature (R) of the connecting channel is related to the arc length L_c , the crossover angle ϕ and the branch angle θ_b as follows:

$$R = L_c / \tan(\phi - 2 \theta_b) \quad (7-7)$$

It is quite important to make this radius larger than some minimum radius

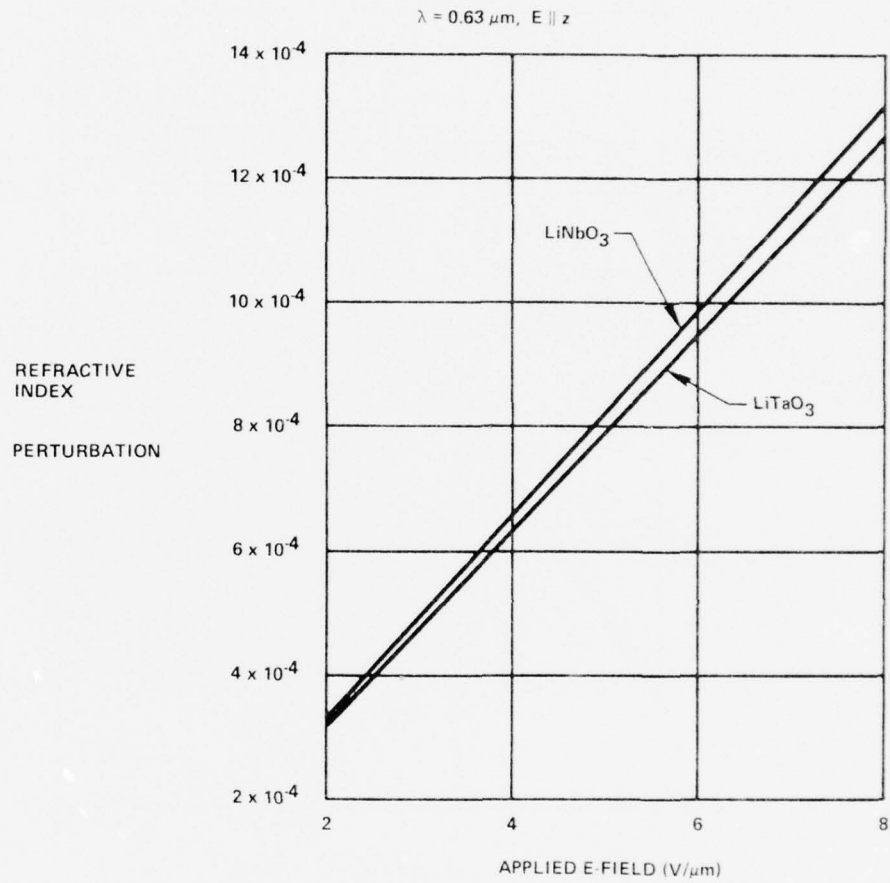


FIG. 31 Induced index perturbation in LiNbO_3 and LiTaO_3 as a function of applied field.

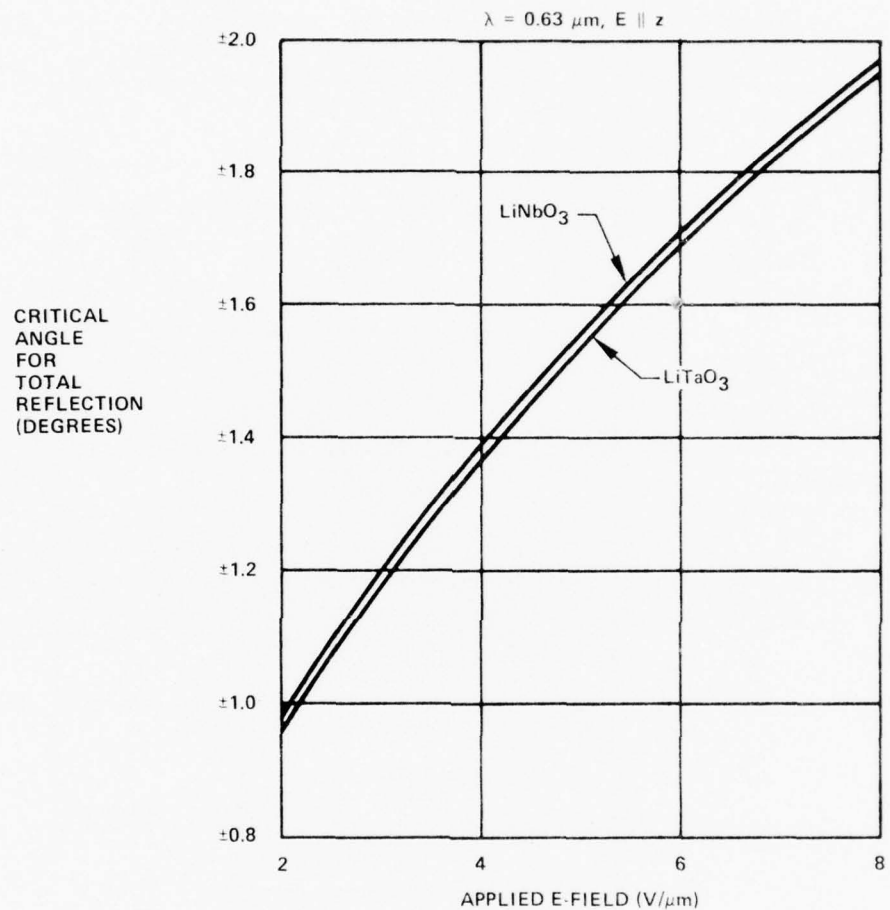
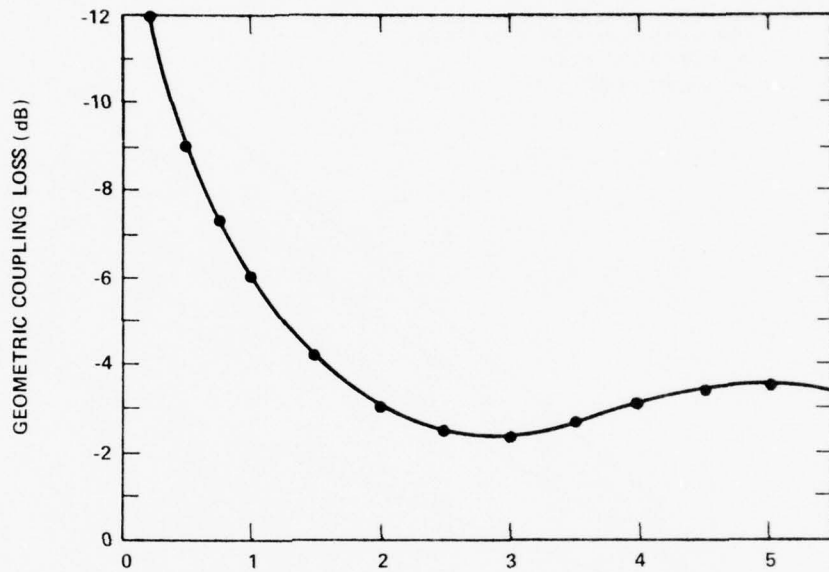


FIG. 32 Critical angle in LiNbO_3 and LiTaO_3 as a function of applied field.



θ_L/θ_B = RATIO OF HALF ANGLE OF LIGHT DIVERGENCE TO BRANCH ANGLE

FIG. 33 Geometric coupling loss versus light-divergence-angle/branch-angle ratio.

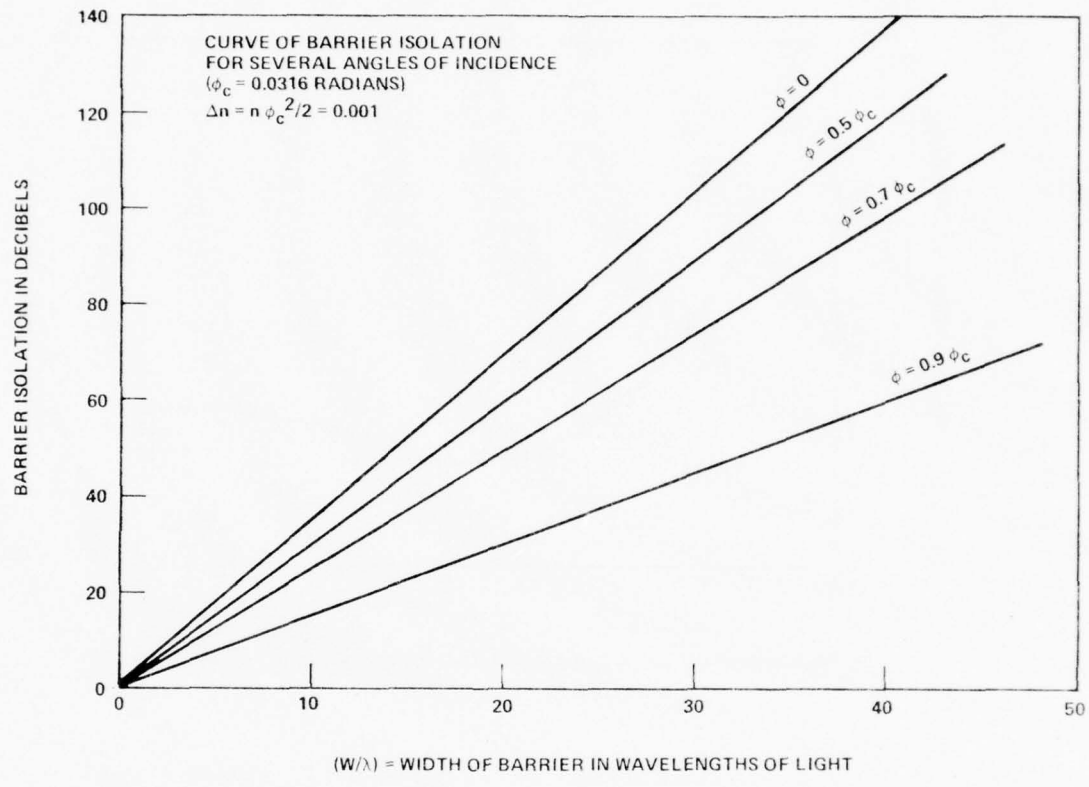


FIG. 34 Optical isolation of barrier as a function of barrier width.

(R_{\min}) in order to keep radiation loss (the unguided leakage out of the curved channel) to a minimum. Multimode waveguide theory yields the approximate relation

$$R_{\min} = 2 W_e / \theta_c^2 \quad (7-8)$$

in which W_e is the effective optical width of the multimode curved channel. The θ_c -dependence of R_{\min} is plotted in Fig. 35. For the initial compound crosspoint, we assumed optical confinement within a 1-mil-wide region of the curved channel, and that $\theta_c = 1.83^\circ$ as above. Hence, from Eq. (7-8), R_{\min} is 4.8 cm.

The crossing angle ϕ enters into Eq. (7-7) for R . Note that small ϕ -values are undesirable because they allow crossguide scattering. On the other hand, as ϕ goes up, crosstalk decreases but R gets smaller, eventually going below the acceptable level R_{\min} . So, a compromise ϕ is needed. We took $\phi = 6^\circ$ for the initial compound crosspoint, giving $R = 8.5$ cm which is greater than R_{\min} computed above.

7.2 EXPERIMENTAL RESULTS

Two versions of the first-generation compound crosspoint, with and without spoiler electrodes, were built. The first version, called CC-1A-2, used the photoresist masks CC-1A and CC-2 shown in Figures 36 and 37. In a third mask, CC-1B, the curved channel of the 1A design was widened to 7 mils, and 1-mil-wide spoiler electrodes were attached to each of the two independent gates (midway along the curve), to give the modified mask shown in Fig. 38. A compound crosspoint with spoilers, designated CC-1B-2 was constructed using the CC-1B and CC-2 masks.

The experimental set-up is similar to that shown in Fig. 21. Light was focussed into the gated channel with a 10x or 20x microscope objective, and both channel outputs were imaged onto detectors. Outputs are observed sequentially; the near-field lens and PMT detector being moved in sequence into position for each channel. Aperture stops are provided for the output lens and the detector.

The compound crosspoint gates could be turned on and off individually, but for most experiments they were connected together. Both devices had some passive channeling, so it was necessary to "reverse bias" the gates ($+V_g$),

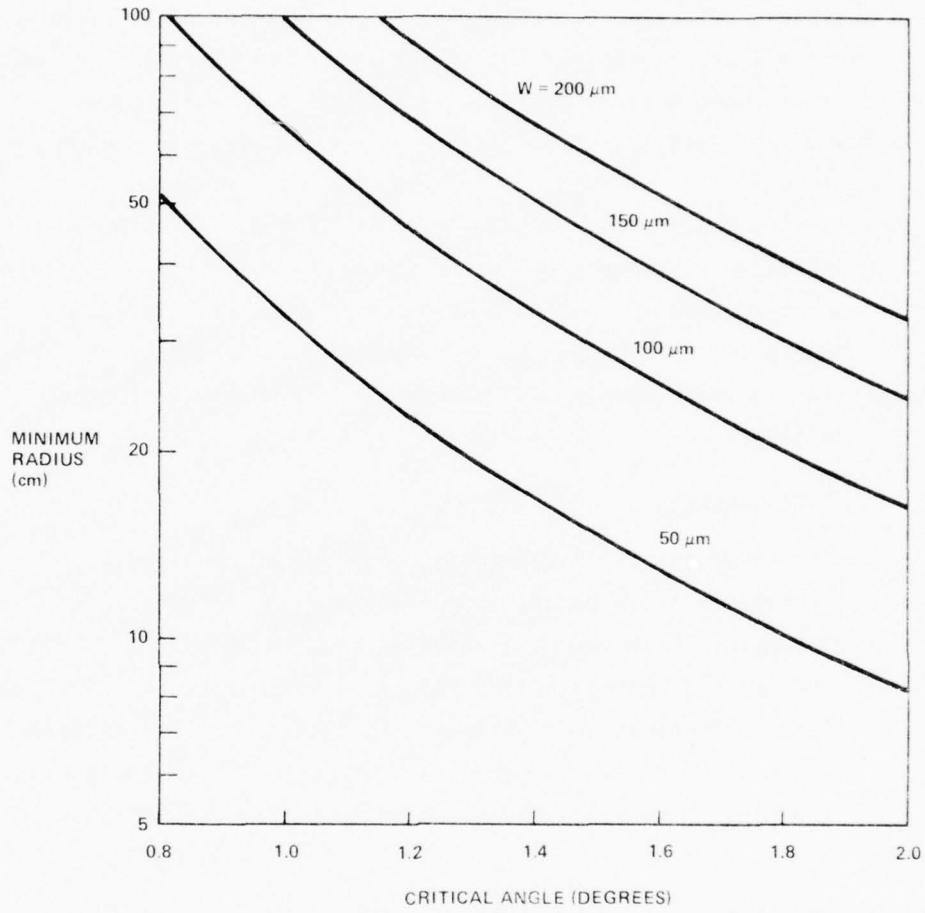


FIG. 35 Minimum bend radius of multimode channel versus channel critical angle.

COMPOUND CROSSPOINT – MASK CC-1A (TOP SURFACE)

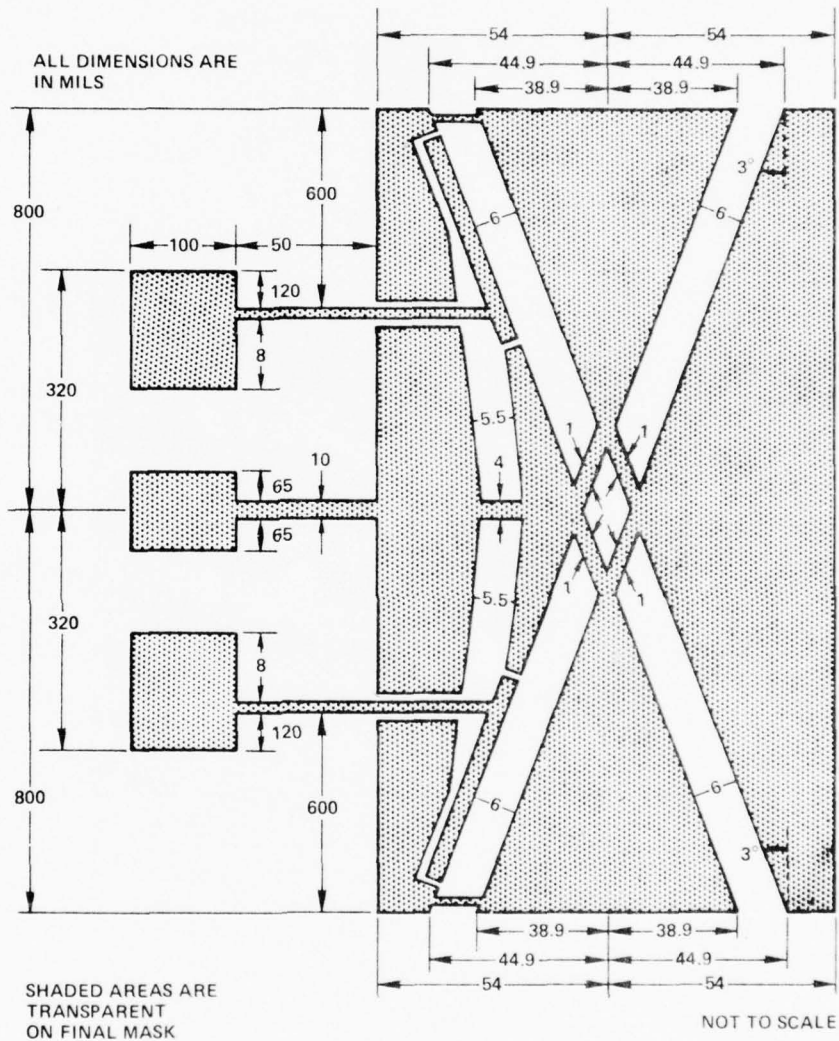


FIG. 36 Photoresist mask for actual Fig. 30 device (side A).

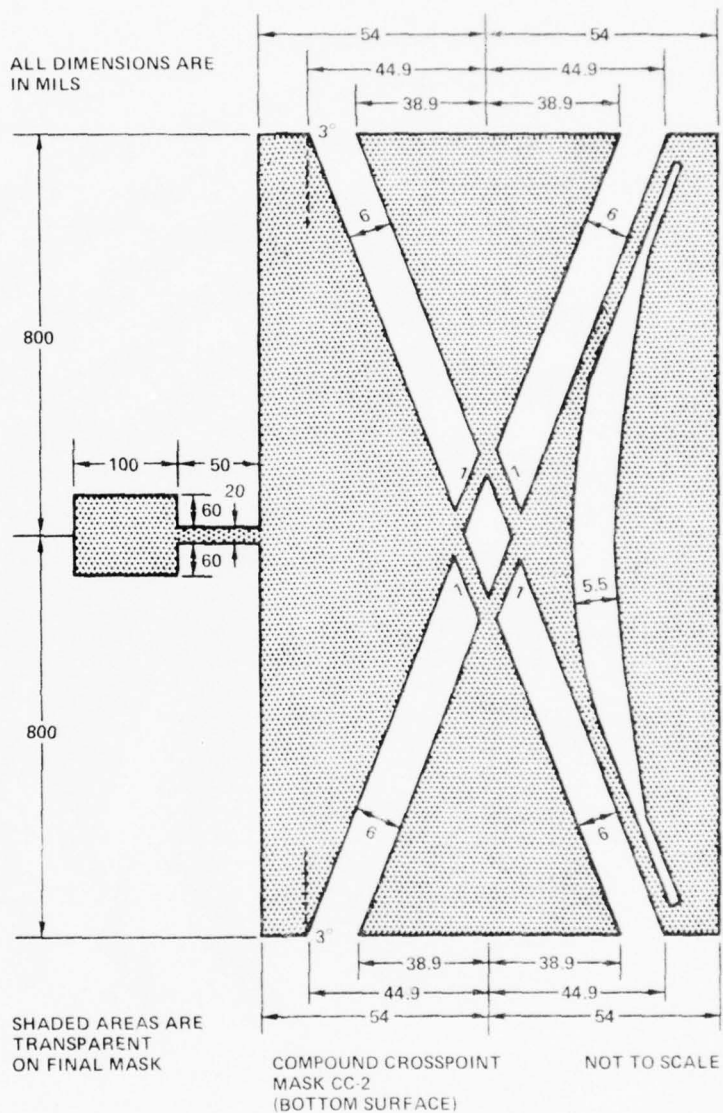


FIG. 37 Photoresist mask for actual Fig. 30 device (side B).

COMPOUND CROSSPOINT - MASK CC-1B (TOP SURFACE)

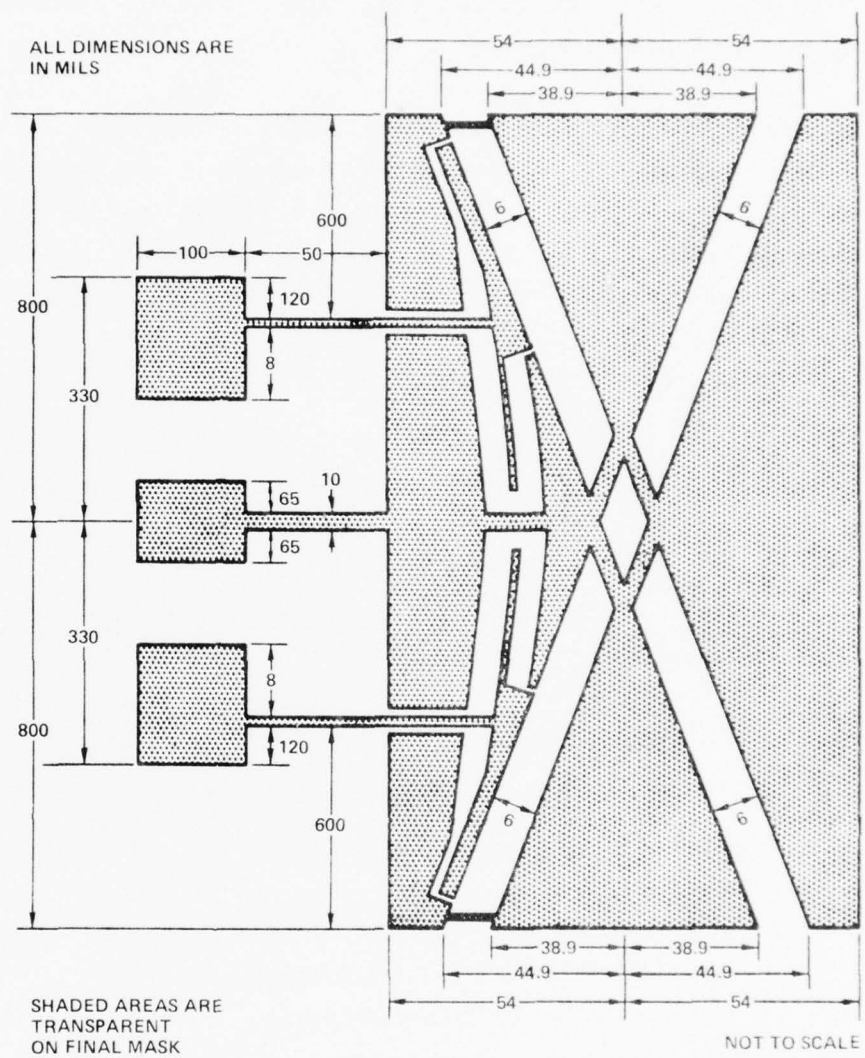


FIG. 38 Photoresist mask for actual Fig. 30 device (side A) with spoiler electrodes.

cancelling out their passive effect to completely "open" them (allowing light to pass). Negative voltage on the gates made them close. They become reflective, and light is also deflected out of the curved channel in the spoiler case.

The observed output intensity from the cross-channel and straight-through channel is plotted on a dB scale as a function of gate potential (V_g) in Fig. 39 for both polarities of applied voltage (CC-1A-2 device). A similar measurement for CC-1B-2 versus gate-and-spoiler potential is presented in Fig. 40. The solid lines refer to on-axis optical excitation of the input channel. The shaded regions show what happens when the input beam is translated slightly off the channel axis.

The switched throughput was largest in the positive voltage regime at values corresponding to the passive background. The on-axis tapoff ratios were smaller than expected, although the switching was several dB greater for off-axis incidence. The straight-through intensity decreased by 1 - 2 dB at $V_g = + 100$ Vdc. The experimental results are summarized below, together with a synopsis of device parameters and test conditions.

Compound Crosspoint (Initial Version)

STRUCTURE, DEVICE CC-1A-2 (No spoilers)

- LiTaO₃, Z-cut plate
- 70 μm plate thickness
- 150 μm straight channel width (electrode gap)
- 137 μm curved channel width (electrode gap)
- 25 μm gate electrode width (both)
- 0.94 cm gate electrode length (both)
- 1.0° branchoff angle, curved channel from crosspoints
- 6.0° channel crossover angle
- 0.63 cm arc-length of curved channel
- 8.5 cm radius of curvature
- 3.0 cm overall length of device
- passive channeling equivalent to -70Vdc

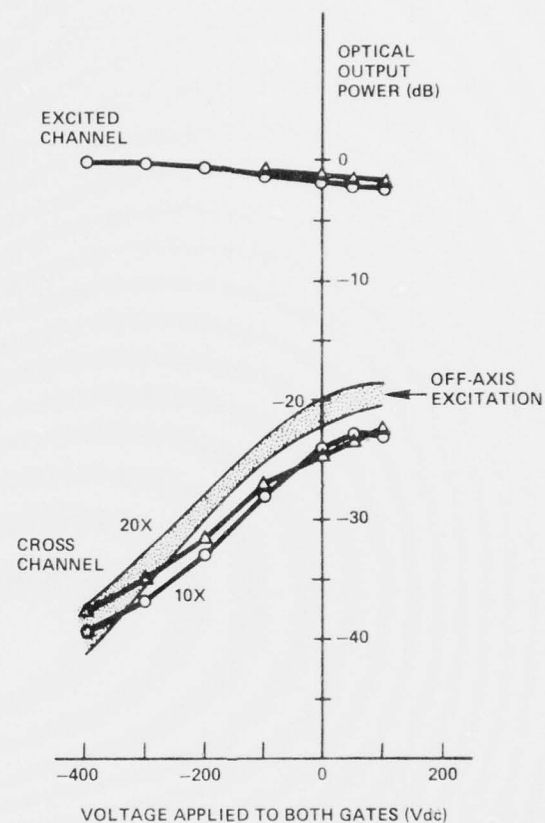


FIG. 39 Measured output of straight-through and crosschannels as a function of gate potential for a compound crosspoint device CC-1A-2.

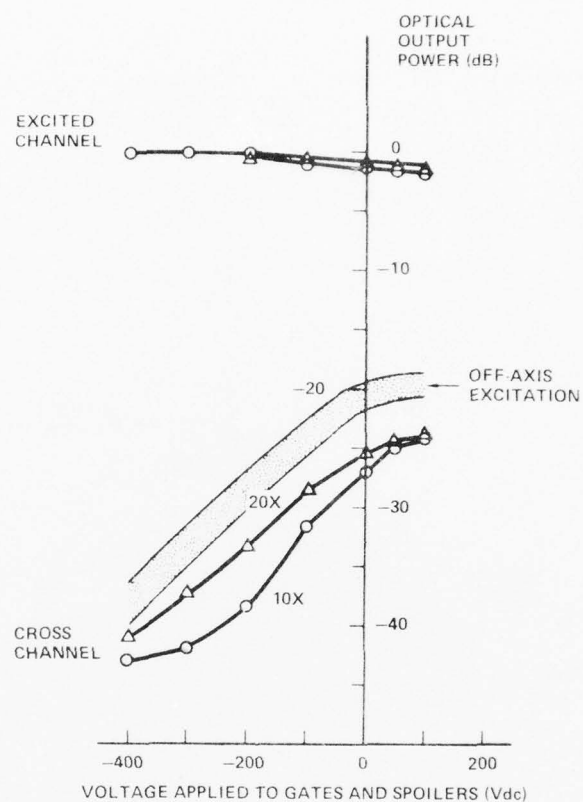


FIG. 40 Measured output of straight-through and crosschannels as a function of gate-and-spoiler potential for a compound crosspoint device CC-1B-2.

TEST CONDITIONS (Fig. 39)

- focussed laser beam input ($\lambda = 0.63 \mu\text{m}$,
1.1 mm beam diam)
- TM polarized, $E \parallel Z$
- 20x input lens
- $\pm 1.8^\circ$ input cone in crystal
- $\pm 4.0^\circ$ input cone in air (0.07 NA)
- $\pm 2.0^\circ$ input cone in air for 10x lens
- $\pm 2.2^\circ$ collection cone in air
- 3 mm x 6 mm detector aperture on 39x image plane
- -350 Vdc channel wall bias

RESULTS

- -22.5 dB optical tapoff ratio, on-axis (crosschannel, $V_g = +100$ Vdc
vs excited channel $V_g = -400$ Vdc).
- 16 dB optical switching ratio (signal-to-crosstalk of crosschannel,
 $V_g = +100$ Vdc vs $V_g = -400$ Vdc).
- 2.4 dB estimated throughput loss (excited channel, $V_g = -400$ Vdc)
including both reflection losses.
- 8.5 pF capacitance of gate electrodes
- 360 pF capacitance of bias electrodes (all channel walls)

STRUCTURE, DEVICE CC-1B-2 (With spoilers)

Same as CC-1A-2 except:

- 72 μm plate thickness
- 225 curved channel width (electrode gap)
- 25 μm spoiler electrode width
- spoiler on midline of curved channel
- spoiler and gate connected electrically
- 3.1 overall length of device
- passive channeling equivalent to -80 Vdc

TEST CONDITIONS (Fig. 40)

Same as for CC-1A-2

RESULTS

- -24 dB optical tapoff ratio, on-axis (crosschannel, $V_g = +100$ Vdc vs excited channel $V_g = -400$ Vdc).
- 17 dB optical switching ratio (signal-to-crosstalk of crosschannel, $V_g = +100$ Vdc vs $V_g = -400$ Vdc).
- 2.4 dB estimated throughput loss (excited channel, $V_g = -400$ Vdc) including both reflection losses.
- 9.6 pF capacitance of gate electrodes
- 380 pF capacitance of bias electrodes (all channel walls)

In gathering the Fig. 39 and 40 data, we noticed that a considerable amount of light emerged from the device "between" the channels as illustrated in Fig. 41 (this was true for both devices). This "midlight" could be extinguished with the first gate closed and the second gate open. Also, when both gates were opened and closed in unison, the midlight was not switched as strongly as the crosschannel output. Therefore, we concluded this light was radiating out of the curved guide as Fig. 41 indicates, implying that the radius of curvature was too small.

In this way, the crosschannel was robbed of light, which explains why the tapoff ratios were low for both compound switches. This radiation effect was the main problem area for CC-1A-2 and CC-1B-2. The intergate radiation also had the effect of masking the spoiler action.

A more gratifying result was obtained for the on/off switching ratio of the crosschannel. Here, in both Figures 39 and 40, the signal-to-crosstalk ratio was in the 17 to 20 dB range, which is approximately twice the observed S/C ratio of the simple crosspoint as predicted by theory. In theory, the isolation of the crosschannel with gates closed should be as great as that found in passive crossover devices, namely ~ 40 dB below the input level (Sec. 5.5). This prediction was indeed borne out in the Fig. 39 and 40 results.

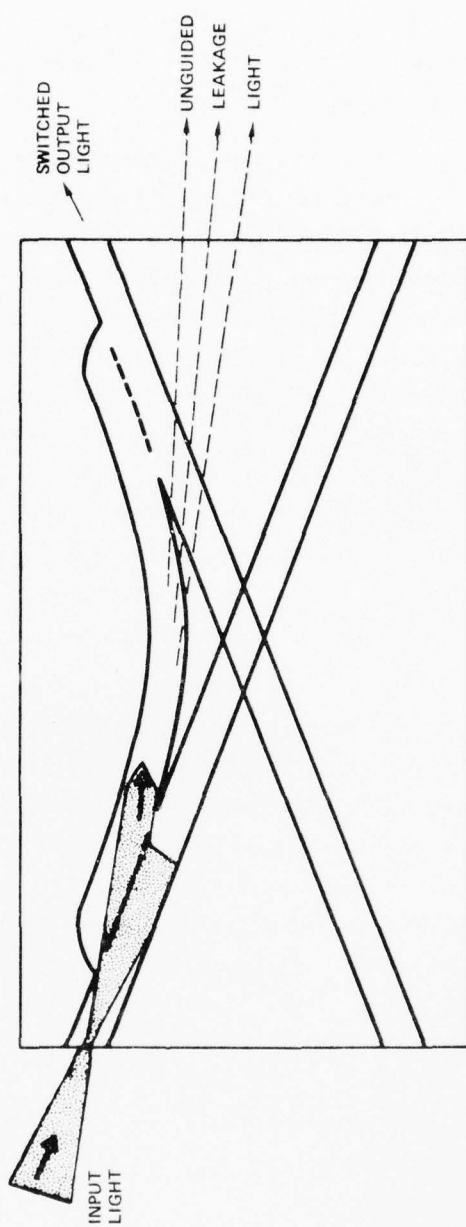


FIG. 41 Top view of initial compound crosspoint showing location of undesired radiation.

Returning to the Sec. 7.1 design procedure, reasons can be found for the curved channel leakage; the light-trapping angles were smaller than anticipated, and the trapping region wider.

For a given voltage on the curved channel stripes, the largest possible index shift at the channel axis will be obtained if the channel midpoint is field-free. However, in practice, there will be z-components of field in the midregion due to fringing-field overlap. This overlap can be significant because the surface electrode gap is only two to three times as large as the plate thickness (t). Hence, the full range, $0 \leq E_z \leq V_g/t$, is not available for channeling. A. R. Nelson has calculated the fringing field strength vs lateral position for plane-parallel electrodes with the result shown in Fig. 42. At a distance of $1.2t$ from the electrode edge (the present experiment), fringing from quadripole stripes is 30 to 40% of the understripe field. Thus, Δn_z for the channel is only 60 to 70% of its ideal value. Hence, because of its square-root dependence on Δn_z , the effective confinement angle of the electro-optic channel is 77 to 84% of its ideal value, which produces a 60 to 70% increase in R_{\min} .

Also, the effective optical width of the channel was, in retrospect, greater than the 1-mil value assumed. It is a complex problem to determine how an index-gradient channel is "filled" with light. As a rough estimate, we now feel that most of the light will be confined within 50% of the electrode spacing, which would be ~ 3 mils in the CC-1-2 case. Consequently, the minimum bend radius for the CC-1A-2 and CC-1B-2 switches was actually much greater than the radius calculated above (Sec. 7.1) and the inequality, $R > R_{\min}$, was not satisfied.

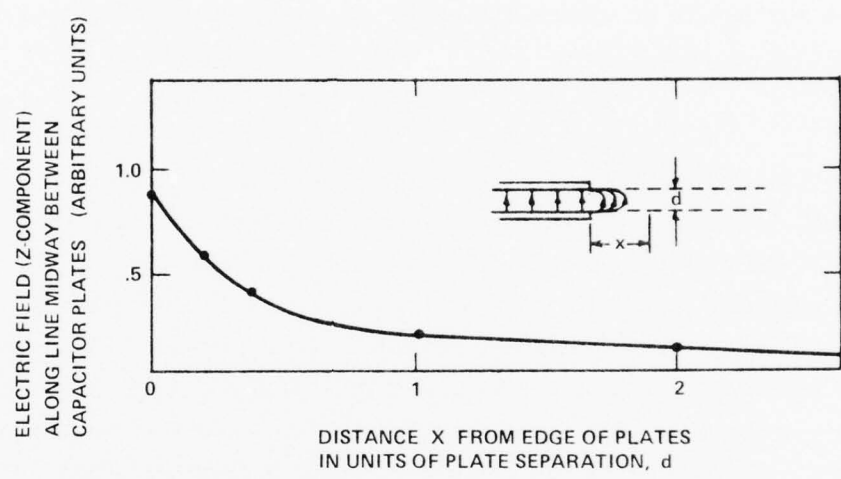


FIG. 42 Z-component of electric field along a line midway between two "capacitor plates."

Section 8

COMPOUND CROSSPOINT (IMPROVED VERSION)

The purpose of building the second-generation compound switch was to achieve higher switching ratios and higher tapoff ratios than in CC-1-2. The Sec. 7 results indicated that this could be done if the bend radius for the connecting channel was increased (which would lengthen the crosspoint). We felt it was worthwhile to demonstrate good switching performance even if the new device took up more space.

8.1 DESIGN

The starting point was to select the overall switch length based upon crystal availability. Polished, optical quality LiTaO_3 crystals, 2.5 mils thick and $\frac{1}{2}$ " wide, were available from Crystal Technology Inc. in two to three inch lengths. Since the cost and fragility of this material go up (at a greater-than-linear rate) with increasing length, we chose 2.4 inches as a compromise crosspoint length. This permitted a 400% increase in the connecting channel length over CC-1-2 because the simple crosspoint lengths could be held at about the same values as in CC-1-2 (their gating performance was adequate).

Photoresist masks, designated CC-3 and CC-4, were made by Photronics Company in a sub-contracting arrangement with Computer Drafting Company, who fabricated the curved-waveguide sections out of 40 pairs of parallel straight-line segments in a piece-wise-linear approximation. From the Sec. 6 results, we chose a 1-mil-wide spoiler electrode to go down the midline of the curved channel on both top and bottom crystal surfaces. This spoiler contacted both gates electrically, so all three electrodes are at the same potential. (It was not felt necessary to have the gates independent of one another, and the electrode layout is simplified in the unified-gate condition.) As before, all electro-optic channels in device were of the four-stripe variety. Figure 43 shows a perspective drawing of the compound crosspoint device (crystal only; electrical leads and protective glass plates on top and bottom are not shown).

Short-circuiting between surface electrodes (gate and wall) was

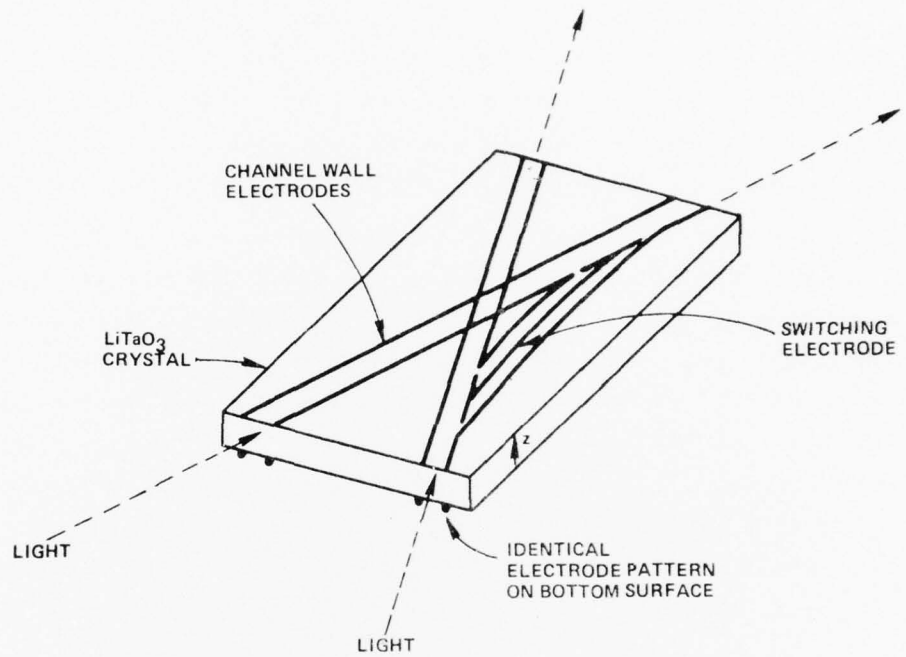


FIG. 43 Layout of four-port compound crosspoint device (improved version).

prevented by making the minimum gap between these electrodes 3 mils, a spacing that should stand off at least 500 V when covered with glycol phthalate. The width of the curved channel is thus 7 mils (3 mils on either side of the 1-mil spoiler). The same width was chosen for the straight channels.

As discussed in Sec. 7.2, the critical angle for light-trapping will be $\pm 1.4^\circ$ to $\pm 1.5^\circ$, rather than the ideal $\pm 1.8^\circ$ value. Also, most of the light in the curved guide will be confined to a 3- to 4-mil band. Using these estimates, we find from Fig. 35 that the minimum bend radius is about 30 cm, so we chose the actual radius to be 36 cm, which provides a margin of safety.

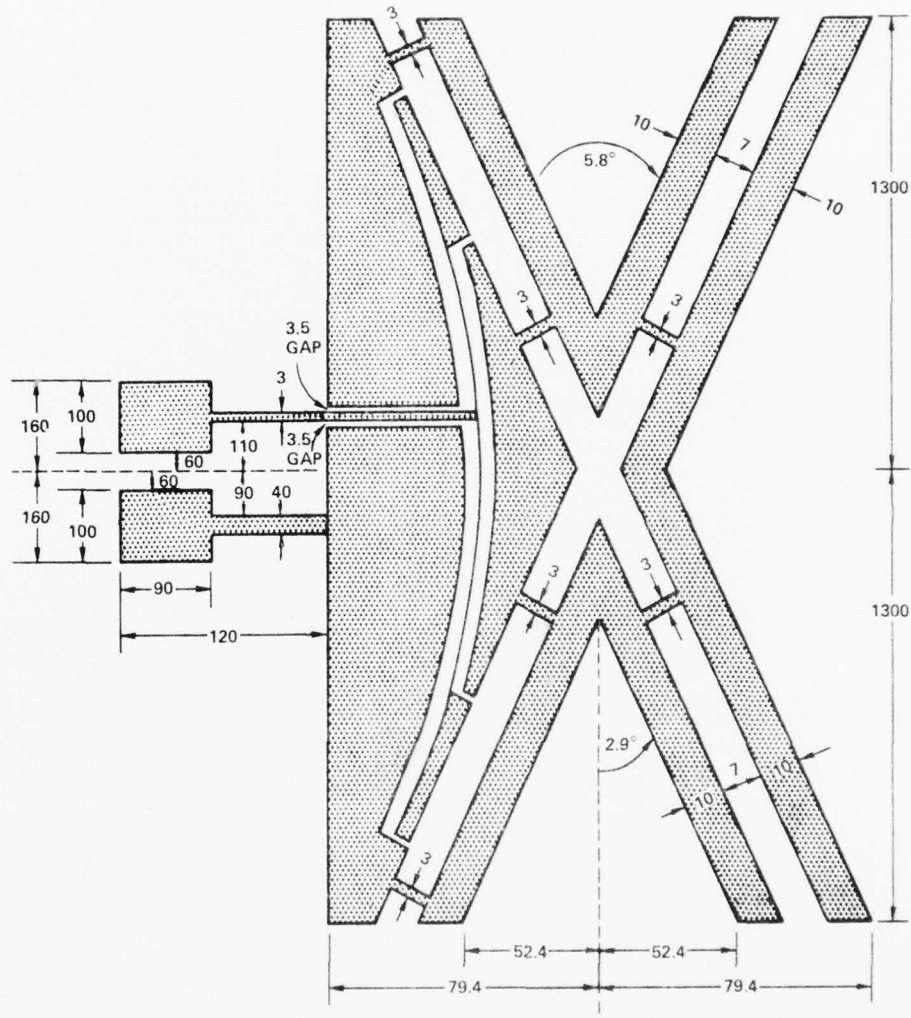
To tapoff large amounts of light as desired, the initial fan-out (or fan-in) angle of the curved guide from the simple crosspoints was chosen to be 0.8° , slightly more than half the effective critical angle. This gave a gate length of 1.44 cm as per Eq. 7-5. With lead-in waveguides 0.26 cm long, the simple crosspoint length is now 1.7 cm. A length of 2.6 cm remains for the curved guide because $L_c = L_{cc} - 2L_{sc} = 6.0 \text{ cm} - 3.4 \text{ cm} = 2.6 \text{ cm}$. Since a 6° intersection angle in CC-1-2 gave a high off-state isolation, a crossover angle close to this is desired here. We found that a crossing angle of 5.8° was consistent with the aforementioned $\theta_b = 0.8^\circ$, $L_c = 2.6 \text{ cm}$, and $R = 35.8 \text{ cm}$, in accordance with Eq. 7-2.

The resulting photomasks, CC-3 and CC-4, which are registered directly atop one another on opposite surfaces of the crystalline plate, are shown in Figures 44 through 47. The drawings show electrode pads to which external contact is made.

8.2 DEVICE CONSTRUCTION

Two devices, nominally identical, were prepared. Device #2 had excellent mask registration, although there was a small 0.5 mil registration error at one end of the 2.4" crystal in Device #1. During the final stage of processing, Device #1 was heated to 170°C for 1 min, while Device #2 was heated to 185° for 2 min. Passive channeling was initially large in Device #1, about -350 Vdc equivalent, but the passive effect faded to a -60 Vdc level after three days. Device #2 was similar, with its initial passive guiding fading to -40 Vdc-equivalent in the same interval.

COMPOUND CROSSPOINT – MASK CC-3



SHADED AREAS TRANSPARENT ON FINAL MASK:
DIMENSIONS IN MILS.

FIG. 44 Photoresist mask for actual Fig. 43 device (side A).

DETAIL OF MASK CC-3

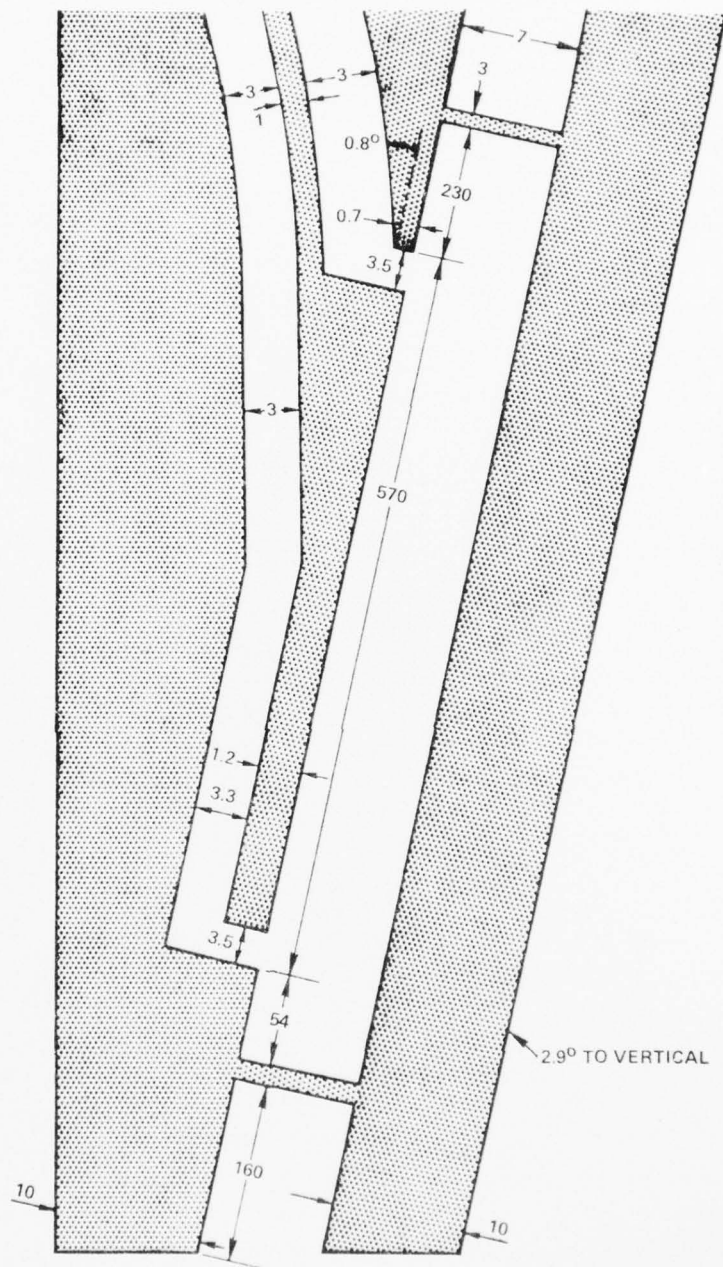


FIG. 45 Detail of side A photoresist mask for Fig. 43 device.

ADDITIONAL DETAIL OF MASK CC-3

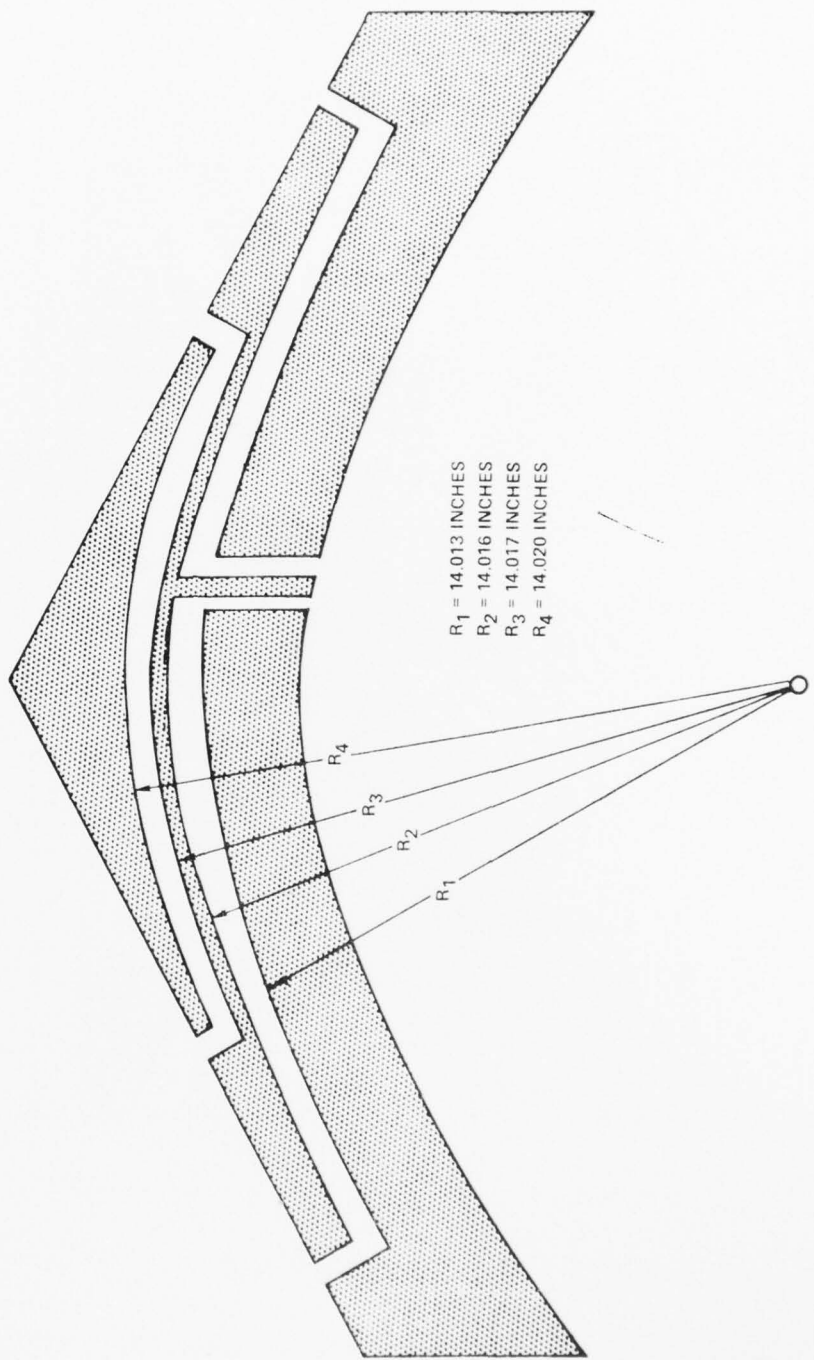


FIG. 46 Further detail of side A photoresist mask for Fig. 43 device.

COMPOUND CROSSPOINT - MASK CC-4

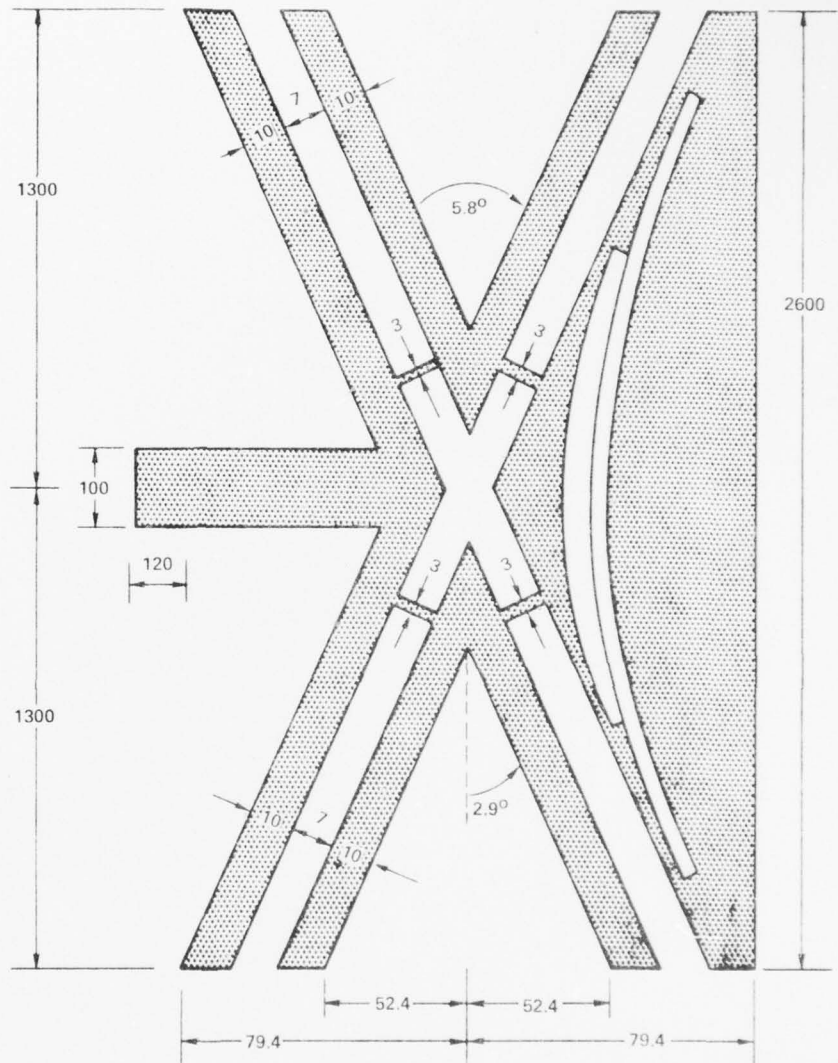


FIG. 47 Photoresist mask for actual Fig. 43 device (side B).

AD-A044 208

SPERRY RESEARCH CENTER SUDBURY MASS
OPTOSWITCH CROSSTALK STUDY. (U)

F/6 17/2

AUG 77 R A SOREF

SCRC-CR-77-22

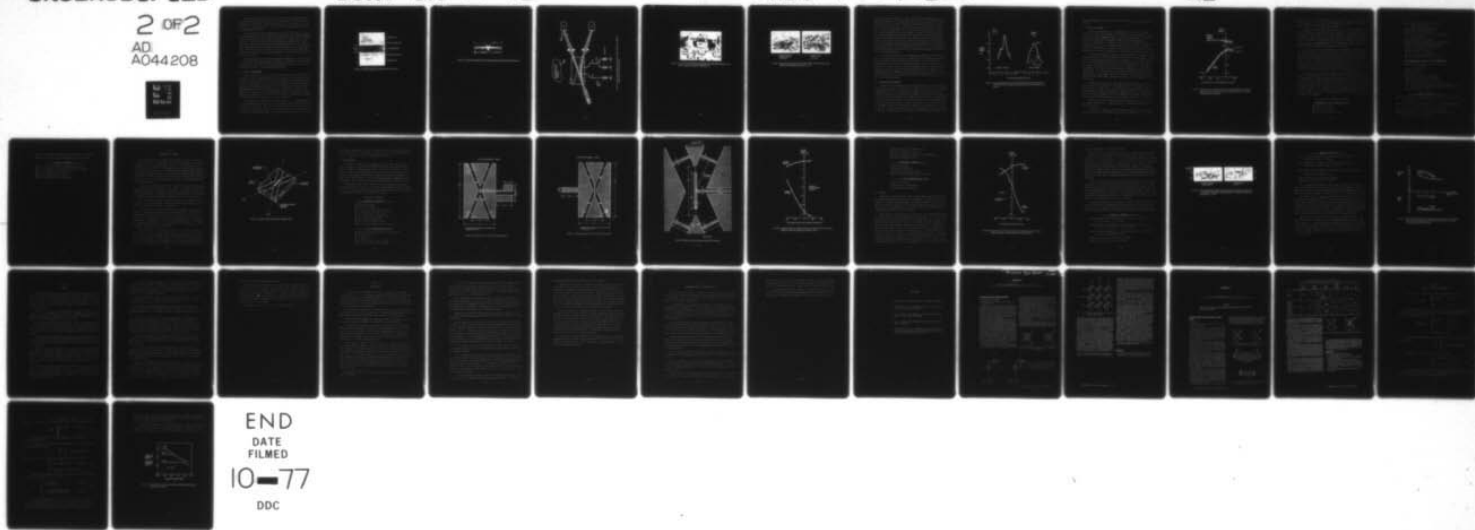
F30602-76-C-0129

UNCLASSIFIED

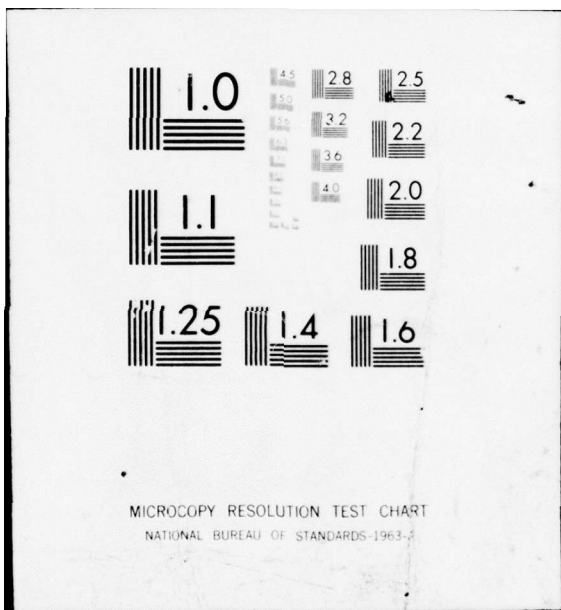
RADC-TR-77-260

NL

2 OF 2
AD
A044208



END
DATE
FILED
10-77
DDC



After the optical polishing steps, the ends of the crosspoint device have the appearance shown in the microscope photograph of Fig. 48, which illustrates the "sandwich" nature of the construction. A top view of the completed device (before wires are attached to the electrode pads) is shown in the photograph of Fig. 49.

The metalization layers applied to Devices #1 and #2 consisted of 500 Å of gold deposited on a 40 Å initial flash of chromium. Joule heating problems were encountered when these layers were "thinned". A third device was built 290 Å Au + 20 Å Cr electrodes, and when 400 Vdc was applied between surface electrodes, open circuits developed in high-resistance areas of the metal pattern. Thermal burn-out occurred in the narrow bridges across channels (Fig. 44). This difficulty did not arise in Devices #1 and #2. As an added precaution, current-limiting resistors (22 megohms in series) were introduced into the test circuit.

Although prior devices have withstood 550 V applied, we set "safe" limits lower than this during testing. To eliminate breakdown, potential differences of 450 V across the 2.5 mil crystal and 500 V across the 3 mil surface electrode gap were not exceeded during measurements.

8.3 INITIAL MEASUREMENTS

The set-up for the electro-optical measurements is shown in Fig. 50 and is similar to those employed before. Starting with a 20 µW cw focussed laser beam (that simulates fiber excitation), the switched and unswitched optical outputs are observed as shown. Light is collected with a near-field imaging lens (4x objective) whose aperture can be controlled with an iris (thereby determining the solid angle of observation). The magnified image of each channel-end is directed to a photomultiplier detector as indicated. The PMT aperture is adjusted so it looks at the channel end and nothing more. The PMT can be mechanically scanned in the transverse direction.

The crosspoint in operation is shown in Fig. 51. We took photographs of the near-field radiation pattern of the compound crosspoint under the Fig. 50 experimental conditions. The results are shown in Fig. 52. Much of the optical detail is obscured by the film's response, and it is more revealing to examine the intensity profile with a detector-plus-narrow-slit that is scanned

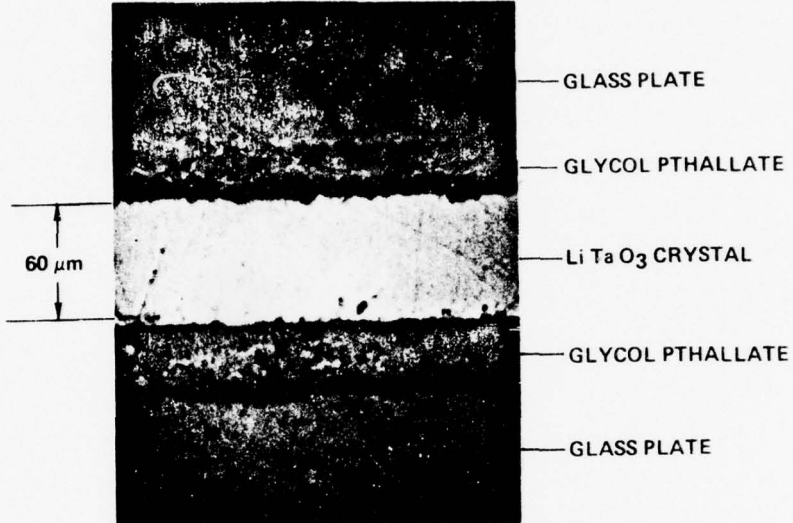


FIG. 48 Photomicrograph of polished end of CC-3-4 device.

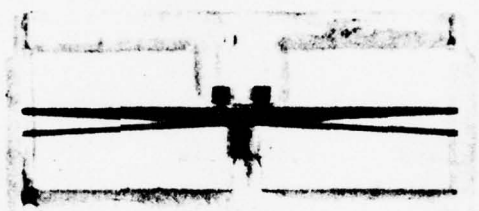


FIG. 49 Top view of actual CC-3-4 compound crosspoint device (improved version).

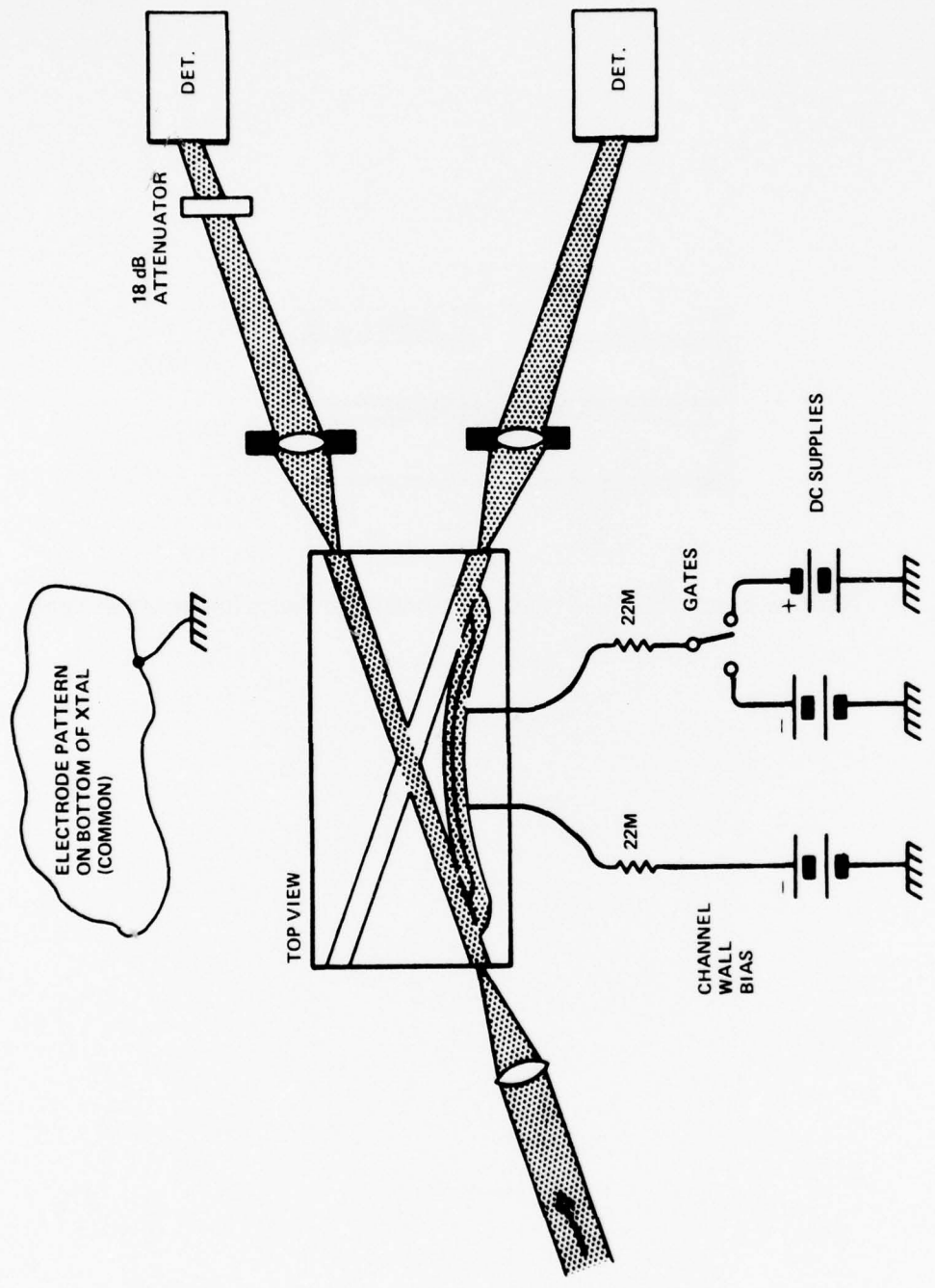


FIG. 50 Experimental arrangement for electro-optical signal and crosstalk measurements on CC-3-4 devices.

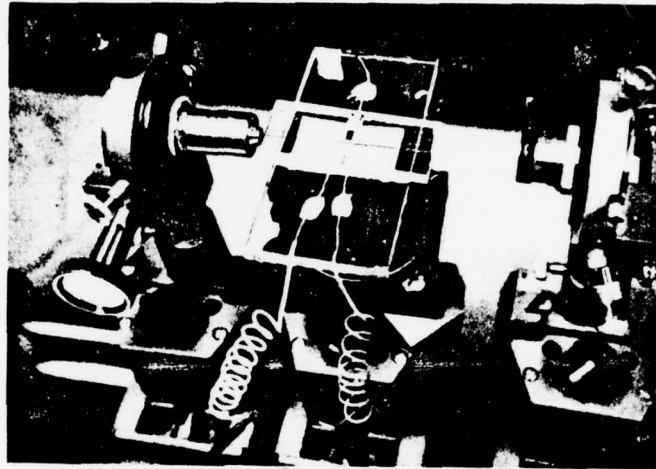


FIG. 51 Test of CC-3-4 device with convergent input light (20x objective at left) and 4x collector at right with adjustable iris.

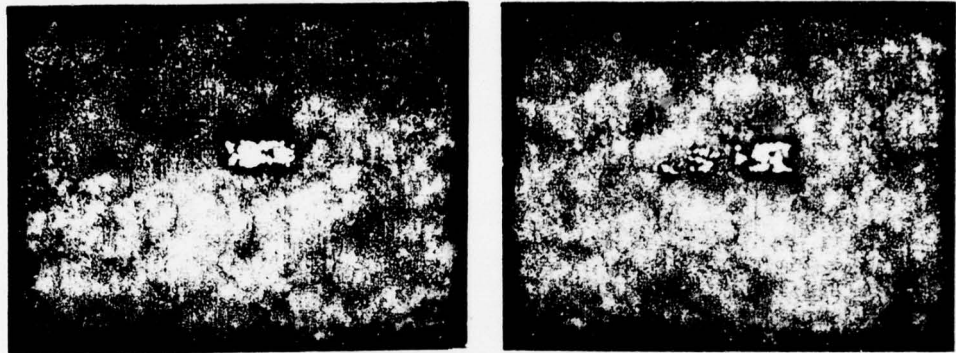


FIG. 52 Output light (both channels, near-field pattern) of CC-3-4 device with -385 Vdc wall bias, 20x input and $\theta_0 = \pm 10^\circ$.

across the optical emission. A 3 mm x 3 mm "slit" on the 42x image plane (which corresponds to a 3-mil-diameter fiber at the crosspoint end) was translated laterally over several cm with the near-field lens fixed in position exactly on the channel axis. This PMT scan was repeated for both channels. The voltages applied during the test were those that made the gates fully open or fully closed (See Sec. 8.5 below). The input electro-optic channel was excited symmetrically (on-axis) with the laser beam. The measured profiles of the excited-channel output and cross-channel output are plotted on a dB scale in Fig. 53. The exact location of the crosschannel on the image plane was determined from the peak of the light distribution seen in Fig. 53. The utility of this method was supported by the fact that the observed 30.1 cm separation between crosschannel and excited channel peaks was close to the 30.3 cm calculated spacing.

It is seen in Fig. 52 that opening the gates depletes the right-hand side of the excited channel by 1.5 to 3 dB, which is reasonable because only one side of the channel is opened electronically. With gates open, the switched light peak is down 9.8 dB from the input. It then drops 26 dB when the gates are closed. This is the scattered light profile or crosstalk distribution shown by the dotted line at the right in Fig. 53. There is an intensity minimum that coincides with the gates-open peak, and "wings" of leakage light are found on both sides of the valley. This behavior may be due in part to the spoiler action.

8.4 THROUGHPUT MEASUREMENTS

Throughput was measured by collecting light from an excited channel and comparing its strength to a free-space transmission value. All of the trapped light emerging from a 6-cm electro-optic channel in the crosspoint (gates closed) was collected and recorded with the PMT. The crosspoint was removed and the input light re-imaged onto the PMT. This measurement was repeated for 4x, 10x, and 20x input lenses. An optical reflection loss of 1.5 dB (air-to-crystal and crystal-to-air) was assumed in all three cases. We found the total throughput loss of the channel was 2.0 dB for 4x, 2.5 dB for 10x and 3.1 dB for 20x. Subtracting reflection loss, the propagation losses were 0.5 dB, 1.0 dB, and 1.6 dB respectively, over the 6 cm channel length; therefore, the

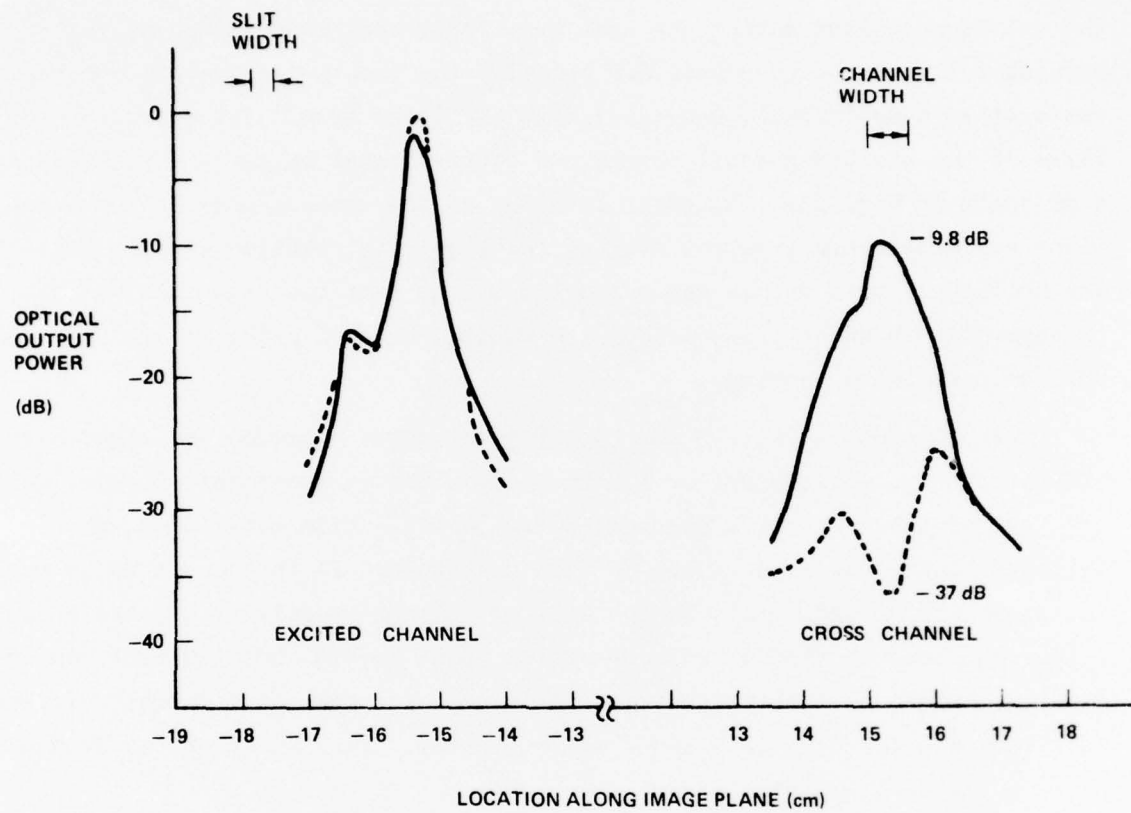


FIG. 53 Intensity distributions from straight-through channel and crosschannel of CC-3-4 device with gates closed (dotted curves) and gates open (solid curves).

observed propagation loss-constants were 0.09, 0.17, and 0.27 dB/cm, respectively.

8.5 FINAL MEASUREMENTS

Signal and crosstalk data was gathered with the Fig. 50 equipment. Setting the channel wall voltage at a constant value of -385 Vdc, the optical output of both compound-crosspoint channels was measured as a function of gate potential (V_g) in both polarity regimes. The negative-polarity lowers the crystal index and serves to close the gates. Though the gates are nominally open at $V_g = 0$, a "forward voltage" of 50 to 100 V is actually needed to cancel out the -50 V passive effect existing at the gates. The observed intensities for both devices (on a dB scale) are presented in Fig. 54.

Let us first discuss the tapoff ratio, which reaches a maximum at about +50 Vdc on the gate. Maximum tapoffs of -11 dB and -13 dB are found, at which point the excited channel power has been depleted by 1.5 to 2.5 dB. Conservation of energy indicates that the tap ratio should be greater: for example, in an ideal crosspoint, if the input channel is "drained" by 1.5 dB (71% throughput), then 29% of the energy should be transferred to the crosschannel, which is a -5.4 dB tap ratio. In practice, some of the initially gated light does not end up confined in the crosschannel. In the present example, 21% of the input (29% - 8%) is dispersed to other locations besides the cross-channel exit.

We find that the radiated light appears between channels and on the outer side of the crosschannel. We attribute most of this leakage in the CC-3-4 device to imperfections in the photoresist masks, primarily a small "scallop" effect in the curved channel. However, CC-3-4 has a 13 dB improvement in switched throughput over CC-1-2, therefore, the amount of light leaking out of the curved channel was much smaller than in CC-1-2 as planned.

Off-axis excitation of CC-3-4 gave an improvement of at most 1.5 dB in the tapoff, unlike CC-1-2. Perhaps the modes are more thermalized in the CC-3-4 input guide.

Turning to the switching ratio (crosschannel with gates open vs. gates closed), the results are favorable. These ratios ranged from 23 to 25 dB in

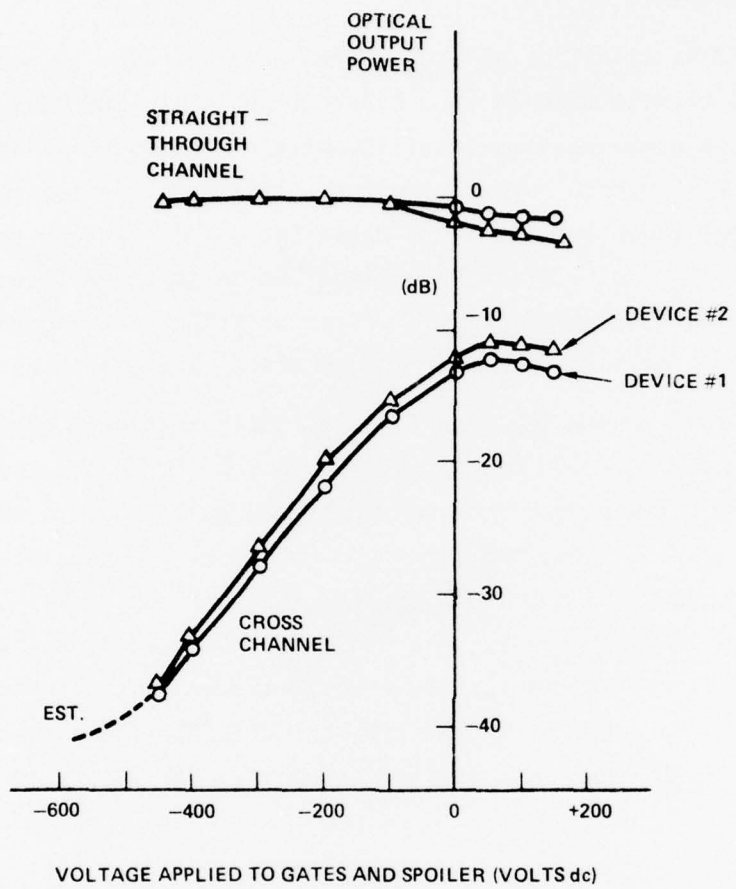


FIG. 54 Observed output of straight-through and crosschannels (on-axis optical excitation) for two improved compound crosspoint devices as a function of gate-and-spoiler potential.

Device #1 and 24 to 26 dB in Device #2, the largest we have observed thus far. It is interesting to note that these S/C ratios are as high as the largest values reported for single-mode switching (Ref. 4).

Before the passive effect faded, we were able to use wall biases of -100 to -200 Vdc and could make $|V_{\text{gate}}| > > |V_{\text{wall}}|$. In that case, it was found that the "noise level" in the crosschannel fell asymptotically to a plateau around -40 dB at highly negative gate voltages. Extrapolating from that result, we estimate that the crosstalk in Fig. 54 will decrease to a saturation value about -41 dB (dashed line in the Figure) at negative potentials of 550 to 600 V (not applied to avoid damaging the device).

For the most part, the curved-channel leakage problem in CC-1-2 has been solved in CC-3-4 in agreement with theory, as a comparison of tapoff results shows. Also, the optical isolation of the crosschannel with the gates closed is near -40 dB which agrees with our results for passive crossovers (Sec. 5.5, similar conditions), showing an internal consistency in the experimental results. Most importantly, the CC-3-4 devices have met the goal in the RADC Work Statement, that the optical switching ratio shall be within 5 dB of twice the switching ratio (in dB) achieved for the simple crossover.

The main drawback of this crosspoint is its length, which would be excessive for multimode optical matrix applications. It would be difficult, if not impossible, to integrate several CC-3-4 devices ($L \approx 6$ cm) into one crystal substrate for a complex, highly moded switching array. The reason is that present-day LiTaO_3 crystal plates (optical quality, Z-cut, 2-3mil) are limited in length to about 8 cm. Of course, a modular approach is possible -- column switching arrays, 6 to 8 cm wide, would be butt-coupled together into a matrix -- however, this is not a preferred approach, and a monolithic technique is judged to be superior.

Compound Crosspoint (Improved Version)

STRUCTURE, CC-3-4, DEVICES #1 and #2

- LiTaO_3 , Z-cut plate
- 62 μm plate thickness
- 5.8° channel crossover angle

- 175 μm channel width (electrode gap for straight and curved)
- 30 μm gate electrode width (both)
- 1.44 cm gate electrode length
- 0.8° initial branchoff angle of curved channel from crosspoints
- 25 μm spoiler electrode width
- spoiler located along midline of curved channel
- spoiler and gates connected electrically
- 2.6 cm arc length of curved channel
- 35.8 cm radius of curvature
- 6.0 cm overall length of device
- passive channeling equivalent to -40 Vdc

TEST CONDITIONS, DEVICES #1 and #2 (Fig. 54)

- focussed laser beam input ($\lambda = 0.63 \mu\text{m}$, 1.1 mm beam diam)
- TM polarized, $E \parallel z$
- 20x input lens
- $\pm 1.8^\circ$ input light cone in crystal
- $\pm 4.0^\circ$ input cone in air (0.07 NA)
- $\pm 2.2^\circ$ output collection cone in air
- 3 mm x 6 mm detector aperture on 42x image plane (collects from 72 μm x 144 μm region at channel end)
- -385 Vdc channel wall bias

RESULTS, DEVICE #1

- -9 to -11 dB optical tapoff ratio into crosschannel at $V_g = +50 \text{ Vdc}$ vs excited channel at $V_g = -450 \text{ Vdc}$.
- 24 to 26 dB optical switching ratio in crosschannel (signal-to-cross-talk ratio: open/closed gates; $V_g = +50 \text{ Vdc}$ vs $V_g = -450 \text{ Vdc}$)
- 1.5 dB optical reflection losses, input and output
- 1.6 dB estimated optical throughput loss of 6-cm-long excited channel at $V_g = -450 \text{ Vdc}$ (20x input)

- 36 pF capacitance of switching electrodes (gates and spoiler)
- 750 pF capacitance of bias electrodes (all channel walls)

RESULTS, DEVICE #2

- -11 to -13 optical tapoff ratio, device #1 voltages
- 23 to 25 dB optical switching ratio, device #1 voltages
- same transmission losses as device #1
- 35 pF gate-and-spoiler capacitance
- 720 pF capacitance of bias electrodes

Section 9
DEFLECTION CROSSPOINT

Modal properties of the fibers and crosspoints were not mentioned in the RADC Work Statement. Implicitly, the devices were supposed to work with single mode fibers and with multimode fibers up to some mode number to be specified at a future date. Since progress has been made by other researchers in single-mode matrixing, we concluded that the "highly moded" regime had the greatest unfulfilled needs, and that crosspoints would make the greatest contributions in fiber systems with ~ 0.14 NA and $75 - 85 \mu\text{m}$ fiber core diameter -- rather than in "quasi-single-mode" systems or in "weakly populated" fibers like NEC Selfoc.

However, this mode choice confronted us with the "real estate" problem for compound crosspoints discussed in Sec. 8.5. We therefore sought an approach more amenable to matrixing and looked for a switching structure that would offer performance comparable to (or better than) CC-3-4 in a much shorter switching length, while retaining simplicity and ease of manufacture.

This investigation occupied a brief period and was an exploration of alternatives to tandem switching. However, we did keep the four-port geometry and the four-stripe electro-optic channeling.

We used some novel concepts proposed by D. H. McMahon of our laboratory. Light was controllably directed between merged channels by a single, compact light-deflection structure. The electrically alterable deflection element was placed at the intersection of in-plane crossed channels. We arrived at the four-port switching device shown in the drawing of Fig. 55. Our familiar top-and-bottom electrode layers were included, and the crosspoint was again a monolithic, all-electro-optic structure.

The switch operates as follows. First, if the deflection stripe is at zero potential, there is no index perturbation in the crystal and this region is transparent to incoming light. Thus, trapped light beams intersect without interacting, giving a "perfect cross" state. For the second switching state, a negative potential is applied to the deflection-bar, thereby lowering the crystal's index locally in a vertical plane, creating a mirror (or more

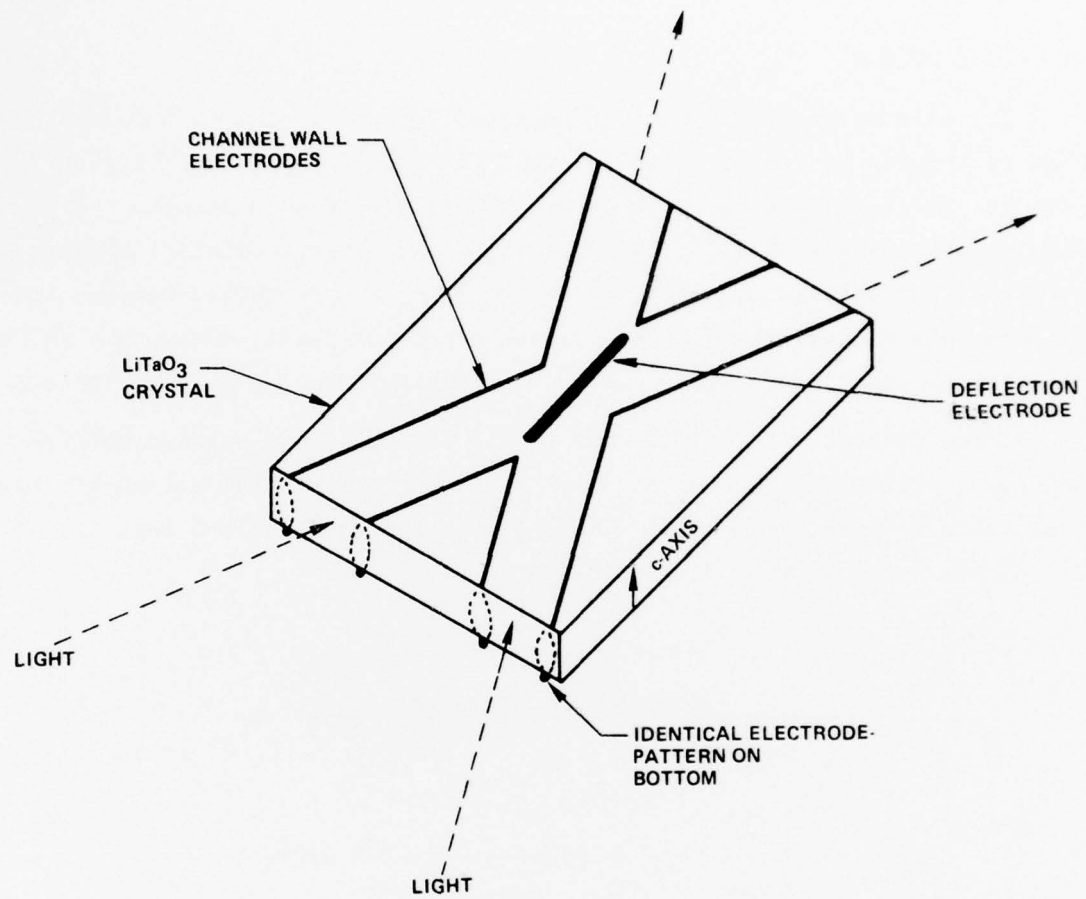


FIG. 55 Layout of four-port deflection crosspoint device.

accurately, a beamsplitter) along the angle-bisector of the channel intersection. Part of the incident light is sent (tapped) to the crosschannel, which again is a multimode, achromatic power-division process.

9.1 CONSTRUCTION

The pair of photoresist masks employed for crosspoint construction are shown in Figures 56 and 57, with a detail in Fig. 58. The 1-mil deflector width was chosen by analogy with previous spoiler and gate results. A waveguide crossing angle of 3.6° , which is twice the maximum critical angle, was selected. For voltage standoff, 4-mil separations were chosen between the deflector and channel walls at the closest-approach point, making the channels 9 mils wide. The interaction length or switching region was 300 mils long.

Three devices were constructed and tested. All had passive optical channeling equivalent to -100 to -180 Vdc. The measurement set-up was identical to that shown in Fig. 50. The crosspoint parameters and test conditions are summarized below for two representative samples.

Deflection Crosspoint

STRUCTURE, DEVICE #1

- LiTaO₃, Z-cut plate
- 75 μm plate thickness
- 225 μm channel width (electrode gap)
- 25 μm deflector electrode width
- 0.71 cm deflector electrode length
- 3.6° channel crossing angle
- 1.7 cm overall length of device
- passive channeling equivalent to -120 Vdc

TEST CONDITIONS (Fig. 59)

- focussed 0.63 μm laser beam, (1.1 mm beam diam)
- TM polarized, E \parallel Z
- 20x input lens
- $\pm 1.8^{\circ}$ input light cone in crystal
- $\pm 4.0^{\circ}$ input cone in air (0.07 NA)

DEFLECTION CROSSPOINT - MASK-1

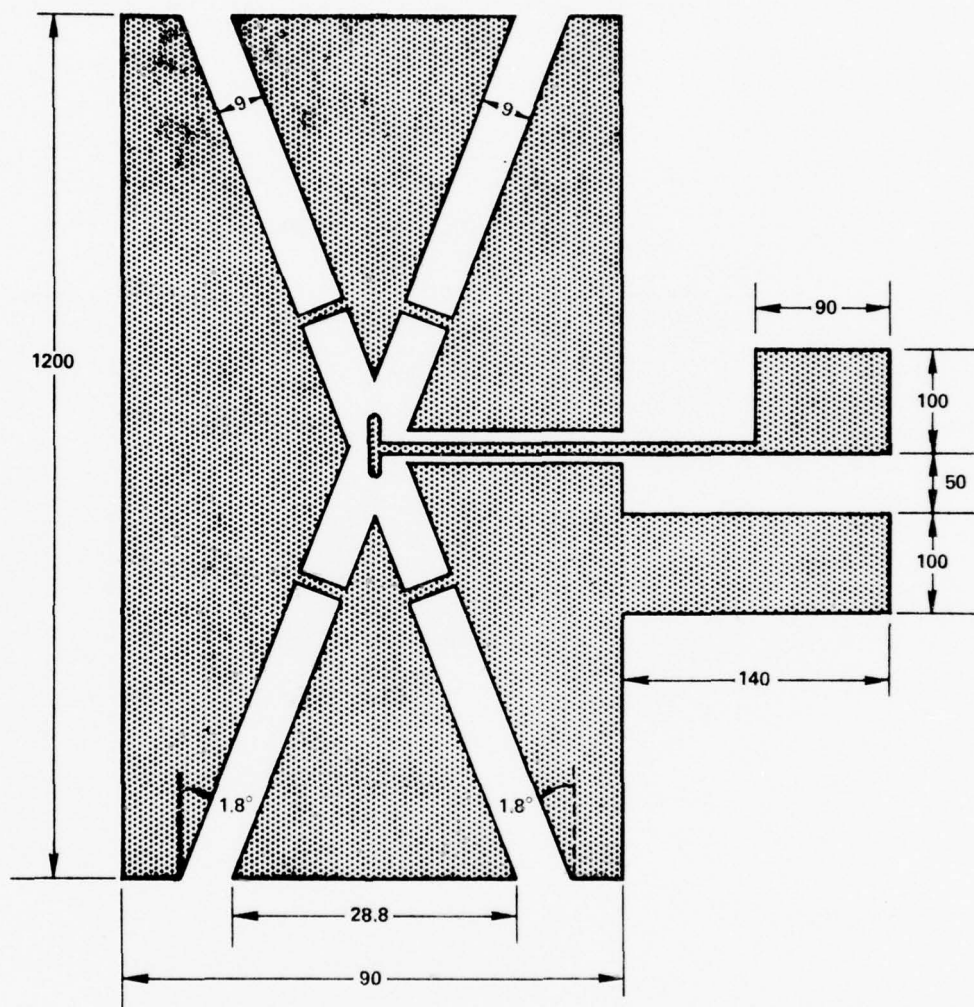
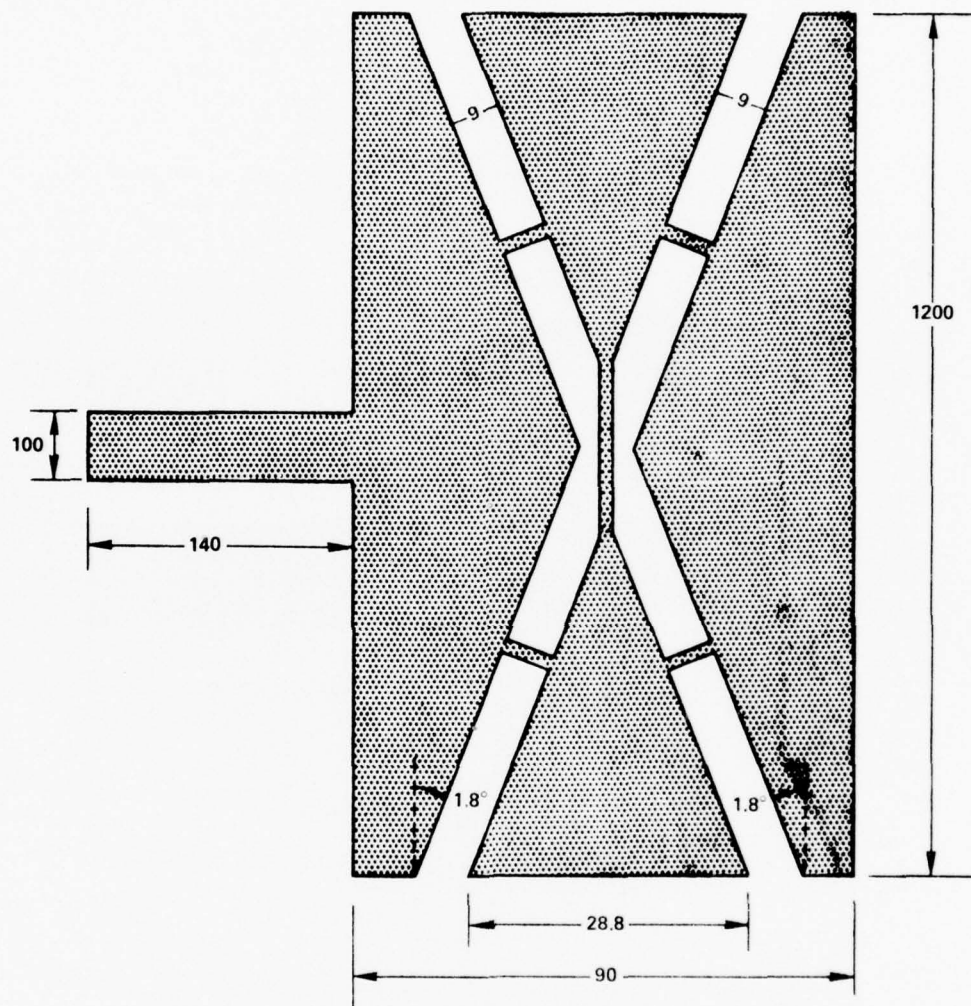


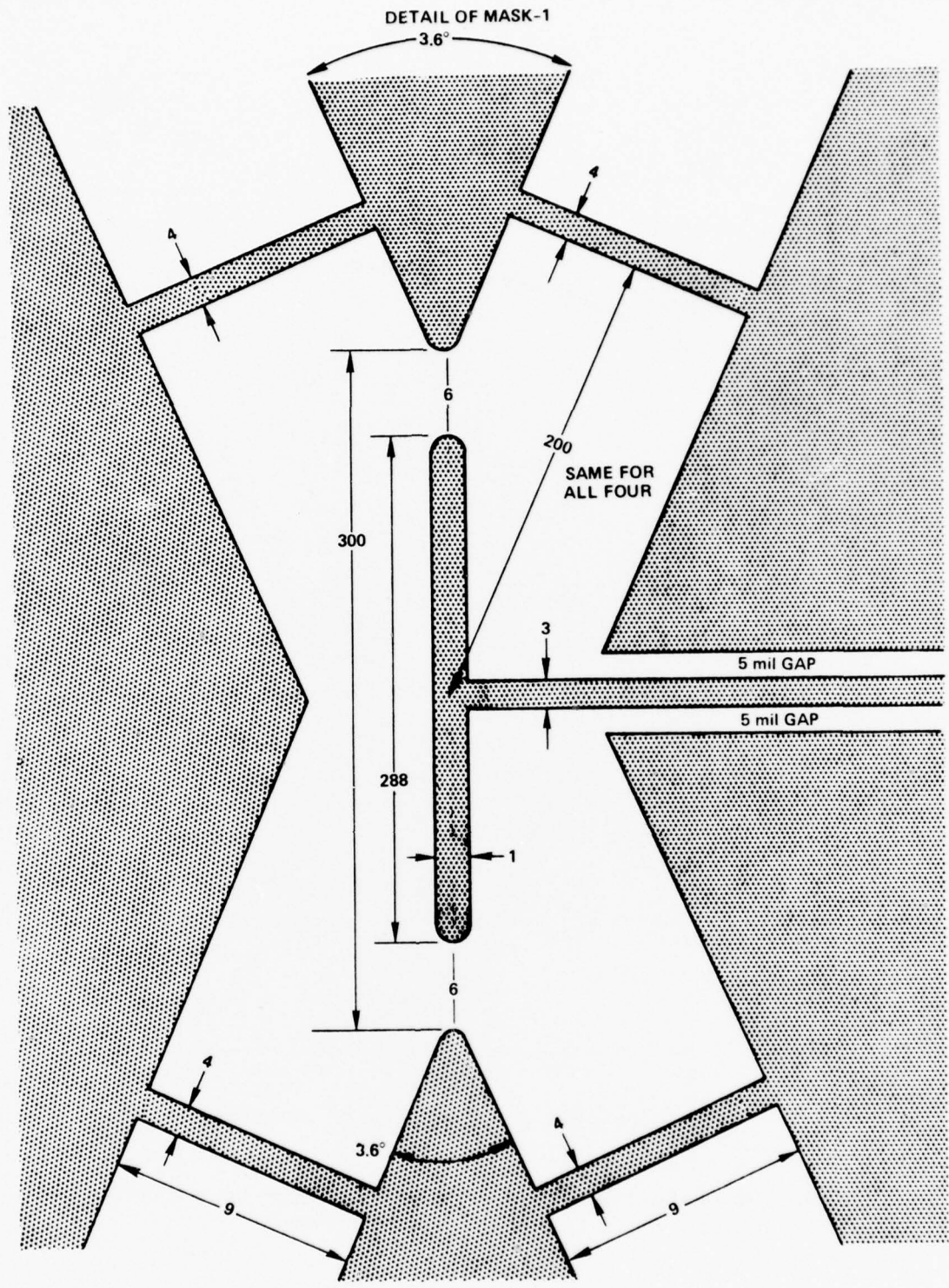
FIG. 56 Photoresist mask for actual Fig. 55 device (side A).

DEFLECTION CROSSPOINT - MASK-2



SHADED AREAS TRANSPARENT ON FINAL MASK.
DIMENSIONS IN MILS

FIG. 57 Photoresist mask for actual Fig. 55 device (side B).



NOT TO SCALE

FIG. 58 Detail of side A photoresist mask for Fig. 55 device.

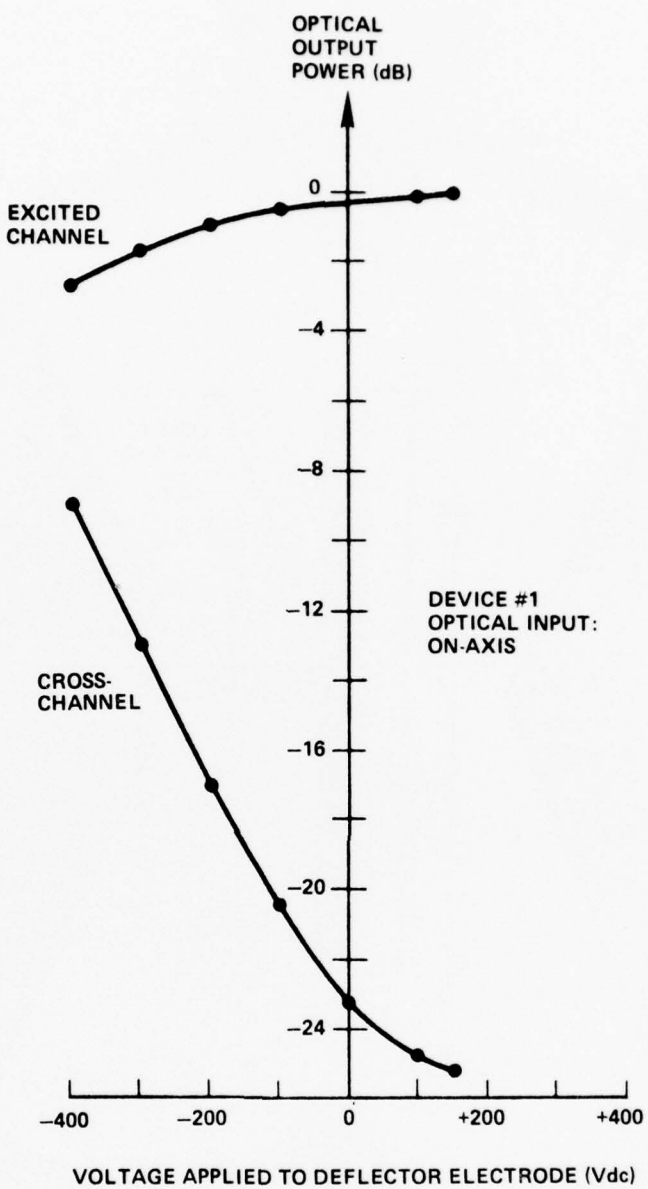


FIG. 59 Observed output of straight-through and crosschannels as a function of deflector voltage for a deflection-crosspoint device.

- input beam is on the channel axis
- $\pm 2.0^\circ$ collection cone in air
- 3 mm x 6 mm detector aperture on 40x image plane
- -250 Vdc channel wall bias

STRUCTURE, DEVICE #2

Same as #1, except:

- 53 μm plate thickness
- 2.9 cm overall length of device
- passive channeling equivalent to -180 Vdc

TEST CONDITIONS (Fig. 60)

Same as #1, except:

- input beam is 25 μm off-axis
- -100 Vdc channel wall bias

9.2 RESULTS

Preliminary results are given here. The observed outputs of the switched and unswitched channels in Device #1 are given on a dB scale in Fig. 59 as a function of deflector voltage (V_d) in both polarity regimes. As in prior devices, a positive potential on the switching electrode was needed to cancel out the passive lower-index effect under this stripe. The negative applied voltage induces reflective power splitting.

This sample was optically excited on the axis of one electro-optic channel; (the input beam was collinear with the axis and centered on it). But it is not clear that the mode distribution is "thermalized" when it reaches the deflector (that might require several cm of travel). For the symmetrical optical excitation, the measured tapoff ratio was -8.8 dB at $V_d = -400$ Vdc (a potential that differs by 500 V from the channel wall bias). There is evidence to suggest that the optical tapoff would reach a plateau of -7 dB at about -600 V, but that would have exceeded our safe-voltage limit. Generally, the light transfer was as good as in the improved compound crosspoint. The on/off switching ratio of this deflection crosspoint was 16 to 17 dB under the above-mentioned conditions. Optical throughput loss of the unswitched channel,

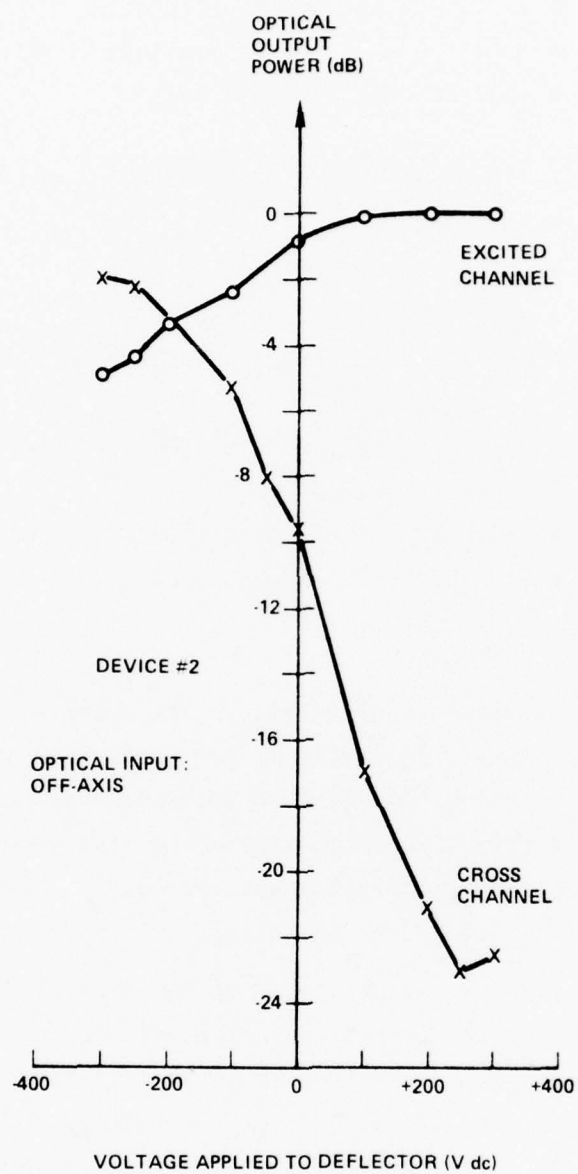


FIG. 60 Observed output of straight-through and crosschannels as a function of deflector voltage for a second deflection-crosspoint device.

including reflections was estimated at 2 dB.

The percent of input light diverted into the crosschannel went up when the optical input was off-axis. In the experiment, the convergent input beam was moved 25 μm laterally off-axis in the crystallographic X-direction, though the beam axis was still parallel to the channel axis. As a result, light rays did not bounce symmetrically in the channel. For an input "packet", the bounce locations on one wall did not line up with a similar set of bounce-points on the opposite wall. Rays may have bounced just before the intersection in the present off-axis experiment, or in the crosschannel beyond the deflector. In other words, a compound deflection may be occurring in the off-axis case.

Optical switching results for Device #2 with off-axis input are presented in Fig. 60. Here, the induced reflection was strong, with a -2 dB tapoff being found, along with a 5 dB depletion of the optical input beam. The observed switching ratio was 21 dB in this case, which is nearly as high as that in the improved compound crosspoint. In the reflective state ($V_d = -300$ Vdc), power division reached a maximum, and a minimum optical scattering level was found in the "transparent" state at $V_d = +250$ Vdc.

Near-field radiation patterns from the output end of crosspoint #2 are shown in the Fig. 61 photographs (for both switching states). The channel cross-sections are elongated because this device was only 53 μm thick. The electro-optical performance of the deflection crosspoints is tabulated here:

RESULTS, DEVICE #1

- -8.8 dB optical tapoff ratio (crosschannel, $V_d = -400$ Vdc vs excited channel, $V_d = +150$ Vdc)
- 16.6 dB optical switching ratio (signal-to-crosstalk of cross-channel, $V_d = -400$ Vdc vs $V_d = +150$ Vdc)
- 2 dB estimated throughput loss (excited channel, $V_d = +150$ Vdc) including both reflection losses
- 5.9 pF capacitance of deflector electrode
- 128 pF capacitance of bias electrodes



FIG. 61 Light output (both channels, near-field pattern) of deflection crosspoint in reflective and transparent-deflector states with -100 Vdc wall bias, 20x input, and $\theta_0 = \pm 1.2^\circ$.

RESULTS, DEVICE #2

- -2.0 dB optical tapoff ratio (crosschannel, $V_d = -300$ Vdc vs excited channel, $V_d = +250$ Vdc)
- 21.0 dB optical switching ratio (signal-to-crosstalk of cross-channel, $V_d = -300$ Vdc vs $V_d = +250$ Vdc)
- 2.3 dB estimated throughput loss (excited channel, $V_d = +250$ Vdc) including both reflection losses
- 6.7 pF capacitance of deflector electrode
- 198 pF capacitance of bias electrodes

We also measured the influence of the output collection cone. The results are presented in Fig. 62. The switching ratio increased at small cone angles but the tap ratio was unaffected. Not shown in the Figure is a 5 dB decrease in optical throughput in going from $\pm 3^\circ$ to $\pm 1^\circ$ (input fixed at $\pm 4^\circ$).

Time did not permit a thorough analysis of the optical noise sources in the deflection crosspoint, but the 3.6° crossing angle seemed to play an important role. Because this angle is relatively small, the observed crosschannel isolation was about -25 dB compared to the -39 dB gate-closed isolation of CC-3-4, whose crossover angle was 5.8° . We attribute most of the optical crosstalk to trapped scattering at the channel intersection (a single-scattering process unlike the two-fold process deduced for the compound switch).

There are several means for improving the crosstalk performance of the deflection switch. Clearly, one way is to raise the channel crossing angle. This can be done, in principle, without significantly reducing the tap ratio. A 20 to 30% increase seems feasible. As the crossover angle is increased, the single-scattering diminishes in intensity until a weaker, higher-order scattering is observed. Additional crosstalk-reduction techniques are discussed in Sec. 11 below.

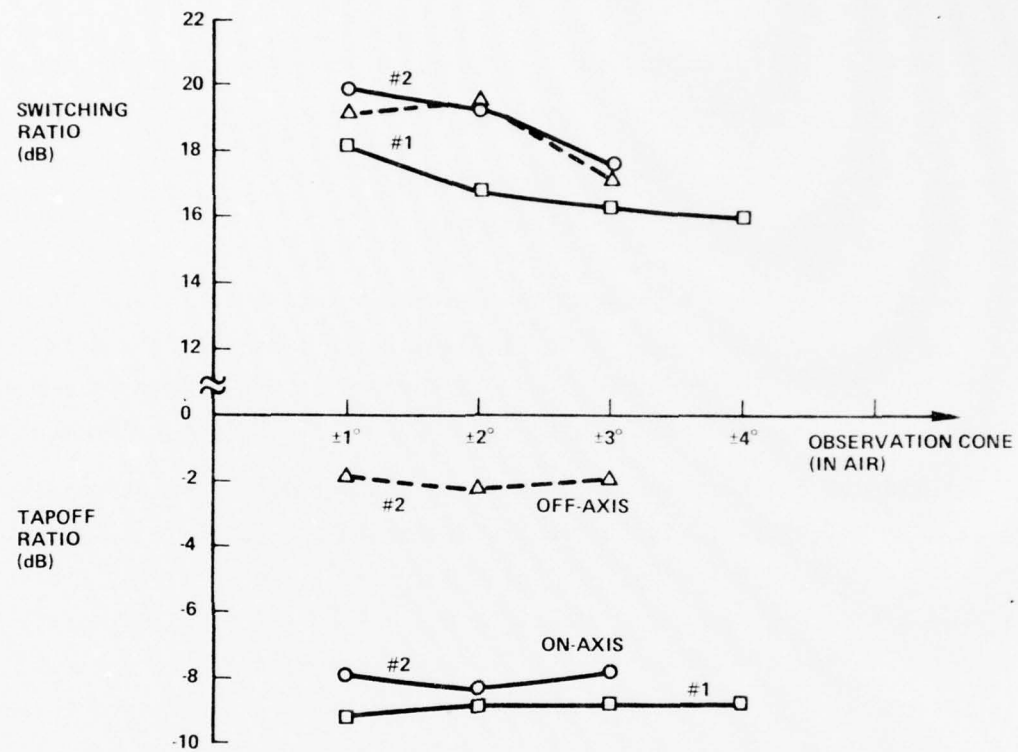


FIG. 62 Optical switching ratio and optical tapoff ratio as a function of observation cone angle for two deflection-crosspoint devices. Data for on-axis and off-axis optical excitation is shown.

Section 10

SUMMARY

A variety of multimode optical waveguiding and switching structures have been demonstrated experimentally: straight and gently curved channels, channels that intersected in a plane at 3.6° to 6.3° , simple crosspoint switches, compound crosspoint switches, and deflection crosspoint switches. All of the crosspoint devices are tapoff switches intended for integration into an optical crossbar matrix.

Early in the contract, an all-electro-optic approach in LiTaO_3 was chosen over a solid-state-diffusion approach (Cu^{++} in LiNbO_3). The reasons included lower attenuation, simpler construction, better interfacing with fibers, and a higher probability of success in switching.

The electro-optic substrate consisted of an optically polished, single-crystal Z-cut plate of LiTaO_3 or LiNbO_3 . A 50 to 75 μm plate thickness was chosen for low-loss butt coupling to commercial multimode fibers having similar core sizes. Crystals are ultrapure (undoped) and free from striae and domains.

Technology has been developed for handling and processing these thin plates, including photolithographic methods for defining metal electrodes on both plate surfaces and optical polishing of the crystal ends for direct coupling to fibers.

Waveguiding regions were created in the crystal by steady applied electric fields. A quadripole structure was preferred for channeling, with light guided in the crystal between parallel stripe electrodes, two on the top surface and two on the bottom. (Low propagation losses made it unnecessary to have a lower-index dielectric cladding layer between each electrode and the crystal).

For optical switching, electrically controlled reflection was used. A portion of the optical channel wall was turned on and off electrically to gate the multimode trapped light. Or, a controllable deflection element (top-and-bottom line-segment electrodes) was inserted into the optical channel at a small angle to the axis.

All devices used the principle of total reflection by grazing incidence on a lower-index "barrier". The barrier is a localized region of lower index induced in the crystal by external fields. These index gradients are capable of reflecting multimode light over a $\pm 1.6^\circ$ range of angles and they are achromatic (not wavelength-sensitive).

Multimode optical excitation of the devices was obtained with a focussed He-Ne laser beam ($\lambda = 0.63 \mu\text{m}$) that simulated optical fiber excitation. The convergent input beam had a numerical aperture of 0.07.

The following experimental results were obtained. The electro-optic channels intersecting at 6° were optically isolated from one another by 36 to 44 dB, depending upon the solid angle of light collected from the channel outputs.

The simple crosspoint was a three-port switch with an 0.9° separation between main and branch channels, and a gate electrode located where those channels joined. The gate-closed isolation of the branch was improved by positioning a thin, negative-potential electrode ("spoiler") down the midline of the branch to divert stray light. The optical tapoff ratio was about -5 dB and the gate-open/gate-closed optical switching ratio was about 12 dB.

The compound crosspoint is a four-port device comprised of two simple crosspoints and a 5.8° channel crossover. Each of the intersecting channels had a gate in one wall, and those gates were connected optically by a gently curved channel.

In an initial version of the compound crosspoint, the tapoff ratio was unexpectedly low because large amounts of light leaked out of the curved guide. The radius of curvature had been made too small. This difficulty was remedied in a second-generation device whose length was greater in order to accomodate a more gradual bend.

The improved compound crosspoint had a tapoff ratio of -9 to -12 dB, and the optical switching ratio (signal-to-crosstalk ratio of the crosschannel) ranged from 24 to 26 dB. The gates-closed crosstalk level of the crosschannel was approximately 40 dB below the optical input level. The control voltage in dc tests was about 450 Vdc and a 390 Vdc bias was also required on the channel walls. Optical transmission loss through the 6-cm-long device was 3 dB,

including both switch/air reflection losses.

A deflection crosspoint with an 0.8 cm switching length (about 15% of the compound crosspoint length) was demonstrated. This four-port switch contained a 3.6° channel crossover. Under test conditions similar to the compound device, the deflector switch had a -2 to -9 dB tapoff ratio (depending on whether the input beam was aligned on or off the channel axis) and the optical switching ratio ranged from 16 to 20 dB, with the control voltages again in the 400 to 500 V range.

The implications of these results are discussed below.

Section 11

CONCLUSIONS

The optical crosstalk between channels is an inplane electro-optic crossover for $\phi \geq 5^\circ$ is limited by a double-scattering process. The optical noise consists mainly of unguided light. It is scattered at the input surface and travels to the output surface where it is re-scattered. The signal-to-crosstalk ratio of the compound crosspoint (as presently constructed) is governed by this scattering process.

The signal-to-crosstalk ratio of the deflection crosspoint (as presently constructed with $\phi = 3.6^\circ$) is governed by a single-scattering process in which guided light is redirected into the other channel at the intersection.

Between LiTaO_3 and LiNbO_3 , the preferred material is LiTaO_3 because of its purity, quality, and minimal susceptibility to optical damage.

The 0.07 NA focussed laser beam input is a good simulation of 0.14 NA fiber excitation because the 2:1 input collimation procedure recently demonstrated by Nelson and McMahon of our laboratory (Ref. 5) will give the same optical input distribution in the crystal, starting with a 0.14 NA fiber. Using this 2:1 arrangement, our 3-mil \times \sim 8-mil electro-optic channels are compatible with a 3-mil core-diameter fiber.

When fibers are coupled at normal incidence, the 3 dB insertion loss of a polarizer should be added to the loss cited above. However, in practice, one is likely to use non-normal incidence (Snell's Law collimation) for both the input and output fibers. Typically, the fibers are terminated at 73° and the crystal cut at 44° (See Fig. 3). In that case, no polarizer is needed and the crosspoints will switch both the TE and TM polarizations launched by the fiber. (Switching is 50% weaker for TE light since the r_{13} coefficient is about 25% that of r_{33}). If anti-reflection coatings are put on the crystal ends, the reflection losses are about 1 dB (mostly TM loss) in the fiber-collimation case.

The present devices can couple to graded or step index fibers and will work with either.

How well are the goals of the Work Statement met in the compound crosspoint? The goal of attaining a switching ratio within 5 dB of twice the switching ratio (in dB) of the simple crosspoint has been met. Because the propagation loss was 0.3 dB/cm, we have come close to meeting the goal of 0.5 dB transmission loss in the unswitched state.

The measured optical isolation was four to five orders of magnitude away from the 80 dB goal. We do not know whether this goal will be met in future multimode (or single mode) switches, but we believe that improvement over the present level is possible. We speculate that a 10 to 20 dB decrease in scattering will be obtainable by means spelled out below.

Inherently, the Pockel's effect response of LiTaO_3 is very fast, so the 100 nanosecond switching rate goal should be attainable, but this has not been verified yet.

The wavelength goal has been met. Because the electro-optic coefficient is "flat" and the crystal is transparent in the near-infrared, we fully expect the 1- μm switching performance to equal that at 0.63 μm . In a brief experiment, we took a $\lambda = 0.90 \mu\text{m}$ pulsed GaAs diode laser, launched its emission into a Corning fiber and butt-coupled this infrared fiber light into the deflection crosspoint. A thin Polaroid HR infrared polarizer was interposed between the switch and the two butt-coupled fibers at the output. Qualitatively, the observed switching action was the same as for the visible laser input.

A transmission of 10% to 15% was attained in the compound crosspoint's switched state, which is not very far from the 32% goal. Lower transmission loss appears feasible.

It is interesting to compare the compound crosspoint performance to that of state-of-the-art single-mode switches. Probably the best single-mode results are found in the reversed ΔS switch of Schmidt and Kogelnick (Ref. 4). There the minimum crosstalk level was -26 dB which is comparable with our multimode result. The single mode energy switched into the crossarm was 80%, compared to the 12% (multimode) achieved here. In these respects, the crosspoint compares favorably.

The maximum length of optical quality Z-cut LiTaO_3 is presently 6 to 8 cm; hence the 6 cm length of the improved compound crosspoint is prohibitive

for making monolithic arrays (matrices) of these devices.

Although overly long for a matrix, the compound crosspoint has value as a switchable access coupler for an optical data bus, particularly if the crosspoint is modified by adding a second pair of gates and a second curved connecting channel symmetric with the first. Using the four ports, this device can serve as a terminal that sends and receives information. Its tapoff ratio is adjustable, its off-state isolation is high, it is end-fire compatible with a variety of fibers, and its insertion loss is "moderate" (although not as low as passive couplers). Generally speaking, the electro-optic devices of this contract have applications in addition to matrixing.

The 0.8 cm deflector crosspoint length is well suited for fabricating integrated arrays in existing crystals. Design changes are available for increasing the optical switching ratio of the deflection crosspoint, possibly into the 30 to 40 dB range. Among the means for crosstalk reduction are: 1) volume absorbers put into the crystal to absorb unguided light, but not to interfere with optical signal paths; 2) surface absorbers put on to stop stray light; and 3) electro-optic spoiler electrodes added to the crystal perimeter to deviate undesired light. In-diffusion, sputtering, and ion-implantation can be used to make the absorbers.

A two-fold or three-fold reduction in crosspoint length is possible by shrinking the channel width in that proportion. But that would necessitate reducing the plate thickness to $\sim 25 \mu\text{m}$, which in turn would require a small-core, quasi-single-mode fiber.

Section 12

RECOMMENDATIONS FOR FURTHER WORK

The deflection crosspoint is useful as it stands, but improved switching ratios are feasible and desireable. We recommend experiments with intersection angles in the 4 to 5° range and channel widths in the 8 to 10 mil range to find optimum performance.

We recommend that an optical matrix switch be constructed from optimized deflection crosspoints. A 3 × 3 crossbar array of these switches (including connecting waveguides) could be monolithically integrated into a 3" × $\frac{1}{2}$ " × 2.5 mil LiTaO₃ substrate. The processing techniques to do this are already in hand because similar-size devices have been constructed under the present contract.

We recommend mating the matrix to commercial multimode fibers (e.g. Corning, step index, 85 μm core, 0.14 NA) with a 2.5:1 Snell's Law collimation at input and output ends of the crossbar. Crystal ends would be cut at 44° to the channel axis and fibers terminated at 73° for oblique butt coupling to the matrix (a single strand being used for each information channel).

Further elucidation of optical crosstalk sources and mechanisms is needed. For example, volume and surface scattering from crystal imperfections has been discussed, but other sources may have been overlooked, such as scattering from irregularities in the fringing-field boundaries of the electro-optic channels.

From a device-manufacturing standpoint, it would be worthwhile to understand the passive waveguiding effect better and to control it more accurately.

Practical solid-state materials with higher electro-optic coefficients would allow smaller crosspoints with better switching performance. However, this is a long-term proposition as the history of electro-optic crystal development has shown.

Liquid crystal materials (primarily nematics) offer a means for getting better multimode crosspoints if millisecond response times are acceptable.

which may be the case in message-switching applications. The electrically controlled birefringence, $\Delta n \sim 0.2$, would be a boon to switching if scattering losses could be kept beneath 1 dB/cm with stabilizing electric fields.

By reducing the dimensions of present structures, novel devices should result in the realm of single-mode switching (or of switching just a few modes). This may require new techniques to handle the thinner crystals.

REFERENCES

1. D. J. Channin, Appl. Phys. Letters, 19, 128 (1971).
2. A. R. Nelson, D. H. McMahon, and R. L. Gravel, Appl. Phys. Letters, 28, 32 (1976).
3. R. A. Soref, D. H. McMahon, and A. R. Nelson, Appl. Phys. Letters, 28, 718 (1976).
4. R. V. Schmidt and H. Kogelnick, Appl. Phys. Letters, 28, 503 (1976).
5. A. R. Nelson and D. H. McMahon, Electro-Optics/Laser Conference, paper II.2, (Digest of Technical Papers, page 36) New York, Sept. 14, 1976.

APPENDIX A

Reprinted from **APPLIED OPTICS**, Vol. 14, page 2559, November 1975
 Copyright 1975 by the Optical Society of America and reprinted by permission of the copyright owner

Crosstalk reduction in optical switching

R. A. Soref and L. R. Schissler

Sperry Research Center, Sudbury, Massachusetts 01776.
 Received 31 May 1975.

All optical switches, in practice, send some fraction of their input light to the wrong output ports. This optical crosstalk occurs because the structural and operational parameters of the optical switch cannot be controlled with sufficient accuracy or because of sensitivity to changes in ambient conditions. The attempt to achieve low crosstalk may impose constraints on the switch's construction or environment that cannot readily be met. Therefore, an alternate way of reducing crosstalk is needed.

This Letter presents a technique for improving the crosstalk properties of any type of optical switch. The technique proposed here is to build a composite optical switch from two or more individual switches and to absorb leakage light by terminating the unused ports of the composite. The composite is functionally equivalent to a single switch but reduces the crosstalk geometrically in proportion to the number of single-switch structures used. Although the increased number of elementary switches increases the system complexity, it does represent a means for achieving higher switching performance. It also may reduce over-all cost by relaxing manufacturing tolerances. The compounding of optical switches is analogous to a method found in the electrical art where an improved on/off ratio in rf switching has been attained with a series-shunt or series-shunt-series arrangement of transistors.

An important application of low crosstalk optical switches is in an optical matrix whose function is to make an alterable interconnection of m optical fibers with a second

group of m fibers. A one-to-one mapping of inputs onto outputs is generally desired. For this function, an $m \times m$ array of composite low crosstalk four-port optical reversing switches can be used in a crossbar geometry where m out of m^2 crosspoints are actuated (one per row and one per column). For the composite crosspoint switches, one can use a pair of elementary four-port reversing switches.

The two states of each elementary optical switch are shown symbolically in Fig. 1. The optical leakage or crosstalk is denoted by ϵ_a in state A (the off-state) and ϵ_b in state B (the on-state). In the X and Y input channels, the optical signal strength is assumed to be unity, though the leakages ϵ_a and ϵ_b are, by definition, much less than unity. At each output port of the switch, the signal-to-crosstalk ratio (S/C ratio) is $(1 - \epsilon_a)/\epsilon_a$ in the off-state and $(1 - \epsilon_b)/\epsilon_b$ in the on-state.

Figure 2 illustrates symbolically how a low-crosstalk switch is created by joining two elementary devices with their off-state leakages in cascade. Figure 2 shows the on- and off-states of the composite in the circuit representa-

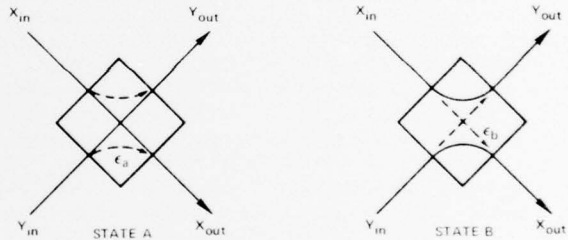


Fig. 1. Schematic model of four-port optical reversing switch (both states). Solid lines are desired signal paths; dashed lines denote crosstalk paths.

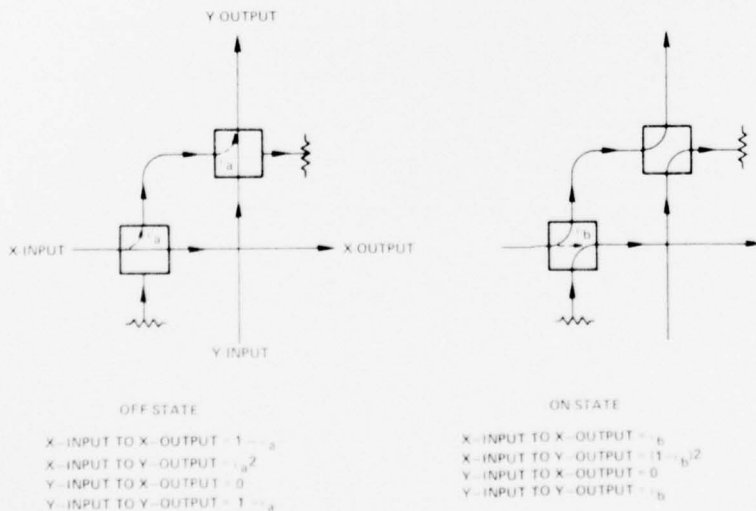


Fig. 2. Circuit representation of low crosstalk optical crosspoint switch constructed from two four-port reversing switches. On- and off-states of composite switch are shown. Output signal and crosstalk levels are indicated.

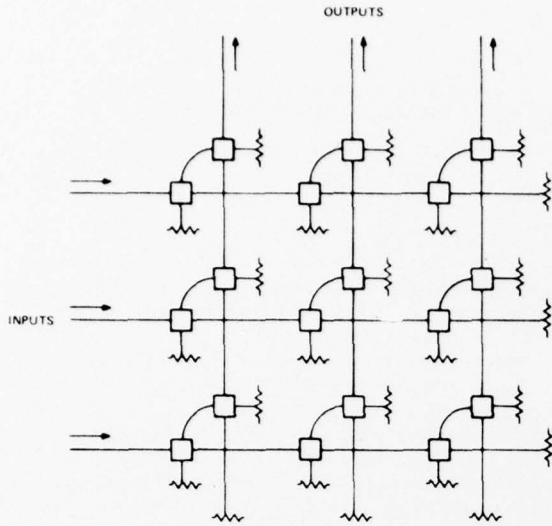


Fig. 3. Low crosstalk 3×3 optical matrix switch comprised of composite optical crosspoints.

tion, where the arrowed lines denote light paths, the squares are optical switches, and the resistors denote non-reflecting optical terminations. These terminations could be portions of the optical waveguide material that have been doped to have a strong absorption band at the wavelengths of interest. The tandem switch has the property that its S/C ratio at the Y output port is $(1 - \epsilon_a)/\epsilon_a^2$ in the off-state and $(1 - \epsilon_b)^2/\epsilon_b$ in the on-state. It is clear that the Fig. 2 scheme can be extended to more than two switches per composite to improve performance still further.

We now consider the matrix signal and crosstalk properties of the Fig. 2 tandem structure. The Fig. 2 composites are connected into a crossbar array with the X channels as matrix rows and the Y channels as matrix columns. The matrix inputs and outputs are X inputs and Y outputs, respectively. The X outputs at the end of each row are unused, and these m ports are terminated to suppress the on-state leakage ϵ_b . This aids considerably in minimizing crosstalk at the matrix outputs. Similarly, the m unused Y inputs at the beginning of each column are terminated to minimize spurious signals. The matrix procedure described here is illustrated in Fig. 3 for the example of $m = 3$.

The S/C ratio varies from port to port among the m output ports of the matrix. Also, the S/C ratio depends on

which set of crosspoints has been addressed. We have analyzed the matrix S/C ratio and have determined that the lowest S/C values are found at the first-column output of the matrix. Examining the m addressing possibilities for this column, we further find that the minimum S/C ratio (which is the worst case S/C ratio for the entire tandemized $m \times m$ matrix) is approximately $(1 - \epsilon_b)^2/(m - 1)\epsilon_a^2$. In obtaining this result, the approximations $\epsilon_a \ll 1$ and $\epsilon_a < \epsilon_b$ were used.

For comparison, consider the S/C ratio of a simple $m \times m$ matrix having only one elementary switch per crosspoint. By the same analytic procedure, we find that the worst case S/C ratio of the conventional $m \times m$ matrix is approximately $(1 - \epsilon_b)/(m - 1)\epsilon_a$. Therefore, the tandemizing technique increases the S/C ratio by the large factor $(1 - \epsilon_b)/\epsilon_a$. Note that the crosstalk problem is severe in the simple matrix for large m (when m is comparable with ϵ_a^{-1}). Then the S/C ratio is very poor; and the matrix will be unusable, depending in detail on the sensitivity of the optical detectors and the power of the optical sources. Because of the S/C enhancement, our composite switch approach makes optical matrixing feasible in situations where it otherwise would not be feasible.

Low crosstalk optical switches can be realized readily with thin-film integrated-optic structures. Several electrooptic crosspoint candidates, such as mode converters, Bragg gratings, and directional couplers, have been compared in a recent report.¹ Layout drawings are given for a low crosstalk matrix employing electrically controlled optical couplers as tandem crosspoints, and a matrix design including pairs of switchable gratings is also presented.

To summarize, the Fig. 3 matrix design provides approximately twice the S/C ratio in dB of the conventional design. Or, for a prescribed S/C ratio, the manufacturing tolerances on individual switches are looser than in the conventional approach. The disadvantage of the design is that it requires $2m^2$ switches rather than m^2 , and there are m^2 waveguide crossovers in the matrix. However, the light beams can pass through one another without three-dimensional crossovers if the matrix array is contained in a slab waveguide, as it would be for Bragg diffraction devices.

This work was supported by the Rome Air Development Center, Contract F30602-74-C-0168.

References

1. R. A. Soref and L. R. Schissler, "Optical Switch Study" (February 1975), available from Rome Air Development Center as RADC Rpt. TR-75-3, Griffiss Air Force Base, New York 13441.

APPENDIX B

Reprinted from **APPLIED OPTICS**, Vol. 15, page 2950, December 1976
Copyright 1976 by the Optical Society of America and reprinted by permission of the copyright owner

ERRATA

I_1 and I_2 are reversed in left-hand side of the Fig. 3 hybrid state, and the $4N^2$ entry in Table 1 should read $2N^2$.

Properties of the terminated optical crossbar matrix

R. A. Soref

Sperry Research Center, Sudbury, Massachusetts 01776.
Received 24 July 1976.

Optical switching networks are comprised of individual optical switches connected by optical waveguides. These switches, known as simple crosspoints, are four-port electrooptic devices that operate in the cross state \otimes or the bar state \ominus , illustrated in Fig. 1. The crosspoint permutes, or does not permute, optical signals between two guides as shown. In general, optical crosstalk is present in both switch states, the fractional crosstalk being denoted by ϵ_a and ϵ_b , respectively, in Fig. 1.

Previous work on optical switching networks (optical matrices) has been concerned with the permutation network¹⁻³ which has N successive stages capable of permuting N optical inputs onto N optical outputs. For this network to give a high signal-to-crosstalk ratio at each of its output ports, it is necessary that the individual switches have low crosstalk in *both* states, that is, $\epsilon_a \ll 1$ and $\epsilon_b \ll 1$.

We recently reported on a terminated crossbar array for use with compound crosspoints.⁴ The purpose of this Letter is to show that the terminated crossbar is much more tolerant of incomplete energy transfer in individual switches than is the permutation matrix. Only one state is required to have high isolation: $\epsilon_a \ll 1$. The other state is allowed to have large crosscoupling, for example $0.4 < \epsilon_b < 0.6$. This opens up new categories of optical crosspoints for use in optical matrices. However, there is a trade-off between the wider crosspoint acceptance of the crossbar and its relatively large size and complexity.

The terminated crossbar is shown in Fig. 2(a) for the example $N = 4$. The resistor symbols denote optical absorbers or terminations at the ends of the row and column waveguides. This is a full crossbar matrix with elementary switches at all row-column intersections. For comparison, we show in Fig. 2(b) the minimal form of the $N \times N$ permutation network for the same example, $N = 4$. This network does not have any waveguide crossings in the regions between switches, which is also true of the Fig. 2(a) array.

The row and column guides in the crossbar are oriented at

a small angle to one another, rather than at 90° . This layout is used for two reasons. First, the optical crosspoints are highly elongated structures. (Optical switches are typically 10^3 to 10^4 wavelengths long and less than 10^2 wavelengths wide.) Second, the channels that interconnect the crosspoints are

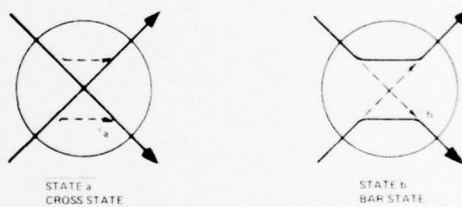


Fig. 1. Binary-state optical crosspoint. Solid lines denote optical signal paths. Dashed lines denote crosstalk.

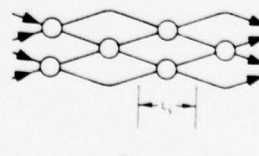
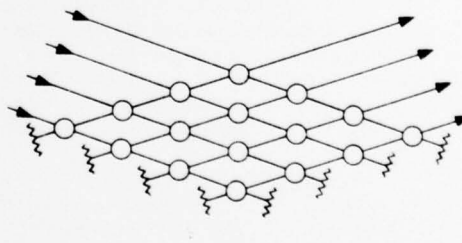


Fig. 2. Layout of (a) terminated optical crossbar matrix, and (b) optical permutation matrix. $N = 4$ for both.

Table I. Comparison of Permutation and Crossbar Switching Approaches

	Number of Elementary Switches	Optical Crosspoint Switch Requirement	Matrix S/C Ratio (Minimum Value)	Optical Insertion Loss thru Matrix (Fractional Loss)	Length of Matrix	Width of Matrix
Permutation Matrix	$\frac{N^2}{2} - \frac{N}{2}$	$\epsilon_a \ll 1$ for (\times) $\epsilon_b \ll 1$ for (\equiv)	$\frac{1}{N\epsilon_b}$ ($\epsilon_b > \epsilon_a$) $\frac{1}{(N-1)\epsilon_a + \epsilon_b}$ ($\epsilon_a > \epsilon_b$)	$1 - (1 - \epsilon_b)^N$ ≈ 0	$N L_s$	$(N-1)W_s$
Terminated Crossbar Matrix (Simple Crosspoints)	N^2	$\epsilon_a \ll 1$ for (\times) $0 < \epsilon_b < 0.6$ for (\equiv)	$\frac{1 - \epsilon_b}{(N-1)\epsilon_a}$	$1 - (1 - \epsilon_b)(1 - \epsilon_a)^{N-1}$ $\approx \epsilon_b$	$(2N-1)L_s$	$(2N-1)W_s$
Terminated Crossbar Matrix (Compound Crosspoints, Ref. 4)	$4N^2$	$\epsilon_a \ll 1$ for (\times) $0 < \epsilon_b < 0.6$ for (\equiv)	$\frac{(1 - \epsilon_b)^2}{(N-1)\epsilon_a^2}$	$1 - (1 - \epsilon_b)^2(1 - \epsilon_a)^{N-1}$ $\approx 2\epsilon_b\epsilon_a^2$	$2(2N-1)L_s$	$2(2N-1)W_s$

relatively short, curved guides that bend gradually to minimize propagation loss. Bends of 90° would take up too much space because the matrix area is limited by the size of available electrooptic crystals.

The asymmetric Fig. 2(a) matrix will accommodate an asymmetry between the a and b states of its switches in the manner shown in Fig. 3. The cross state should have high isolation to maximize S/C, but the bar state can be a hybrid, half-bar and half-cross with $\epsilon_b \sim 0.5$ because unswitched energy in the b state travels to a termination and is absorbed. The worst-case signal-to-crosstalk ratio⁵ at any output port of the terminated matrix is $(1 - \epsilon_b)(1 - \epsilon_a)^{N-1}/[1 - (1 - \epsilon_a)^{N-1}]$. Thus, if the crosspoints are optical power dividers (~ 3 -dB couplers) in state b , the S/C ratio will decrease by ~ 3 dB relative to the ideal case, $\epsilon_b = 0$; and the insertion loss will increase by ~ 3 dB. These 3-dB changes will usually be acceptable in practice.

We have examined the theoretical limits of the permutation and terminated crossbar matrices. Our results are summarized in Table I, which shows the trade-offs between these two approaches. The crossbar array has the advantage of permitting partial coupling in one switch state; but it requires approximately twice the substrate length of the permutation array, more than twice the number of switches, and it has a larger throughput loss. The matrix width is small in both cases.

The coupler switches can be implemented in multimode and single-mode versions. Experiments in our laboratory have shown that it is possible to build a multimode optical switch that has a reasonable off-state isolation and 3-dB power splitting in its on-state.⁶ Manufacturing tolerances are fairly loose because the switch does not rely on mode interference, and the switch length is not excessive. The multimode switch length is given approximately by $L_s = 2D/\theta_c = D(2n/\Delta n)^{1/2}$, where D is the diameter of the multimode optical channels,

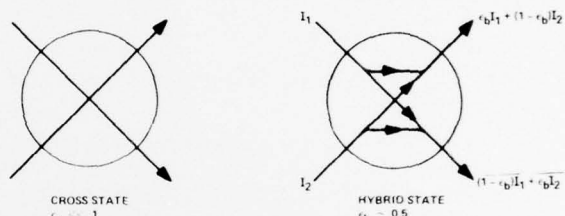


Fig. 3. Usable states of crosspoint in terminated crossbar matrix.

θ_c is the critical angle for internal reflection within the channels, n is the channel index, and Δn is the voltage-controlled (field-induced) index perturbation in the interchannel region.⁶ We find, in practice, $0.5 \text{ cm} < L_s < 1.0 \text{ cm}$, which is comparable with the result obtained in single-mode switching. We have designed multimode switches for $\epsilon_a \ll 1$ and $\epsilon_b \ll 1$, but L_s is about 0.5 cm longer in that case.

References

1. H. F. Taylor, Electron. Lett. **10**, 41 (1974).
2. H. F. Taylor, NELC Tech. Rep. 1913 (1974).
3. J. C. Shelton, IEEE Trans. Microwave Theory Tech. **MTT-24**, (1976) (to be published).
4. R. A. Soref and L. R. Schissler, Appl. Opt. **14**, 2559 (1975).
5. This ratio is equal to $P_1(\min)/P_0(\max)$ as described in Ref. 3. Minimum P_1 and maximum P_0 are found at the first-column output of the crossbar when the crosspoint in the N th row of that column is addressed. The input levels are $(0, 0, \dots, 0, 1)$ for P_1 and $(1, 1, \dots, 1, 0)$ for P_0 .
6. R. A. Soref, D. H. McMahon, and A. R. Nelson, Appl. Phys. Lett. **28**, 716 (1976).

Appendix C
CROSSTALK MODEL FOR CROSSOVER

The signal is calculated by assuming a uniform input intensity

$$I_{in}(\theta) = \begin{cases} P_{in}/\pi\theta_i^2 & \text{for } \theta < \theta_i \\ 0 & \text{for } \theta \geq \theta_i \end{cases}$$

The optical input power, P_{in} , is fixed. Because θ_c may be larger or smaller than θ_i , we note that the output signal intensity, S_{out} , is truncated at the minimal angle, θ_{ci} .

$$S_{out}(\theta) = \begin{cases} P_{in}/\pi\theta_i^2 & \text{for } \theta < \theta_{ci} \\ 0 & \text{for } \theta \geq \theta_{ci} \end{cases}$$

$$\theta_{ci} = \text{the smaller of } \theta_c \text{ and } \theta_i$$

The observed signal power, S , is integrated over the full range of collection angles

$$S = \int_0^{2\pi} \int_0^{\theta_o} S_{out}(\theta) \sin\theta d\theta d\psi$$

Performing the integration with $\sin\theta \approx \theta$, we obtain

$$S = \begin{cases} P_{in} (\theta_o/\theta_i)^2 & \text{for } \theta_o < \theta_{ci} \\ P_{in} (\theta_{ci}/\theta_i)^2 & \text{for } \theta_o \geq \theta_{ci} \end{cases} \quad (1)$$

The output crosstalk intensity, C_{out} , is comprised of two terms: a single-scattering term proportional to the trapped signal, $\mathcal{J}(\theta')$, reoriented at the intersection, and a double-scattering term, $B(\phi)$:

$$C_{\text{out}} = A(\phi) \mathcal{J}(\theta') + B(\phi) \quad (2)$$

where θ' is the bounce angle measured with respect to the crosschannel axis, and

$$\mathcal{J}(\theta') = \begin{cases} P_{\text{in}} / \pi \theta_i^2 & \text{for } \theta' < \theta_{ci} \\ 0 & \text{for } \theta' \geq \theta_{ci} \end{cases} \quad (3)$$

The A and B coefficients decrease rapidly with increasing ϕ and $\phi > 2\theta_c$ by hypothesis.

The crosstalk is then computed by integrating the crosstalk intensity over the observation range:

$$C = \int_0^{2\pi} \int_0^{\theta_o} C_{\text{out}}(\theta') \sin \theta' d\theta' d\psi$$

Which, from Eqs. 2 and 3, gives the observed crosstalk C as follows:

$$C = \begin{cases} A P_{\text{in}} (\theta_o / \theta_i)^2 + \pi B \theta_o^2 & \text{for } \theta_o < \theta_{ci} \\ A P_{\text{in}} (\theta_{ci} / \theta_i)^2 + \pi B \theta_o^2 & \text{for } \theta_o \geq \theta_{ci} \end{cases} \quad (4)$$

Therefore, the observed signal-to-crosstalk ratio of the passive cross-over is calculated from Eqs. 1 and 4 to be:

$$S/C = \begin{cases} \frac{1}{A + \pi B \theta_i^2 / P_{\text{in}}} & \text{for } \theta_o < \theta_{ci} \\ \frac{1}{A + [\pi B \theta_i^2 / P_{\text{in}}] (\theta_o / \theta_{ci})^2} & \text{for } \theta_o \geq \theta_{ci} \end{cases} \quad (5)$$

The theoretical signal-to-crosstalk ratio (Eq. 5) for the choice, $A = 2.0 (\pi B \theta_i^2 / P_{\text{in}})$, is shown in Fig. C-1, on the same scale as used in Figures 13 through 16. The agreement between experiment and theory is only fair. Agreement is fairly good for the 4x input, but poor for 20x. This

comparison implies that a more sophisticated model is needed. For example, the present model could be improved by assuming a Gaussian intensity distribution at the input rather than a square one.

Correlation of the observed 4x shape with theory suggests that the two-component crosstalk model has some validity. Equation 5 shows how the A-term dominates in the limit, $\theta_o \rightarrow 0$, and how the B-term takes over when $\theta_o \gg \theta_{ci}$.

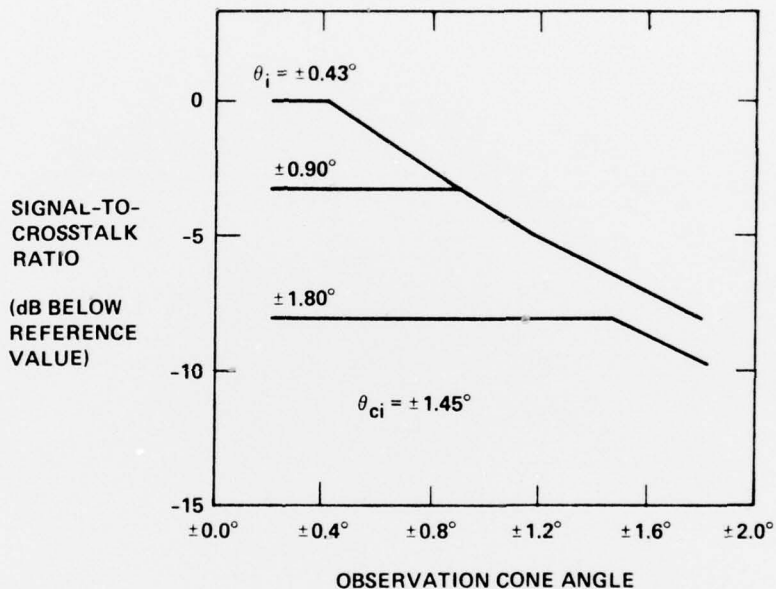


FIG. C-1 Theoretical S/C ratios of multimode intersecting channels versus observation cone angle.